



uOttawa

L'Université canadienne
Canada's university

**FACULTÉ DES ÉTUDES SUPÉRIEURES
ET POSTDOCTORALES**



**FACULTY OF GRADUATE AND
POSTDOCTORAL STUDIES**

Shahrzad Hashemi

AUTEUR DE LA THÈSE / AUTHOR OF THESIS

Ph.D. (Chemical Engineering)

GRADE / DEGREE

Department of Chemical and Biological Engineering

FACULTÉ, ÉCOLE, DÉPARTEMENT / FACULTY, SCHOOL, DEPARTMENT

Carbon Dioxide Hydrate Formation in a Three-Phase Slurry Bubble Column

TITRE DE LA THÈSE / TITLE OF THESIS

A. Macchi

DIRECTEUR (DIRECTRICE) DE LA THÈSE / THESIS SUPERVISOR

CO-DIRECTEUR (CO-DIRECTRICE) DE LA THÈSE / THESIS CO-SUPERVISOR

EXAMINATEURS (EXAMINATRICES) DE LA THÈSE / THESIS EXAMINERS

P. Englezos

D. Taylor

M. Ternan

J. Thibault

Gary W. Slater

Le Doyen de la Faculté des études supérieures et postdoctorales / Dean of the Faculty of Graduate and Postdoctoral Studies

Carbon Dioxide Hydrate Formation in a Three-Phase Slurry Bubble Column

By

Shahrzad Hashemi

Thesis submitted to the Faculty of Graduate and Postdoctoral Studies
In Partial Fulfillment of the Requirements for the Degree of Doctor of
Philosophy in Chemical Engineering

Department of Chemical and Biological Engineering
University of Ottawa
April 2009

©Shahrzad Hashemi, Ottawa, Canada, 2009



Library and Archives
Canada

Published Heritage
Branch

395 Wellington Street
Ottawa ON K1A 0N4
Canada

Bibliothèque et
Archives Canada

Direction du
Patrimoine de l'édition

395, rue Wellington
Ottawa ON K1A 0N4
Canada

Your file *Votre référence*
ISBN: 978-0-494-59499-5
Our file *Notre référence*
ISBN: 978-0-494-59499-5

NOTICE:

The author has granted a non-exclusive license allowing Library and Archives Canada to reproduce, publish, archive, preserve, conserve, communicate to the public by telecommunication or on the Internet, loan, distribute and sell theses worldwide, for commercial or non-commercial purposes, in microform, paper, electronic and/or any other formats.

The author retains copyright ownership and moral rights in this thesis. Neither the thesis nor substantial extracts from it may be printed or otherwise reproduced without the author's permission.

In compliance with the Canadian Privacy Act some supporting forms may have been removed from this thesis.

While these forms may be included in the document page count, their removal does not represent any loss of content from the thesis.

AVIS:

L'auteur a accordé une licence non exclusive permettant à la Bibliothèque et Archives Canada de reproduire, publier, archiver, sauvegarder, conserver, transmettre au public par télécommunication ou par l'Internet, prêter, distribuer et vendre des thèses partout dans le monde, à des fins commerciales ou autres, sur support microforme, papier, électronique et/ou autres formats.

L'auteur conserve la propriété du droit d'auteur et des droits moraux qui protègent cette thèse. Ni la thèse ni des extraits substantiels de celle-ci ne doivent être imprimés ou autrement reproduits sans son autorisation.

Conformément à la loi canadienne sur la protection de la vie privée, quelques formulaires secondaires ont été enlevés de cette thèse.

Bien que ces formulaires aient inclus dans la pagination, il n'y aura aucun contenu manquant.


Canada

Statement of Contribution of Collaborators

I hereby declare that I am the sole author of this thesis. The hydrodynamic experiments as well as the development of computer codes in MATLAB[®] for thermodynamic and kinetic studies, and dynamic simulations were performed by me. The newly-adjusted parameters associated with Chapter 2 were optimized by Sebastien Bergeron (Chemical Engineering Department, McGill University) under my co-supervision and using my computer codes.

My supervisor, Dr. Arturo Macchi, of the Department of Chemical and Biological Engineering, University of Ottawa supervised my work during the Ph.D. program and provided editorial corrections.

Signature: Shahzad Hushemi

Date: Apr. 28, 09

Abstract

Gas hydrates are non-stoichiometric crystalline compounds made of ice-like lattice linked together through hydrogen bonding. Hydrates are being considered as an alternate means of transportation and storage of natural gas as hydrate metastability can be achieved at higher temperature and lower pressure than those required for liquefaction and compression, respectively. Since the mass production of gas hydrates is a developing technology, there is very little data on reactor design and performance available in the open literature. The multiphase reactor of choice is a continuous sparged slurry bubble column which allows relatively high heat and mass transfer rates. The thermodynamics, kinetics and hydrodynamics of this system were studied in this work.

In order to predict the solubility of carbon dioxide and methane in water in the presence of hydrate, a model was assembled based on the Trebble-Bishnoi equation of state (1987, *Fluid Phase Equil.*, 35, 1-18), the van der Waals and Platteeuw model (1959, *Adv. Chem. Phys.*, 2, 1-57) and the Holder model (1980, *Ind. Eng. Chem. Fund.*, 19, 282-286). The accuracy of the model was improved by re-adjusting its parameters with recent vapor-liquid water and vapor-liquid water-hydrate equilibrium data of methane-water and carbon dioxide-water systems.

In order to estimate the intrinsic kinetic rate constant of hydrate growth, Englezos model (1987, *Chem. Eng. Sci.*, 42, 2647-2658) was reformulated based on a concentration driving force which takes interphase heat transfer into account. The estimation of the intrinsic

kinetic rate constant depends on the accuracy of hydrate surface area. The hydrate surface area estimated using a population balance was found to be in good agreement with that based on recently measured data (Bergeron and Servio, 2008, AIChE J, 54 (11), 2964-2970).

Gas-liquid interphase mass transfer coefficients were investigated in a three-phase slurry bubble column under CO₂ hydrate forming operating conditions. The pressure was varied from 0.1 MPa to 4 MPa while gas velocity was increased up to 0.20 m/s. The effect of temperature was investigated by performing experiment at ambient as well as 277 K. Wettable ion-exchange resin particles were used to simulate the CO₂ hydrate. The slurry concentration was varied up to 10 vol.%. Volumetric mass transfer coefficient was found to increase with pressure and superficial gas velocity while it decreased with temperature. No effect of solid was noticed within the range investigated as the rheology of the slurry remained similar to that of water alone.

Finally, a reactor model was developed that incorporates the hydrate formation kinetics as well as the system hydrodynamics and interphase mass and heat transfer rates. The model uses a population balance to account for the hydrate growth rate. The mole consumption rate was evaluated as a function of time, temperature, pressure and superficial gas velocity. Moreover, the effect of flow regimes as well as the relative importance of interphase mass transfer and growth kinetics as a function of time and process conditions was discussed.

Sommaire

Les hydrates de gaz sont des composés cristallins non-stoechiométriques dont les molécules d'eau sont liées par des ponts d'hydrogène. Les hydrates sont considérés comme moyen de transport alternatif du gaz naturel puisque la meta-stabilité de l'hydrate peut être réalisée à des températures plus élevées et pressions plus faibles que celles pour la liquéfaction et la compression, respectivement. Puisque la production industrielle des hydrates de gaz est une technologie en voie de développement, il y a très peu de données disponibles dans la littérature sur la conception et la performance du réacteur. Le réacteur multiphasé de choix est une colonne à bulle où les taux de transfert de la chaleur et de matière sont relativement élevés. La thermodynamique, la cinétique et l'hydrodynamique de ce système ont été étudiées dans cette thèse.

Afin de prévoir la solubilité du dioxyde de carbone et du méthane dans l'eau en présence de l'hydrate, un modèle a été assemblé basé sur l'équation d'état de Trebble-Bishnoi (1987, Fluid Phase Equil., 35, 1-18), le modèle de van der Waals et Platteeuw (1959, Adv. Chem. Phys., 2, 1-57) et le modèle de Holder (1980, Ind. Eng. Chem. Fund., 19, 282-286). L'exactitude du modèle a été améliorée en ajustant ses paramètres avec des données récentes d'équilibre vapeur-eau liquide et vapeur-eau liquide-hydrate des systèmes méthane-eau et dioxyde de carbone-eau.

Afin d'estimer la constante cinétique intrinsèque du taux de croissance de l'hydrate, le modèle d'Englezos (1987, Chem. Eng. Sci., 42, 2647-2658) a été reformulé basé sur une

force motrice de concentration qui prend en considération le transfert de chaleur interphase. L'évaluation de la constante cinétique intrinsèque dépend de l'exactitude de la superficie des hydrates et celle extraite utilisant un bilan de population s'est avérée en bon accord avec celle basée sur la superficie récemment mesurée expérimentalement (Bergeron et Servio, 2008, AIChE J, 54 (11), 2964-2970).

Des coefficients de transfert de matière gaz-liquide ont été obtenus dans une colonne à bulle sous des conditions propices à la formation d'hydrate de CO₂. La pression a été variée de 0.1 à 4 MPa alors que la vitesse superficielle du gaz était augmentée jusqu'à 0.20 m/s. L'effet de la température a été étudié aux conditions ambiantes et à 277 K. Des particules d'échange ions mouillables en résine ont été employées pour simuler l'hydrate de CO₂. La concentration de particules a été variée jusqu'à 10 vol.%. Le coefficient de transfert de matière volumique augmente avec la pression et la vitesse superficielle de gaz tandis qu'il diminue avec la température. Aucun effet de solide n'a été noté pour les concentrations étudiées puisque la rhéologie de la suspension demeure semblable à celle de l'eau.

En conclusion, on a développé un modèle de réacteur qui incorpore la cinétique de formation des hydrates ainsi que l'hydrodynamique du système et les taux de transfert interphase de la matière et de chaleur. Le modèle emploie un bilan de population pour déterminer le taux de croissance d'hydrate. Le taux de consommation du gaz a été évalué en fonction du temps, de la température, de la pression et de la vitesse superficielle du gaz. De plus, l'effet des régimes d'écoulement et l'importance relative de la cinétique de croissance et du transfert de matière en fonction du temps et des conditions d'opération ont été discutés.

Acknowledgements

I would like to express my gratitude to Dr. Arturo Macchi for giving me the opportunity to work on this project and for inspiration and support throughout the program.

I would like to thank Dr. Phillip Servio from the Department of Chemical Engineering at McGill University for his helpful comments and insights.

I would also like to thank people in the Chemical and Biological Engineering Department who helped me during this program. Special thanks go to Louis G. Tremblay, Franco Zirolto, Gérard Nina, Dr. Poupak Mehrani, Siamak Lashkari, Dr. Jules Thibault, Philippe Malouf and Andrew Sowinski.

Finally, I would like to thank my family and friends for their support.

Table of Contents

Statement of Contribution of Collaborators	ii
Abstract	iii
Sommaire	v
Acknowledgements	vii
Table of Contents	viii
List of Tables	x
List of Figures	xi
Chapter 1. Introduction	1
1.1 Hydrate Structure	1
1.2 Importance of Gas Hydrate	3
1.3 Methods for Transporting Gas	5
1.4 Gas Hydrate Forming Processes	8
1.4.1 Systems with Liquid Water as the Dispersed Phase	8
1.4.2 Systems with Gas as the Dispersed Phase	10
1.5 Research Objectives	14
1.6 Research Outline	15
Nomenclature	16
References	17
Chapter 2. Prediction of Methane and Carbon Dioxide Solubility in Water in the Presence of Hydrate	21
Abstract	22
2.1 Introduction	23
2.2 Theory	27
2.3 Results and Discussion	31
2.4 Conclusions	42
Nomenclature	42
Acknowledgments	44
References	44
Chapter 3. Gas Hydrate Growth Model in a Semi-Batch Stirred Tank Reactor	48
Abstract	49
3.1 Introduction	50
3.2 Hydrate Formation Model	52
3.2.1 Two-Phase Versus Three-Phase Equilibrium	56
3.3 Results and Discussion	59
3.3.1 Intrinsic Kinetic Rate Constant	60
3.3.2 Supersaturation	63
3.4 Conclusions	65
Nomenclature	66
Acknowledgements	68
References	69

Chapter 4. Gas-Liquid Mass Transfer in a Slurry Bubble Column Operated at Hydrate Forming Conditions	72
Abstract	73
4.1 Introduction	74
4.2 Experimental	75
4.2.1 Apparatus	75
4.2.2 Procedure	77
4.2.3 Particles	81
4.3 Results and Discussion	84
4.4 Conclusions	103
Nomenclature	104
Acknowledgements	105
References	105
 Chapter 5. Dynamic Simulation of Gas Hydrate Formation in a Three-Phase Slurry Reactor	 111
Abstract	112
5.1 Introduction	113
5.2 Model Development	114
5.2.1 Mass Balance	115
5.2.2 Energy Balance	124
5.2.3 Pressure Balance	129
5.3 Results and Discussion	129
5.4 Conclusion	147
Nomenclature	148
Acknowledgements	151
References	151
 Chapter 6. Conclusions and Future Research	 155
6.1 Conclusions	155
6.2 Future Research	160

List of Tables

Table (2.1). Vapor-liquid water experimental data for methane-water and carbon dioxide-water(*) systems.	35
Table (2.2). Mixing rule binary interaction parameters	35
Table (2.3). Hydrate-liquid water-vapor experimental data for methane-water and carbon dioxide-water(*) systems.	37
Table (2.4). Hydrate-liquid water experimental data for methane-water and carbon dioxide-water(*) systems.	38

List of Figures

Figure (1.1). Schematic of the experimental apparatus of Iwasaki et al. (2002).	8
Figure (1.2). Schematic of the experimental apparatus of Heinemann et al. (2001).	9
Figure (1.3). Schematic of the experimental apparatus of Waycuilis and York (2002).	12
Figure (1.4). Schematic of the slurry bubble column in this work.	14
Figure (2.1). Phase diagram of methane-water system (Sloan, 1998; Servio and Englezos, 2002).	25
Figure (2.2). Comparison of calculated methane solubility in liquid water by the present model using the original parameters with experimental data of Servio and Englezos (2002).	32
Figure (2.3). Comparison of calculated methane solubility in liquid water by the present model using the re-optimized parameters with experimental data of Servio and Englezos (2002).	39
Figure (2.4). Comparison of calculated carbon dioxide solubility in liquid water by the present model using the re-optimized parameters with experimental data of Servio and Englezos (2001).	40
Figure (3.1). Carbon dioxide solubility in water under liquid water-vapor and liquid water-hydrate equilibrium at 35 bar (Hashemi et al., 2006).	58
Figure (3.2). Temperature, pressure and concentration driving forces within the liquid phase. Dashed lines represent the liquid film boundary.	59
Figure (3.3). Supersaturation as a function of time at 277.15 K and 21.87 bar.	64
Figure (4.1). Slurry bubble column setup.	77
Figure (4.2)a. Oxygen absorption dynamics for water at 0.5, 1 and 2.5 MPa in the bubble column.	80
Figure (4.2)b. Oxygen absorption dynamics for water at 4MPa in the bubble column.	80
Figure (4.3). Rheology for ion-exchange resin slurry in water.	83
Figure (4.4). Effect of pressure on gas holdup in the bubble column at ambient temperature.	85
Figure (4.5). Effect of pressure on volumetric mass transfer coefficient in the bubble column at ambient temperature.	86
Figure (4.6). Effect of solid volume concentration on gas holdup at 2.5 MPa and ambient temperature.	87
Figure (4.7). Effect of solid volume concentration on volumetric mass transfer coefficient at 2.5 MPa and ambient temperature.	88
Figure (4.8). Effect of solid volume concentration and pressure on gas holdup at ambient temperature. closed symbols: 0%; open symbols: 10%.	89
Figure (4.9). Effect of solid volume concentration and pressure on volumetric mass transfer coefficient at ambient temperature. closed symbols: 0%; open symbols: 10%.	90
Figure (4.10). Effect of temperature on gas holdup at 2.5MPa. closed symbols: 0%; open symbols: 10%.	91
Figure (4.11). Effect of temperature on volumetric mass transfer coefficient at 2.5MPa. closed symbols: 0%; open symbols: 10%.	92
Figure (4.12). Mass transfer versus gas holdup in the bubble column at ambient temperature.	93

Figure (4.13). Mass transfer coefficient-to-bubble diameter ratio in the bubble column at ambient temperature.	95
Figure (4.14). Mass transfer coefficient-to-gas holdup ratio in the bubble column at ambient temperature.	96
Figure (4.15)a. Gas holdup in the bubble column at 2.5 MPa and 295K comparing the current experimental data with Luo et al. as well as Behkish et al. correlations.	97
Figure (4.15)b. Gas holdup in the bubble column at 0.1 MPa and 295K comparing the current experimental data with Luo et al. as well as Behkish et al. correlations.	98
Figure (4.15)c. Gas holdup in the bubble column at 2.5 MPa and 277K comparing the current experimental data with Luo et al. as well as Behkish et al. correlations.	99
Figure (4.16)a. Volumetric mass transfer coefficient in the bubble column at 2.5 MPa and 295 K comparing the current experimental data with Lau et al. as well as Lemoine et al. correlations.	100
Figure (4.16)b. Volumetric mass transfer coefficient in the bubble column at 0.1 MPa and 295 K comparing the current experimental data with Lau et al. as well as Lemoine et al. correlations.	101
Figure (4.16)c. Volumetric mass transfer coefficient in the bubble column at 2.5 MPa and 277 K comparing the current experimental data with Lau et al. as well as Lemoine et al. correlations.	102
Figure (4.17). The ratio of CO ₂ volumetric mass transfer coefficient and gas holdup to those reported in this work at 295 K.	103
Figure (A.1). Surface tension of water in presence of CO ₂ as a function of pressure at 295 K.	110
Figure (5.1). Temperature, pressure and concentration driving forces within the gas, liquid and solid phases.	115
Figure (5.2)a. Schematic of the experimental apparatus .	116
Figure (5.2)b. Schematic representation of slurry bubble column reactor.	116
Figure (5.3). Phase diagram of carbon dioxide-water system.	127
Figure (5.4). Carbon dioxide solubility in water under liquid water-vapor and liquid water-hydrate equilibrium at 3.5 MPa (Hashemi et al., 2006).	128
Figure (5.5). Supersaturation ratio of carbon dioxide in water as a function of time at 277.15 and 2.187 MPa; PF at $z = H_D$; gas and liquid superficial velocities are 0.025 and 0.002 m/s, respectively.	130
Figure (5.6). Gas consumption rate as a function time at 277.15 K and 2.187 MPa; gas and liquid superficial velocities are 0.025 and 0.002 m/s, respectively; CST for all phases.	132
Figure (5.7). Supersaturation ratio of carbon dioxide in water as a function of time at 277.15 K and 2.187 MPa; liquid velocity is 0.002 m/s; CST for all phases.	134
Figure (5.8). Heat produced as a function of time at 277.15 K and 2.187 MPa; liquid velocity is 0.002 m/s; CST for all phases.	136
Figure (5.9). Effect of pressure at 277.5 K; gas and liquid superficial velocities are 0.01 and 0.002 m/s, respectively. Open and close symbols represent mole consumption rate and supersaturation ratio, respectively; CST for all phases.	138
Figure (5.10). Effect of temperature on supersaturation at 3.04 MPa; gas and liquid superficial velocities are 0.01 and 0.002 m/s, respectively; CST for all phases.	139
Figure (5.11). Effect of temperature on mole consumption rate at 3.04 MPa; gas and liquid superficial velocities are 0.01 and 0.002 m/s, respectively; CST for all phases.	140

Figure (5.12)a. Effect of pressure on the ratio of resistances at 277.5 K; gas and liquid superficial velocities are 0.01 and 0.002 m/s, respectively; CST for all phases.	141
Figure (5.12)b. Effect of pressure on $k_l a_l \varepsilon_l$ at 277.5 K; gas and liquid superficial velocities are 0.01 and 0.002 m/s, respectively; CST for all phases.	142
Figure (5.12)c. Effect of pressure on $k_r a_s$ at 277.5 K; gas and liquid superficial velocities are 0.01 and 0.002 m/s, respectively; CST for all phases.	143
Figure (5.13)a. Effect of temperature on the ratio of resistances at 3.04 MPa; gas and liquid superficial velocities are 0.01 and 0.002 m/s, respectively; CST for all phases.	144
Figure (5.13)b. Effect of temperature on $k_l a_l \varepsilon_l$ at 3.04 MPa; gas and liquid superficial velocities are 0.01 and 0.002 m/s, respectively; CST for all phases.	145
Figure (5.13)c. Effect of temperature on $k_r a_s$ at 3.04 MPa; gas and liquid superficial velocities are 0.01 and 0.002 m/s, respectively; CST for all phases.	146

Chapter 1

Introduction

Natural gas hydrates are considered as a potential cost-effective alternative for transportation and storage of natural gas. Mass production of natural gas hydrates requires high-efficiency continuous hydrate formation reactors. Research has been conducted to overcome the mass and heat transfer issues by enhancing the gas-liquid contact as well as the heat transfer area. Knowledge of thermodynamics, kinetics as well as hydrodynamics is required to address the current issues in gas hydrate formation processes.

1.1 Hydrate Structure

Gas hydrates are non-stoichiometric crystalline compounds that belong to the inclusion group known as Clathrate. Hydrates occur when water molecules attach themselves through hydrogen bonding and form cages that can be occupied by at most one guest molecule each. The presence of an enclathrated guest molecule inside the water network thermodynamically stabilizes the structure through physical bonding via van der Waals forces. The cages in hydrate arrange into different structures known as structure I (sI), structure II (sII) and structure H (sH) (Sloan, 1998). The structure of the water lattice is determined by the size of the guest molecule. Methane gas forms sI hydrates, while natural gas usually forms sII hydrates. Structure H is not discussed here since all natural gas components form either sI or sII.

A unit cell of sI consists of 2 small and 6 large cages. The small cage, the pentagonal dodecahedron denoted 5^{12} , has 12 pentagonal faces with equal edge lengths and equal angles. The large cage, the tetrakaidecahedron, labeled $5^{12}6^2$ has 12 pentagonal and 2 hexagonal faces. There are 46 water molecules inside the one sI unit cell which fits into a 12 Å cube. sII has the pentagonal dodecahedron (5^{12}) as the small cage. The large cage, the hexakaidecahedron labeled $5^{12}6^4$, has 12 pentagonal and 4 hexagonal faces. One unit cell of sII consists of 16 small cages and 8 large cages with 136 water molecules which fit within a 17.3 Å cube (Sloan, 1998).

Each cavity can contain at most one guest molecule if the molecule contains neither a single hydrogen-bond group nor a number of moderately strong hydrogen bonding groups. The molecules of natural gas components do not consist of any hydrogen bonding. Hence, their chemical nature does not limit the hydrate formation. Molecules between 3.5 Å and 7 Å can form sI and sII hydrates. Lower size molecules are not able to stabilize any cavity while larger size molecules do not fit into any cavity in sI or sII. A structure could be stabilized either when the large cavity or both types of cages is occupied, e.g. any guest molecule between 5.5 Å to 6 Å such as ethane stabilizes the $5^{12}6^2$ in sI while any guest molecule between 6 Å to 7 Å such as iso-butane stabilizes $5^{12}6^4$ in sII. However, the small cages are never occupied alone as this does not allow sI or sII to be stable. A guest molecule will fill the large cavities of any structure if it can stabilize the small cavity of that structure. Molecules from 4.5 Å to 5.5 Å such as methane, carbon dioxide and hydrogen sulfide form structure sI as simple hydrates by filling both types of cages. Natural gas with propane and iso-butane typically form structure sII by stabilizing the larger structure. The vacant small cages will hence be filled by methane and carbon dioxide (Sloan, 1998).

The relative water/guest ratio is known as the hydration number. However, a crystal where all the cages are occupied is rarely obtained in reality, which means that the real hydration number is higher than the ideal hydration number. The difference in real and ideal hydration number makes hydrates non-stoichiometric clathrate compounds (Sloan, 1998).

1.2 Importance of Gas Hydrate

Naturally occurring hydrates, containing mostly methane, exist in vast quantities within and below the permafrost zone and in sub-sea sediment where temperature and pressure allow them to remain thermodynamically stable (Sloan, 1998). Methane hydrate is looked upon as a potential natural gas resource due to its immense quantities and wide geographical distribution. It was estimated that world hydrate reserves are as high as 10^{16} m³ at STP (Lee and Holder, 2001). One unit volume of methane hydrates has over 160 volumes of gas at standard conditions. Access to this high gas concentration as a possible future energy resource will also alleviate the potential global warming due to the emission of methane gas. The challenges for an acceptable operational extraction of gas hydrate in Canada has been recently studied (<http://www.scienceadvice.ca/hydrates.html>). Canada has one of the world's most favorable conditions for occurrence of gas hydrate. However, more research and exploration appears to be required to quantify the volume and location of the gas hydrate resource and to determine the technical and economical factors for the gas production. The report also indicates that gas production from gas hydrate is still more costly than comparable conventional natural gas reservoirs. They need compression from the beginning of the process due to the fact that a low pressure is required for hydrate dissociation. On the

other hand, gas reservoirs require compression when the gas production rate is significantly reduced, usually at the end of their life. Water produced from hydrate dissociation should be continuously disposed or lifted which adds more cost. In addition, chemical injection equipment or local heating is also required to avoid reforming of gas hydrate and plugging. However, the production of gas from conventional gas has a faster decline rate when compared to gas hydrate with a stable or increasing rate over time ([http://www.scienceadvice.ca/documents/\(2008-11-05\)%20Report%20on%20GH.pdf](http://www.scienceadvice.ca/documents/(2008-11-05)%20Report%20on%20GH.pdf)).

Carbon dioxide hydrates are also important hydrates being considered as a means to sequester carbon dioxide in the deep ocean thus reducing the emission of greenhouse gases (Tsouris et al., 2007; Brewer et al., 1999). CO₂ hydrate is not stable in seawater due to the difference between the chemical potential of CO₂ in the sea water and in the hydrate. However, the release rate is much smaller for CO₂ hydrate than other methods of sequestration including the liquid and gaseous CO₂ (Lee et al., 2003). Moreover, the density of CO₂ hydrate is greater than seawater at any depth of the ocean resulting in the hydrate particle descending towards the ocean bottom. However, liquid CO₂ is less dense than seawater unless the depth is greater than 3000 m and gaseous CO₂ is much less dense. Hence, sequestered CO₂ will ascend to the sea surface and to the atmosphere (Yamasaki et al., 2003). Gas hydrate has also been considered to recover CO₂ from flue gas by hydrate formation. This can be achieved by forming the mixed hydrate that preferentially removes CO₂ from the gaseous mixture (Seo et al., 2005). They performed the thermodynamic measurement and NMR spectroscopic analysis to study the separation of CO₂ from CO₂/N₂ gas mixture using water dispersed in pores of silica gel. Linga et al. (2007) also studied CO₂ hydrate formation from CO₂/N₂ and CO₂/H₂ mixtures.

Carbon dioxide is also a component of Natural Gas and can lead to hydrate formation in pipelines resulting in pipeline blockage (Englezos, 1993). Pipelines are designed by industry to operate outside the hydrate formation pressure-temperature region. This is typically carried out either by adding inhibitors (e.g. methanol and glycol) or by the dehydration of the gas/condensate fluids (Wu et al., 2007; Koh et al., 2002; Jamaluddin, 1991).

One of the most significant proposed technologies incorporating gas hydrates deals with transportation and storage of natural gas.

1.3 Methods for Transporting Gas

Natural gas produces less carbon dioxide than other conventional fuels, which is crucial for global warming issue worldwide (Lee and Holder, 2001). Natural gas transportation and storage occurs at high pressure and/or low temperature. Hence, an economical transportation and storage process is required to make the natural gas an alternative as a premium fuel to the most commonly used fuels such as oil or coal. Methods to export natural gas include: pipelines, liquefied natural gas (LNG), compressed natural gas (CNG), gas to liquid (GtL) and gas to solids (NGH), i.e. hydrates (Thomas and Dawe, 2003).

Pipelines need high pressure (between 45-76 atm) with the installation cost being approximately proportional to the distance, on average US\$ 1-5 million per mile plus compressor stations. Moreover, pipelines do not have more than one destination (Thomas and Dawe, 2003). Liquefied natural gas has a temperature around $-162\text{ }^{\circ}\text{C}$ at 1 atm with a

volume $\sim 1/600$ that of gas at room temperature. LNG method is only applied on large gas reserves with the facilities requiring large scale refrigerated tanks for the gas transportation and storage and hence is not able to serve the small market or use the small offshore reserves (Thomas and Dawe, 2003). Compressed natural gas has a high pressure typically 123 atm for a rich gas (significant amounts of ethane, propane, etc.) to roughly 246 atm for a lean gas (mainly methane). The compressors needed for CNG process are expensive to purchase, maintain and operate. In addition, heat exchangers needed to remove heat of compression makes the process more expensive (Thomas and Dawe, 2003). Natural gas can also be converted into liquid hydrocarbons via the production of synthesis gas and subsequent Fisher-Tropsch reactions. Sulfur components are removed at first stages of the process which makes the product clean to the environment (Thomas and Dawe, 2003).

Natural gas can be transported as solid (NGH). Natural gas hydrate can form at 80-100 bar and 2-10 °C and contain 160 Sm³ gas per m³ of hydrate. They can be stored and transported at mild temperatures (0 to -10 °C) and pressures (10 to 1 atm) (Thomas and Dawe, 2003). The self-preservation characteristic of NGH was studied by Giavarini and Maccioni (2004). The dissociation rate was reported to be a function of temperature, pressure as well as gas content. The best condition for self- preservation was suggested as 0.3 MPa and -4°C. Self-preservation of natural gas hydrate was also investigated by Mitsui (Watanabe et al., 2008) and the dissociation rate was found minimum at -20°C at atmospheric pressure. However, the dissociation rate was reported as 1% per day at 0°C. Currently used methods of natural gas transportation as mentioned before require high pressure ~ 205 atm for CNG (200 Sm³ per 1 m³ of compressed gas) or low temperature of ~ -162 °C for LNG (637 Sm³ gas per 1 m³). This compared to NGH formation and storage operating conditions explains the

research being conducted on the development of NGH processes (Watanabe et al., 2008; Hao et al., 2008; Javanmardi, 2005; Abdalla and Abdullatef, 2005; Gudmundsson, 2005). It has been estimated that 40% of all natural gas reserves from small gas fields is unutilized due to economical reasons (<http://www.mes.co.jp/english>). By using NGH, the development of unused gas resources could be feasible.

Gudmundsson and Borrehaug (1996) studied the capital costs of LNG and NGH transportation chains from Norway to Europe. The natural gas was assumed to first be piped to shore and then the two alternative gas chains were compared. Both chains consisted of on-land production facilities, sea-transport by tankers and on-land regasification. The capacity of the chains was assumed at 4.1 billion Sm^3 per year, which is the same as one standard LNG train, and the transport distance was assumed to be 6475 km. The capital cost of the NGH technology was found to be about 24% lower than that of the LNG. A similar study was conducted by Mitsui (Kanada, 2006) for cases of 0.6 and 1.4 billion Sm^3 per year natural gas transported over the sea for about 2760 and 6440 km, respectively. The cost for the small LNG chain was estimated based on a general LNG chain of 4.2-7 billion Sm^3 per year, because there is currently no such small LNG chain of 0.6-1.4 billion Sm^3 per year available. The production, transportation and re-gasification costs were calculated for evaluating the economical feasibility of NGH ocean transport chain in two cases. The study shows that the initial cost of the NGH transport chain (as a whole) is lower than that of LNG of the same scale by 25% and 18% in cases 1 and 2, respectively.

1.4 Gas Hydrate Forming Processes

Various systems have been suggested to produce gas hydrate. In this section gas hydrate production processes are divided into two categories such that gas or water can be the dispersed phase.

1.4.1 Systems with Liquid Water as the Dispersed Phase

Iwasaki et al. (2002) proposed the system shown in Fig. (1.1). Super-cooled water is sprayed into the reactor and liquid circulation is started. Temperature is adjusted and the gas supplied pressurizes the reactor to the desired condition. Formed gas hydrate slurry is filtered. Recovered water is mixed with fresh feed water, super-cooled and sprayed into the reactor again.

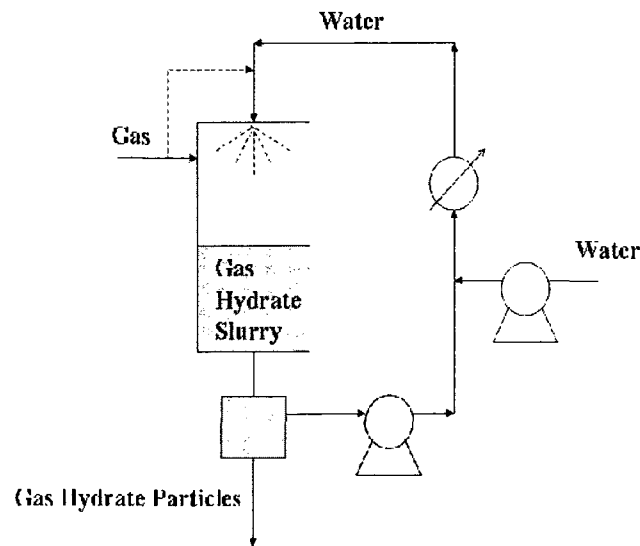


Figure (1.1). Schematic of the experimental apparatus of Iwasaki et al. (2002).

Heinemann et al. (2001) proposed a system which includes a reactor having a fluidized or expanded bed reaction zone as presented in Fig. (1.2). Water and gas are introduced into the reactor vessel from the top and bottom of the reactor respectively in order to have countercurrent flow through the system. Some of the injected water forms seed hydrate particles, while the rest coats already formed particles surrounding the atomizing nozzle. These particles receive successive coats of water and may agglomerate with neighboring particles until they reach a sufficient size and fall by gravity to the bottom of the vessel. The lower section of the vessel has a smaller cross-section and the particles will remain in suspension, absorbing more gas before finally exiting by the bottom of the fluidized bed. Some of the gas hydrate particles withdrawn from the reactor can be recycled to provide the seed crystals. Similarly, Gudmundsson (1996) and Yamasaki et al. (2003) suggested system with the dispersed liquid phase.

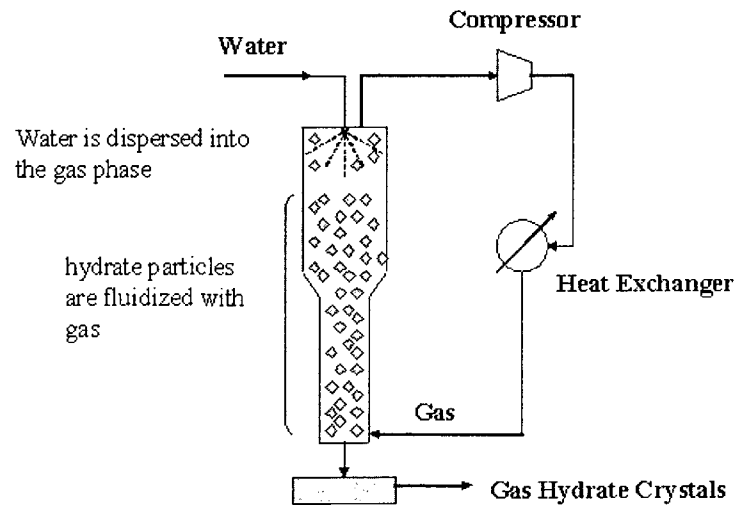


Figure (1.2). Schematic of the experimental apparatus of Heinemann et al. (2001).

A new apparatus has recently been proposed for CO₂ capture by Linga et al. (2008), which is similar to what was shown in Fig. (1.1) including a propeller with an arrangement such that the gas phase could be distributed in the liquid phase through the propeller. This arrangement increases the gas-liquid surface area and enhances internal mixing.

1.4.2 Systems with Gas as the Dispersed Phase

The overall mass transfer coefficient between liquid and gas can be evaluated as follows:

$$\frac{1}{K_l} = \frac{1}{k_l} + \frac{1}{Hk_g} \quad (1.1)$$

where k_l , k_g are the mass transfer coefficient in the liquid and gas phase respectively. H is the Henry's constant which is relatively large for gases of low solubility in liquid e.g. CH₄, O₂, N₂ in water (Levenspiel, 2001). Moreover, k_g is typically considerably larger than k_l according to the two-film theory, i.e. $k = \frac{D}{\Delta x}$. Gas phase diffusivities are vastly greater than those in liquids ($D_{\text{carbon dioxide/air}} \approx 10^4 D_{\text{carbon dioxide/water}}$ at 20°C) and, at the same time, the gas phase film thicknesses are smaller than those of the liquid (Chisti, 1989). Under these circumstances, the second term on the right hand side of the Eq. (1.1) becomes negligible and Eq. (1.1) reduces to:

$$\frac{1}{K_l} \approx \frac{1}{k_l} \quad (1.2)$$

This implies that all the resistance to interfacial mass transfer lies in the liquid film at the interface. In order to maximize the mass transfer coefficient k_f , gas should be bubbled into the liquid phase (Levenspiel, 2001). Hence, systems with gas as the dispersed phase are expected to be more efficient than systems with liquid as the dispersed phase. Moreover, heat removal is an issue in gas hydrate production systems due to the heat of gas hydrate formation. Systems with liquid as the continuous phase benefit from higher heat capacity and hence greater rates of heat removal.

Another application of fluidization in gas hydrate production is the work of Waycuilis and York (2002). The methods described before probably require sub-cooling or large adiabatic pressure drop before the process. Otherwise, the released heat of formation will restrict the conversion. This will increase the cost and complexity of the process. A fluidized bed heat exchanger reactor was proposed by Waycuilis and York (2002) in order to solve the heat transfer issue, which is presented in Fig. (1.3). The heat transfer medium flows in the shell of the reactor, while the hydrate formation occurs in the tubes. Inert particles are added to the fluidized hydrates in order to reduce hydrate deposits on the inner tube wall. Fluid velocities are chosen such that the inert particles remain within the reactor while the small/light hydrate particles are elutriated.

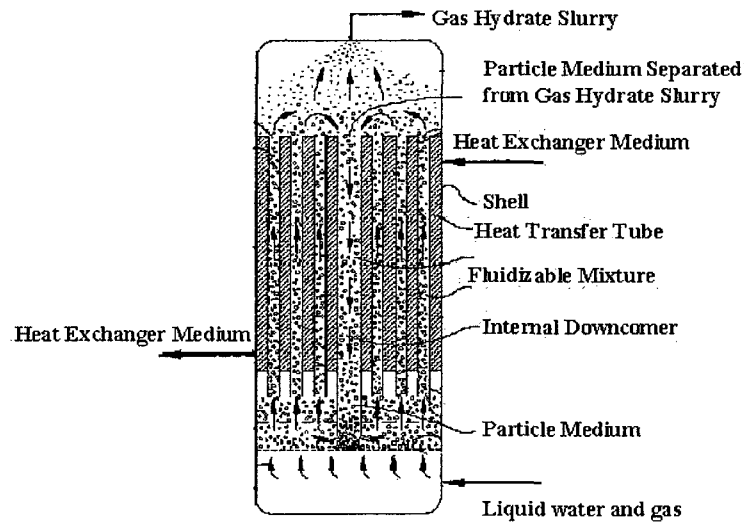


Figure (1.3). Schematic of the experimental apparatus of Waycuilis and York (2002).

Mitsui built a 600 kg/day demonstration plant as the first-stage Process Development Unit (PDU) using a continuously sparged stirred tank slurry reactor operated at 5.5 MPa and 277 K (Iwasaki et al., 2005). However, there is still on-going research to improve the phase contacting and heat removal efficiencies. In the second-stage of NGH production plant called Bench Scale Unit (BSU), the product slurry of the reactor contains 10% hydrate increased to 40% after dehydration. The pelletizer eventually is planned to produce 5 tons per day slurry of 75% hydrate in Fall 2008. The pelletized/granulate hydrate spheres are more stable and easier to move and store (Watanabe et al., 2008). At the reception location, hydrates are turned back into gas and water. Mitsui plans launching a pilot project around 2009, and the commercialization phase around 2012-13 with the capacity of 6000 ton/day. Mork and Gudmundsson (2002) tested a similar hydrate production reactor at the laboratory scale.

A tubular type reactor has been proposed by JFE Engineering Corporation (www.trcm.org/english/ourbusiness04.html). The reactor is 250 m long and has an internal diameter of 16.1 mm, thus providing a relatively large surface area /volume ratio which is beneficial for heat transfer. A static mixer is also used in the tubular reactor to generate micro bubbles and increase the mass transfer surface area.

As was presented, there are a few patents for the mass production of gas hydrates. However, there is no commercial process in operation and the choice of the best multiphase reactor is still unknown. Furthermore, there is very little experimental data and, to my knowledge, no published model available for the design of such reactors.

The system proposed in this work is a high-pressure slurry bubble column shown in Fig. (1.4) where the hydrate forming gas and water are introduced into the bottom of the reactor. The heat produced from hydrate formation is constantly removed. The reactor is maintained at an appropriate temperature and pressure. The system is not operated at steady-state since newly formed hydrate particles are not continuously removed.

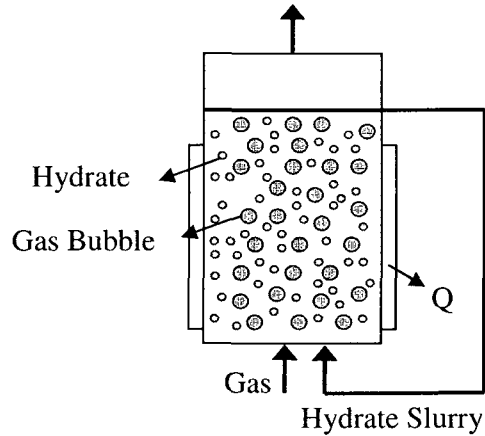


Figure (1.4). Schematic of the slurry bubble column in this work.

1.5 Research Objectives

An efficient method of converting water and gas into hydrate is considered in this work. The multiphase reactor of choice will be a slurry bubble column, which is going to be used to make carbon dioxide gas hydrates. Carbon Dioxide is chosen as the safety requirements are less demanding than other natural gas components such as methane. The research program specific objectives are:

- 1- Develop a reactor model that incorporates the hydrate formation kinetics as well as the system hydrodynamics and interphase heat and mass transfer rates.
- 2- Determine the model parameters including the intrinsic kinetic rate constant, gas hydrate former solubility in the presence of gas hydrate as well as mass transfer data of the slurry bubble column at hydrate forming conditions.

1.6 Research Outline

In order to develop the reactor model, it is necessary to determine the gas solubility at gas-liquid as well as hydrate-liquid interface as this along with the mass transfer coefficient will dictate interphase mass transfer and affect overall conversion. A model was assembled to predict these solubility values using the Trebble-Bishnoi equation of state, the van der Waals and Platteeuw model and the Holder model. With the model developed, the solubility at vapor-liquid, hydrate-liquid and hydrate-liquid-vapor equilibrium can be calculated for methane and carbon dioxide water systems. The paper associated with this work is entitled *“Prediction of Methane and Carbon Dioxide Solubility in Water in the Presence of Hydrate”* and presented in Chapter 2.

The carbon dioxide hydrate formation intrinsic rate constant was evaluated with the available literature data in a semi-batch stirred tank reactor and using a population balance. The hydrate growth model presented to extract the intrinsic rate constant is based on the concentration driving force where the equilibrium concentration at the hydrate surface is determined at the surface pressure and temperature. This work is entitled as *“Gas Hydrate Growth Model in a Semi-Batch Stirred Tank Reactor”* and presented in Chapter 3.

From a reactor modeling point of view, the interphase mass transfer coefficient needs to be measured. There is no data or correlation available in the literature for a high-pressure slurry bubble column corresponding to carbon dioxide hydrate physical properties or forming temperatures. Experiments were thus performed in a high-pressure slurry bubble column system. The effect of solids was simulated by an ion-exchange resin with physical

characteristics similar to those of carbon dioxide hydrates. Gas holdup and volumetric mass transfer coefficient are measured as a function of pressure, temperature, gas superficial velocity and volumetric solid concentration. This work is entitled as “*Gas-liquid Mass Transfer in a Slurry Bubble Column Operated at Hydrate Forming Conditions*” and presented in Chapter 4.

The hydrate growth model was finally developed which takes the kinetic, thermodynamics and hydrodynamics into account. The parameters were taken from the previous work as stated above. The mass balance was coupled with a population balance to represent the hydrate growth. The effect of flow pattern, gas and liquid superficial velocity, temperature and pressure were investigated on the gas hydrate formation rate. This part of work is entitled “*Dynamic Simulation of Gas Hydrate Formation in a Three-Phase Slurry Reactor*” and presented in Chapter 5.

Finally, Chapter 6 summarizes conclusions and recommendations for future research.

Nomenclature

D	diffusion coefficient [$\text{m}^2 \text{s}^{-1}$]
H	Henry’s constant [-]
k_l	liquid side gas-liquid mass transfer coefficient [m s^{-1}]
k_g	gas side gas-liquid mass transfer coefficient [m s^{-1}]
K_l	overall liquid side gas-liquid mass transfer coefficient [m s^{-1}]
x	film thickness [m]

References

- Abdalla, B.K., Abdullatef, N.A., (2005). Simulation and economic evaluation of natural gas hydrates [NGH] as an alternative to liquefied natural gas [LNG]. *Catalysis Today*, 106, 256-258.
- Brewer, P.G., Friederich, G., Peltzer, E.T., Franklin, M. Orr., (1999). Direct experiments on the ocean disposal of fossil fuel CO₂. *Science*, 284, 943-945.
- Chisti, M.Y., (1989). *Airlift bioreactors*. New York: Elsevier Science Publishers.
- Englezos, P., (1993). Clathrate hydrates. *Industrial and Engineering Chemistry Research*, 32, 1251-1274.
- Giavarini, C., Maccioni, F., (2004). Self-preservation at low pressures of methane hydrates with various gas contents. *Industrial and Engineering Chemistry Research*, 43, 6616-6621.
- Gudmundsson, J.S., Borrehaug, A., (1996). Frozen hydrate for transport of natural gas. In: *Proceeding of the 2th International Conference on Gas Hydrates, Toulouse*.
- Gudmundsson, J.S., (1996). Method for production of gas hydrates for transportation and storage. U.S patent 5,536,893.
- Gudmundsson, J.S., Mork, M., Oscar, F.G., (2002). Hydrate non-pipeline technology. In: *Proceeding of the 4th International Conference on Gas Hydrates, Yokohama*.
- Hao, W., Wang, J., Fan, S., Hao, W., (2008). Evaluation and analysis method for natural gas hydrate storage and transportation processes. *Energy Conversion and Management*, 49, 2546-2553.

- Heinemann, R.F., Huang, D. D-T., Long, J., Saeger, R.B., (2001). Methods for producing gas hydrates utilizing a fluidized bed. U.S patent 6,180,843.
- Iwasaki, S., Kimura, T., Yoshikawa, K., Nagayasu, H., (2002). The pre-investigation of natural gas transportation and storage system as gas hydrates for development of marginal natural gas fields. In: Proceeding of the 4th International Conference on Gas Hydrates, Yokohama.
- Iwasaki, T., Katoh, Y., Nagamori, S., Takahashi, S., Oya, N., (2005). Continuous natural gas hydrate pellet production (NGHP) by process development unit (PDU). In: Proceeding of the 5th International Conference on Gas Hydrates, Trondheim.
- Jamaluddin, A.K.M., Kalogerakis, N., Bishnoi, P.R., (1991). Hydrate plugging problems in undersea natural gas pipelines under shutdown conditions. *Journal of Petroleum Science and Engineering*, 5, 323-335.
- Javanmardi, J., Nasrifar, Kh., Najibi, S.H., Moshfeghian, M., (2005). Economic evaluation of natural gas hydrate as an alternative for natural gas transportation. *Applied Thermal Engineering*, 25, 1708-1723.
- Kanada, H. (2006). Economic study on natural gas transportation with natural gas hydrate (NGH) pellets. 23rd World Gas Conference, Amsterdam.
- See also: <http://www.igu.org/html/wgc2006/pdf/paper/add10399.pdf>.
- Koh, C.A., Westacott, R.E., Zhang, W., Hirachand, K., Creek, J.L., Soper, A.K., (2002). Mechanism of gas hydrate formation and inhibition. *Fluid Phase Equilibria*, 194-197, 143-151.
- Lee, S.-Y., Holder, G.D., (2001). Methane hydrate potential as a future energy source. *Fuel Processing Technology*, 71, 181-186.

- Lee, S., Liang, L., Riestenberg, D., West, O.R., Tsouris, C., Adams E., (2003). CO₂ hydrate composite for ocean carbon sequestration. *Environmental Science and Technology*, 37, 3701-3708.
- Levespiel, O., (2001). *Chemical reaction engineering*, 3rd ed. John Wiley & Sons.
- Linga, P., Kumar, R., Englezos, P., (2007). Gas hydrate formation from hydrogen/carbon dioxide and nitrogen/carbon dioxide gas mixtures. *Chemical Engineering Science*, 62, 4268-4276.
- Linga, P., Kumar, K., Ripmeester, J.A., Englezos, P., (2008). Hydrate processes for CO₂ capture and scale up using a new apparatus. In: *Proceeding of the 6th International Conference on Gas Hydrates*, Vancouver.
- Mork, M., Gudmundsson, J.S., (2002). Hydrate formation rate in a continuous stirred tank reactor: Experimental results and bubble-to-crystal model. In: *Proceeding of the 4th International Conference on Gas Hydrates*, Yokohama.
- Seo, Y-T., Moudrakovski, I., Ripmeester J.A., Lee, J-W., Lee, H., (2005). Efficient recovery of CO₂ from flue gas by clathrate hydrate formation in porous silica gels. *Environmental Science and Technology*, 39, 2315-2319.
- Sloan, Jr. E.D., (1998). *Clathrate Hydrates of natural gases*. 2nd ed., New York: Marcel Dekker.
- Thomas, S., Dawe, R.A., (2003). Review of ways to transport natural gas energy from countries which do not need the gas for domestic use. *Energy*, 28, 1461-1477.
- Tsouris, C., McCallum, S., Aaron, D., Riestenberg, D., Gabitto, J., Chow, A., Adams, E., (2007). Scale-up of a continuous-jet hydrate reactor for CO₂ ocean sequestration. *AIChE Journal*, 53, 1017-1027.

- Yamasaki, A., Takano, S., Fujii, M., Yanagisawa, Y., Tajima, H., Kiyono, F., (2003).
Formation and growth of CO₂ hydrate particles in a fluidized bed reactor. F Preprints
of Symposia: American Chemical Society, Division of Fuel Chemistry, 48, 123-124.
- Watanabe, S., Takahashi, S., Mizubayashi, H., Muratal, S., Murakami, H., (2008). A
demonstration project of NGH land transportation system. In: Proceeding of the 6th
International Conference on Gas Hydrates, Vancouver.
- Waycuilis, J.J., York, S.D., (2002). Production of a gas hydrate slurry using a fluidized bed
heat exchanger. US patent 6,350,928.
- Wu, M., Wang, S., Liu, H., (2007). A study on inhibitors for the prevention of hydrate
formation in gas transmission pipeline. Journal of Natural Gas Chemistry, 16, 81-85.

Chapter 2

Prediction of Methane and Carbon Dioxide Solubility in Water in the Presence of Hydrate

S. Hashemi¹, A. Macchi¹, S. Bergeron², P. Servio^{2*}

Fluid Phase Equilibria, (2006), 246 (1-2), 131–136

¹ Department of Chemical and Biological Engineering
University of Ottawa
161 Louis Pasteur Street
Ottawa, Ontario, K1N 6N5, Canada

² Department of Chemical Engineering
McGill University
3610 University Street
Montreal, Quebec, H3A 2B2, Canada

* Corresponding author: Phillip Servio, Tel: +1 514 398 1026, Fax: +1 514 398 6678, E-mail address: phillip.servio@mcgill.ca

Abstract

Most proposed technologies to form gas hydrates use continuously stirred tank reactors where gas is bubbled into the liquid. From a reactor modeling point of view, it is necessary to determine the gas solubility in the liquid with and without hydrates as this will dictate interphase mass transfer and affect overall conversion. This work assembled a model to predict these solubility values using the Trebble-Bishnoi equation of state, the van der Waals and Platteuw model and the Holder model. Model predictions, as well as predictions from Henry's law, were compared to available experimental data of methane-water and carbon dioxide-water systems. Although Henry's law can not be applied under hydrate-liquid water equilibrium, its accuracy was very good due to the small effect of pressure on solubility in that zone. The accuracy of the model in this work has been improved by re-adjusting its parameters with recent vapor-liquid water and vapor-liquid water-hydrate equilibrium data of methane-water and carbon dioxide-water systems.

Keywords: carbon dioxide, gas hydrate, hydrate-liquid water equilibrium, methane, solubility

2.1 Introduction

Gas hydrates are crystalline solids that form when gas or volatile liquid molecules suitable for hydrate formation are enclosed in a cage consisting of water molecules. The presence of the hydrate forming gas molecules leads to stabilization of the water lattice through physical bonding via van der Waals forces. Hydrate compounds are made naturally within the permafrost zone and in sub-sea sediment at temperature and pressure conditions within the thermodynamic stability region (Sloan, 1998). Naturally occurring hydrates, containing mostly methane, exist in vast quantities and are being looked upon as a potential alternative energy source (Sloan, 1998). Carbon dioxide hydrates are also important hydrates. They are being considered as a means to sequester carbon dioxide in the deep ocean thus reducing the emission of greenhouse gases (Brewer et al., 1999). Carbon dioxide is also a component of Natural Gas (the major component being methane) which can lead to hydrate formation in pipelines resulting in pipeline blockage (Englezos, 1993).

One significant proposed technology incorporating gas hydrates deals with transportation and storage of gas. Hydrates are being regarded as an alternate means of transporting natural gas over other currently used methods such as LNG (Liquefied Natural Gas) or CNG (Compressed Natural Gas) as they eliminate the necessity of very low temperatures (-160°C) and very high pressures (200 atm). The hydrate contains about 160 Sm^3 per m^3 of hydrate, which is comparable to the above mentioned technologies (LNG and CNG) (Thomas and Dawe, 2003), at near ambient temperature (0 to -10°C) and pressures (10 to 1 atm).

Attempts at synthesizing hydrate in an efficient manner have used a continuously stirred tank slurry reactor where the hydrate forming gas is sparged into a continuous water phase (Mork and Gudmundsson, 2002). Gas diffuses out of the bubbles into the liquid water where it is eventually consumed at the surface of suspended hydrate crystals. The driving force around the hydrate particle can be defined as the difference between the gas hydrate former concentration in the liquid bulk water and its solubility at the hydrate-liquid interface. The pressure at the hydrate interface has to be equal to the experimental pressure (Sloan, 1998), while the interface temperature can be the three-phase (H-L_w-V) or two-phase (H-L_w) temperature depending on the heat transfer rate. Similarly, the driving force around the gas bubble is assumed to be the difference between the gas hydrate former solubility at the gas bubble-liquid interface and its concentration in the bulk liquid water. Hence, vapor-liquid water (L_w-V), vapor-liquid water-hydrate (H-L_w-V) and hydrate-liquid water (H-L_w) equilibrium are key concepts in the modeling of these systems. Moreover, in order to use gas hydrates for carbon dioxide sequestration, (H-L_w) solubility prediction is required to assess the stability of carbon dioxide hydrates located at the bottom of the ocean. (L_w-V) and (H-L_w-V) equilibrium have been the subject of years of study (Holder et al., 1980; Parrish and Prausnitz, 1972; Klauda and Sandler, 2000; Klauda and Sandler, 2003; Culberson and McKetta, 1951; Battino and Clever, 1966; Lekvam and Bishnoi, 1997; Stewart and Munjal, 1970; Valtz et al., 2004; Bamberger et al., 2000; Wendland et al., 1999; Wang et al., 2003; Sloan, 1998). However, there are only few papers discussing the solubility of gas in water in the hydrate-liquid water two-phase zone. Thus, a general model for predicting the solubility where hydrate and liquid water are in equilibrium is sought in this study.

Due to simplicity and lack of an applicable model, Henry's Law has been employed recently to predict the solubility in hydrate-liquid water equilibrium (Servio and Englezos, 2002; Servio and Englezos, 2001) where it was assumed that gas solubility at (H-L_w) equilibrium, i.e. at (P_{exp.}, T_{exp.}), is equal to that at (P_{eq.}, T_{exp.}) in P-T equilibrium diagram, see Fig. (2.1) (Sloan, 1998; Servio and Englezos, 2002). P_{eq.} and T_{exp.} are located on the three-phase line. Hence, T_{exp.} is also equal to T_{eq.} and the solubility predicted with this assumption would be that at the (H-L_w-V) equilibrium instead of (H-L_w).

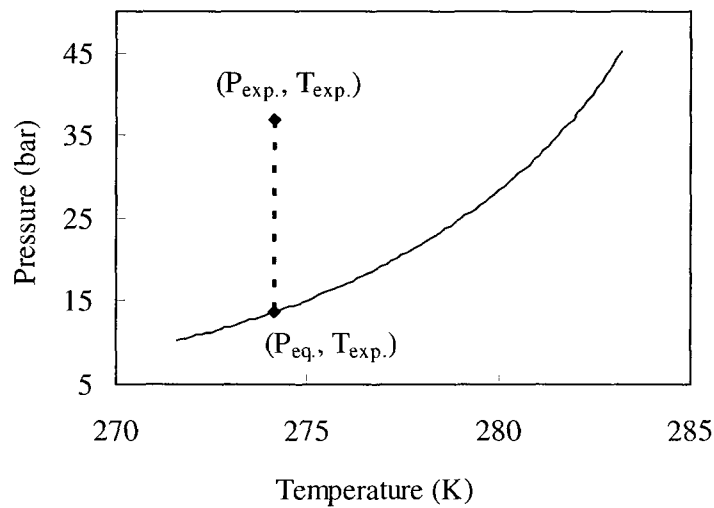


Figure (2.1). Phase diagram of methane-water system (Sloan, 1998; Servio and Englezos, 2002).

One way of determining solubility is the use of a Gibbs energy-solubility diagram (Tabe et al., 1998). This approach seeks the solubility at which the Gibbs energy curve has the lowest value. Minimum of Gibbs energy demonstrates which phases are stable at a certain

temperature and pressure. Although the theory behind the graphical approach is identical to that of the most commonly used fugacity or chemical potential, it cannot be looked upon as a practical model for solubility prediction.

There have also been some attempts to develop a model to predict the solubility based on the van der Waals and Platteeuw (1959) model. Among this group is the work of Handa (1990) which employs the activity coefficient to represent the chemical potential of water in the liquid phase. Handa derived the chemical potential of water in liquid and hydrate phases in terms of the pressure at equilibrium. This led to an equation illustrating the dependency of gas solubility in the liquid phase to pressure. Kim et al. (2003) and Yang et al. (2000, 2001) also employed the van der Waals and Platteeuw model along with the non-random lattice fluid hydrogen bonding equation of state, which requires several physical parameters, binary interaction parameters and hydrogen bonding energy and entropy to be fitted. In these studies, hydrate-liquid water equilibrium discussions were primarily directed towards the influence of pressure on methane and carbon dioxide solubility. The solubility did not significantly vary over the pressure range investigated because the compressibility of both liquid water and hydrate is small. Zatsepina and Buffet (1997) applied the van der Waals and Platteeuw model coupled with the Parrish and Prausnitz (1972) model and the Trebble-Bishnoi equation of state (1987) to show that temperature variations are more significant than pressure variations for establishing the equilibrium conditions in marine sediment. The accuracy of their model was not tested with experimental data. Ballard and Sloan (2002) extended the van der Waals and Platteeuw model which now allows for the distortion of hydrate due to the presence of a guest molecule. Since the standard hydrate volume differs from the volume of the equilibrium hydrate, there should be an energy change that is

proportional to the difference in volume. They account for this distortion via an activity coefficient. However, assuming a constant hydrate volume for pressures lower than 200 bars does not lead to any significant error (Ballard, 2002).

In this work, the van der Waals and Platteeuw (1959) and Holder et al. (1980) models were employed along with the Trebble-Bishnoi (1987) equation of state, which is a four-parameter cubic equation of state. The Trebble-Bishnoi equation of state was chosen due to its simplicity compared to the non-random lattice fluid hydrogen bonding equation of state, and its relative success in predicting (L_w-V) equilibrium of a methane-water system and (H-L_w) equilibrium of a carbon dioxide-water system over other cubic equations of state such as Peng-Robinson (1976) and Soave-Redlich-Kwong (1972). The Peng-Robinson and Soave-Redlich-Kwong equations of state were found to fail in characterizing phase equilibria of a methane-water system (Trebble and Bishnoi, 1988). The gas hydrate former solubility prediction results have been reported using the original (Trebble and Bishnoi, 1988) as well as the re-optimized mixing rule binary interaction parameters obtained in this work.

2.2 Theory

For three-phase hydrate-liquid water-vapor equilibrium, the basic equations for the equilibrium condition are:

$$\mu_i^L = \mu_i^V \quad (i = 1, N) \quad (2.1)$$

$$\mu_i^L = \mu_i^H \quad (i = 1, N) \quad (2.2)$$

where N is the total number of components. For three-phase equilibrium calculations, Eqs. (2.1) and (2.2) are solved simultaneously. Vapor-liquid water equilibrium and hydrate-liquid water equilibrium are defined by solving Eq. (2.1) and (2.2), respectively.

The chemical potential of a component in the vapor or liquid phase may be calculated using a suitable equation of state, Trebble-Bishnoi in this study. The chemical potential of water in the hydrate phase is given by van der Waals and Platteeuw (1959):

$$\mu_w^H = \mu_w^{MT} + RT \sum_m v_m \ln(1 - \sum_j \theta_{mj}) \quad (2.3)$$

where μ_w^{MT} refers to the chemical potential of water in the hypothetical (empty) hydrate lattice, v_m is the number of cavities of type m per water molecule in the lattice and θ_{mj} is the fraction of cavities of type m occupied by gas component j . The fractional occupancy is defined by the following Langmuir expression:

$$\theta_{mj} = \frac{C_{mj} f_j}{1 + \sum_k C_{mk} f_k} \quad (2.4)$$

where C_{mj} is the Langmuir constant and f_j is the fugacity of component j in the phase with which the hydrate phase is in equilibrium. Therefore, in the case of hydrate-liquid water equilibrium, fugacity of the hydrate forming gas component in Eq. (2.4) is equal to that in

the liquid water phase. In this work, Langmuir constants needed to evaluate fractional occupancy were obtained using the correlation proposed by Parrish and Prausnitz (1972).

The equilibrium relation for water from Eq. (2.2) becomes:

$$\mu_w^L = \mu_w^H \quad (2.5)$$

The difference in chemical potential of water in the empty hydrate lattice and that in the pure liquid state at the system temperature and pressure is:

$$\mu_w^{MT} - \mu_w^{L_0} = \Delta\mu_w^{MT-L_0} \quad (2.6)$$

The right hand side of Eq. (2.6) is commonly represented by Holder et al. (1980):

$$\frac{\Delta\mu_w^{MT-L_0}}{RT} = \frac{\Delta\mu_w^{MT-L_0}(T_0)}{RT_0} + \int_{p_0}^p \frac{\Delta v_w^{MT-L_0}}{RT} dp - \int_{T_0}^T \frac{\Delta h_w^{MT-L_0}}{RT^2} dT \quad (2.7)$$

Equations (2.6) and (2.7) can be combined to give the chemical potential of water in the empty hydrate phase:

$$\frac{\mu_w^{MT}}{RT} = \frac{\Delta\mu_w^{MT-L_0}(T_0)}{RT_0} + \int_{p_0}^p \frac{\Delta v_w^{MT-L_0}}{RT} dp - \int_{T_0}^T \frac{\Delta h_w^{MT-L_0}}{RT^2} dT + \frac{\mu_w^{L_0}}{RT} \quad (2.8)$$

The chemical potential of water in the hydrate phase can be obtained from Eq. (2.3) and (2.8).

$$\frac{\mu_w^H}{RT} = \frac{\Delta\mu_w^{MT-L_0}(T_0)}{RT_0} + \int_{p_0}^p \frac{\Delta v_w^{MT-L_0}}{RT} dp - \int_{T_0}^T \frac{\Delta h_w^{MT-L_0}}{RT^2} dT + \frac{\mu_w^{L_0}}{RT} + \sum_m \nu_m \ln(1 - \sum_j \theta_{mj}) \quad (2.9)$$

where

$$\Delta h_w^{MT-L_0} = \Delta h_w^{MT-L_0}(T_0) + \int_{T_0}^T \Delta C_{p_w}^{MT-L_0} dT \quad (2.10)$$

$\Delta h_w^{MT-L_0}(T_0)$ and $\Delta\mu_w^{MT-L_0}(T_0)$ were taken from the work of Holder et al. (1980). These parameters have also been re-optimized in this work using (H-L_w-V) experimental data. The rest of parameters were taken from the work of Holder et al. (1980). The chemical potential of water in the liquid solution phase is:

$$\mu_w^{sol} = \mu_w^{L_0} + RT \ln a_w \quad (2.11)$$

where a_w is the activity of water. At equilibrium, the chemical potential of water in the hydrate phase has to be equal to that in the liquid solution phase. Thus, at equilibrium, Eq. (2.9) and (2.11) give

$$\frac{\Delta\mu_w^{MT-L_0}(T_0)}{RT_0} + \int_{p_0}^p \frac{\Delta v_w^{MT-L_0}}{RT} dp - \int_{T_0}^T \frac{\Delta h_w^{MT-L_0}}{RT^2} dT - \ln a_w = -\sum_m v_m \ln(1 - \sum_j \theta_{mj}) \quad (2.12)$$

Isofugacity criterion does not necessarily lead to the minimum of the Gibbs energy. All components existing in the system have to be distributed among all possible phases such that the Gibbs energy is at minimum. The Gibbs energy of the system as a mixture property is obtained by the following equation:

$$G = \sum_{i,j} X_i^j \mu_i^j \quad (2.13)$$

where X_i^j is the molar fraction of component i in phase j . In deriving Eq. (2.13), the total number of mole fraction in each phase is set equal to one.

2.3 Results and Discussion

Model predictions of methane solubility in liquid water for temperatures between 274 and 285 K and for pressures of 35, 50 and 65 bars are presented in Fig. (2.2) using the original parameters. As shown in Fig. (2.2), hydrate-liquid water phases are stable at the lower temperatures. The maximum amount of gas that can be dissolved in a liquid at a certain temperature and pressure is the solubility. In (H-L_w) equilibrium, hydrate crystals start to decompose as the temperature is increased. As a result, gas transfers to the liquid phase and the solubility of the gas hydrate former increases. This trend continues up to the point where the vapor, liquid water and hydrate phases are at equilibrium. A further increase in temperature results in complete decomposition of the hydrate phase. In (L_w-V) equilibrium,

the solubility-temperature trend is reversed since more gas will enter the vapor phase as the temperature is further increased. The same solubility dependency on temperature is observed with other gas hydrate formers such as carbon dioxide, see Fig. (2.4).

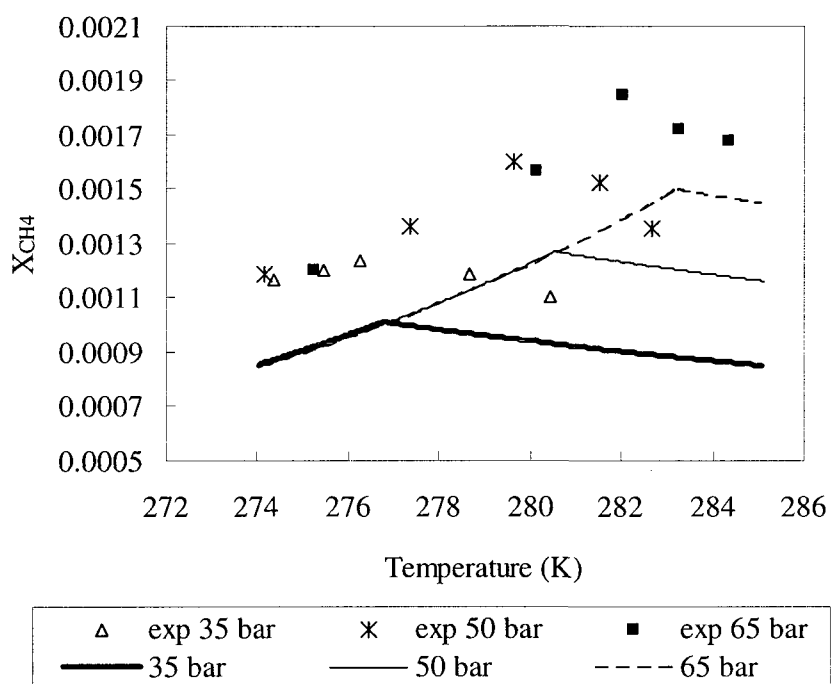


Figure (2.2). Comparison of calculated methane solubility in liquid water by the present model using the original parameters with experimental data of Servio and Englezos (2002).

Model prediction in Fig. (2.2) also shows the effect of pressure on methane-water phase equilibrium. Higher pressures lead to an increase in solubility at vapor-liquid water equilibrium and, by contrast, a decrease in solubility at hydrate-liquid water equilibrium. The influence of pressure is more pronounced in (L_w -V) than in (H- L_w) equilibrium (Handa, 1990). For example, in the present case, a pressure change from 35 to 65 bars causes methane solubility to increase by 69.7% at 284.15 K and decrease by only 1.6% at 274.15 K.

The results of the model in Fig. (2.2) are also compared to the experimental data of Servio and Englezos (2002). The Trebble-Bishnoi equation of state was found to always underestimate the solubility of methane in water at (L_w-V) equilibrium by an average absolute relative error (AARE) of 14.8, 15.3, and 14.3% for six experimental data points of Servio and Englezos (2002) as shown in Fig. (2.2), for six data points of Kim et al. (2003) at 298.15 K, and for eighteen data points of Lekvam and Bishnoi (1997), respectively using the original parameters. The negative bias resulting from the Trebble-Bishnoi equation of state might be attributed to the mixing rule binary interaction parameters taken from Trebble-Bishnoi (1988) which cover different temperature and pressure ranges of 310.9 to 444.3 K and 1 to 680 bar respectively.

The predicted solubility of methane in water at (H-L_w) equilibrium is also lower than the experimental data of Servio and Englezos (2002) as presented in Fig. (2.2) and of Kim et al. (2003) by an average of 24.3% for six and 30.5% for sixteen data points respectively. The model of this work also underestimates the solubility of methane at (H-L_w-V) equilibrium for three data points of Servio and Englezos by an average of 23.5% as presented in Fig. (2.2). However, from Fig. (2.2), the relative error is consistent for (H-L_w-V) and (H-L_w) suggesting that the predicted trend correctly follows the experimental data. The Langmuir constants and the reference parameters that respectively appear in the van der Waals and Platteeuw (Eq. (2.3)) and Holder (Eq. (2.7)) models are all fitted parameters taken from their work. This, with the already mentioned deficiency of the Trebble-Bishnoi equation of state, contributed to the bias of the solubility model.

Carbon dioxide solubility values were always underestimated except for one data point in (L_w-V) equilibrium. The AARE on the solubility data of Servio and Englezos (2001) are 3.6% (for six data points), 9.2% (for three data points) and 15.6% (for ten data points) for (L_w-V), (H-L_w-V) and (H-L_w) equilibrium, respectively. The smaller relative errors compared to those obtained in the methane-water system suggests that the binary interaction parameters of the Trebble-Bishnoi equation of state are a better fit for the carbon dioxide-water system.

In order to improve the vapor-liquid water (L_w-V) equilibrium predictions for methane-water and carbon dioxide-water systems, the mixing rule binary interaction parameters in the Trebble-Bishnoi equation of state were optimized using recent vapor-liquid water equilibrium data that cover a greater temperature range. A total of 54 experimental solubility measurements were used for the methane-water system, while 83 were used for the carbon dioxide-water system, see Table (2.1).

Table (2.1). Vapor-liquid water experimental data for methane-water and carbon dioxide-water(*) systems.

<i>T</i> range (K)	<i>P</i> range (bars)	No. of points	Reference
310.9-444.3	41.4-552	18	Culberson, 1951
274.2-285.7	10.1-70.5	11	Lekvam & Bishnoi, 1997
278.7-284.4	35-65	6	Servio & Englezos, 2002
298.2	23-166	5	Kim et al., 2003
283.2-303.2	20-400.3	14	Wang et al., 2003
273.2-283.2	10.1-38.5	*9	Stewart & Munjal, 1970
278.1-283.2	20-37	*6	Servio & Englezos, 2001
278.2-318.2	4.96-79.6	*42	Valtz et al., 2004
323.2-353.1	50.6-131	*26	Bamberger et al., 2000

The newly optimized mixing rule binary interactions parameters used in the Trebble-Bishnoi equation of state, for both methane-water and carbon dioxide-water systems, are displayed in Table (2.2).

Table (2.2). Mixing rule binary interaction parameters

	K_a	K_b	K_c	K_d
CH₄	0.4199	-0.1727	-0.0001	-1.2274
CO₂	0.9688	0.5181	0.3757	0.1647

To improve the model predictions for the hydrate-liquid water (H-L_w) equilibrium, both the reference chemical potential and the reference enthalpy difference between the unoccupied

hydrate and pure water i.e., $\Delta\mu_w^{MT-L_0}(T_0)$ and $\Delta h_w^{MT-L_0}(T_0)$, at the reference temperature, were optimized using three-phase (H-L_w-V) equilibrium data.

Table (2.3) shows the (H-L_w-V) data used to optimize the model, for both methane-water (69 points) and carbon dioxide-water (131 points) systems. $\Delta\mu_w^{MT-L_0}(T_0)$ used in the present study has a value of 1288 J/mol, compared to 1245 J/mol, as reported by Holder et al. (1980). Similarly, $\Delta h_w^{MT-L_0}(T_0)$ used in the current work has a value of -4671 J/mol, compared to -4327 J/mol, as reported by Holder et al. (1980).

Table (2.3). Hydrate-liquid water-vapor experimental data for methane-water and carbon dioxide-water(*) systems.

<i>T</i> range (K)	<i>P</i> range (bars)	No. of points	Reference
280.9-286.7	58.5-108	3	Sloan, 1998
273.2-294.3	26.5-285.7	8	Sloan, 1998
283.2-288.7	71-131.1	4	Sloan, 1998
273.7-285.9	27.7-97.8	13	Sloan, 1998
295.7-302.0	339.9-775	4	Sloan, 1998
285.7-301.6	96.2-680.4	10	Sloan, 1998
275.2-291.2	30.2-185.5	7	Sloan, 1998
275.4-282.2	28.7-61	6	Sloan, 1998
273.4-286.4	26.8-105.7	11	Sloan, 1998
276.3-282.1	35-65	3	Servio & Englezos, 2002
273.7-282.9	13.2-43.2	*19	Sloan, 1998
277.2-281.9	20.4-36.9	*4	Sloan, 1998
271.8-283.2	10.5-45.0	*36	Sloan, 1998
273.9-282.0	13.8-38.4	*6	Sloan, 1998
279.6-282.8	27.4-43.6	*3	Sloan, 1998
271.6-283.2	10.4-45.1	*44	Sloan, 1998
274.3-282.9	14.2-43.7	*9	Sloan, 1998
277.1-282.6	20-42	*3	Servio & Englezos, 2001
273.9-282.2	13.7-38.5	*7	Wendland et al., 1999

Table (2.4) presents the hydrate-liquid water references used to evaluate the model accuracy under (H-L_w) equilibrium for both methane-water (22 points) and carbon dioxide-water (10 points) systems. The experimental data of Yang et al. (2001) for methane-water was not used as it was found erroneous by Kim et al. (2003).

Table (2.4). Hydrate-liquid water experimental data for methane-water and carbon dioxide-water(*) systems.

T range (K)	P range (bar)	No. of points	References	AARE (%)
274.4-280.2	35-65	6	Servio & Englezos, 2002	2.9
276.2-281.7	50-144	16	Kim et al., 2003	9.0
274.0-278.2	20-60	*10	Servio & Englezos, 2001	5.2

Model predictions of methane and carbon dioxide solubility in water using the re-optimized parameters are displayed in Fig. (2.3) and (2.4), respectively. Single points in the figures correspond to the data obtained by Servio and Englezos (2001, 2002). Using the newly optimized parameters, the current model predicts methane solubility in water under (H-L_w) equilibrium with an AARE of 2.9% for the six data points of Servio and Englezos (2002) and 9.0% for the sixteen data points of Kim et al. (2003). The optimized model predicts carbon dioxide solubility in water under (H-L_w) equilibrium with an AARE of 5.2% for ten data points of Servio and Englezos (2001). Results are summarized in Table (2.4).

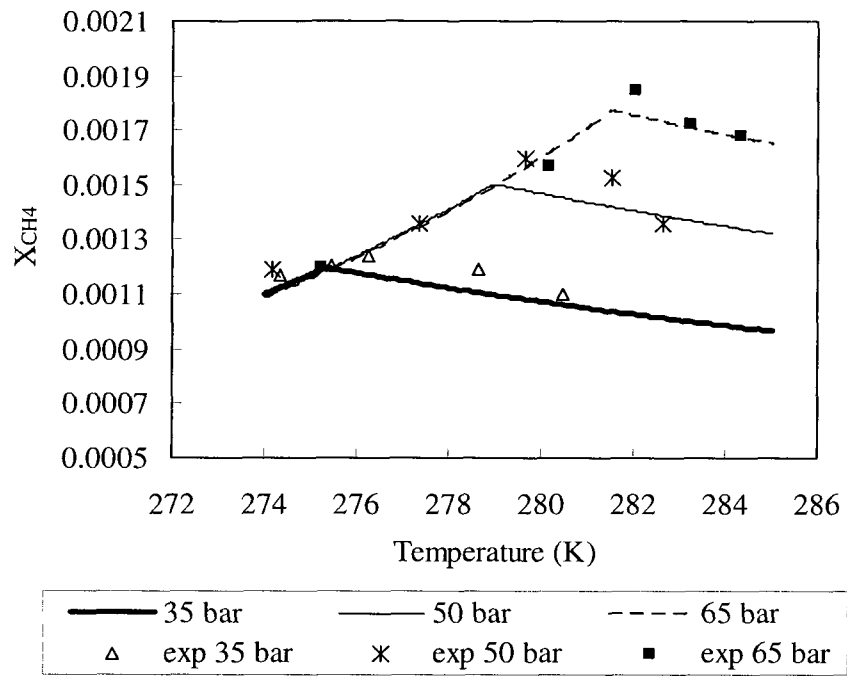


Figure (2.3). Comparison of calculated methane solubility in liquid water by the present model using the re-optimized parameters with experimental data of Servio and Englezos (2002).

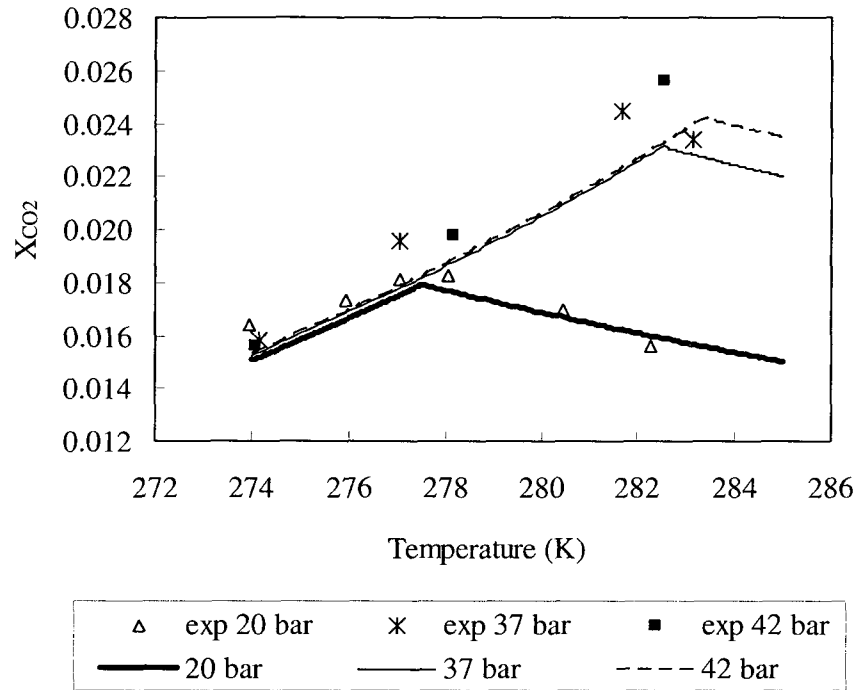


Figure (2.4). Comparison of calculated carbon dioxide solubility in liquid water by the present model using the re-optimized parameters with experimental data of Servio and Englezos (2001).

The bias of the model (F_m) was tested using a statistical technique similar to that proposed by Bolles and Fair cited by Saberian-Broudjenni et al. (1989):

$$F_m = \exp\left(\sum_{i=1}^n \ln(x_{cal} / x_{exp}) / n\right) \quad (2.14)$$

where x_{cal} is the solubility predicted by the model, x_{exp} is the solubility measured experimentally and n is the number of data points. The resulting bias factor at (H-L_w)

equilibrium is 0.93 and 0.95 for methane-water and carbon dioxide-water systems respectively. The fact that the bias values are slightly lower than one demonstrates that the model predictions present only a slight negative bias towards the experimental data.

As mentioned before, Henry's law has been usually employed to determine the gas solubility at (H-L_w) (Servio and Englezos, 2001; Servio and Englezos, 2002) as well as at (H-L_w-V) (Mork and Gudmundsson, 2002). In calculating the (H-L_w) solubility, Servio and Englezos (2001, 2002) assumed that the (H-L_w) experimental pressure could be replaced by the three-phase equilibrium pressure corresponding to the experimental temperature as explained before. This assumption may need the interpolation of the three-phase equilibrium pressure from the experimental data at certain temperatures. The AARE of Henry's law for methane solubility was 2.4% for the six experimental data points of Servio and Englezos (2002). The influence of pressure on the gas solubility in the hydrate-liquid water zone is not significant over the range investigated. Therefore, a slight change in pressure from two-phase (H-L_w) to three-phase (H-L_w-V) equilibrium does not significantly affect the solubility. However, the predicted effect of a pressure increase on methane solubility in the hydrate-liquid water zone resulting from Henry's law is opposite to the present model and to experimental observations, see Fig. (2.3). Henry's constant is a function of temperature and, at a given temperature, gas solubility is proportional to the fugacity of the gas in vapor phase which increases with pressure.

2.4 Conclusions

The Trebble-Bishnoi equation of state was applied along with the van der Waals and Platteeuw, and Holder models to predict the gas solubility in water at (H-L_w) equilibrium for methane-water and carbon dioxide-water systems. The Trebble-Bishnoi equation of state was found to be fairly simple and relatively successful compared to other equation of states employed in the literature. The model, with its original parameters, always underestimated solubility in hydrate-liquid water equilibrium. Solubility prediction using Henry's law, which actually estimates the solubility at the three phase equilibrium (H-L_w-V) and not in two-phase hydrate liquid water equilibrium (H-L_w), were in good agreement with experimental data. The good agreement stems from the small effect of pressure on gas solubility in the presence of hydrate. In order to improve the accuracy of the present model, the interaction parameters of Trebble-Bishnoi equation of state as well as reference parameters of the hydrate model were readjusted to (L_w-V) and (H-L_w-V) equilibrium data, respectively. The model covered a larger temperature range and the AARE for both gases was below 10%.

Nomenclature

a_w water activity

$AARE$ average absolute relative error = $100 * ABS(X_{cal.} - X_{exp.}) / X_{exp}$

C_{mj} Langmuir constant of species j in cavity of type m , Pa⁻¹

f_i fugacity of species i , Pa

F_m bias factor defined by Eq. (14.2)

G Gibbs Energy, kJ kmol⁻¹

h	Enthalpy, kJ kmol^{-1}
N	total number of components
P	pressure, Pa
R	universal gas constant, $\text{kJ kmol}^{-1} \text{K}^{-1}$
T	temperature, K
v	volume, m^3
X	Gas mole fraction in water

Greek Letters

μ	chemical potential, kJ kmol^{-1}
ν_m	number of cavities of type m
θ_{mj}	fraction of cavities type m occupied by component j

Subscripts

w	water
-----	-------

Superscripts

H	hydrate
L	liquid
MT	empty lattice
sol	solution
V	vapor

Acknowledgments

The authors are grateful to the Natural Sciences and Engineering Research Council of Canada for financial assistance.

References

- Ballard, A.L., Sloan, Jr. E.D., (2002). The next generation of hydrate prediction: I. Hydrate standard states and incorporation of spectroscopy. *Fluid Phase Equilibria*, 194-197, 371-383.
- Ballard, A.L. (2002). A non-ideal hydrate solid solution model for a multiphase equilibria program. Ph.D. thesis, Colorado School of Mine, Golden, CO, USA.
- Bamberger, A., Sieder, G., Maurer, G., (2000). High-pressure (vapor plus liquid) equilibrium in binary mixtures of (carbon dioxide plus water or acetic acid) at temperatures from 313 to 353 K. *Journal of Supercritical Fluids*, 17 (2), 97-110.
- Battino, R., Clever, H.I., (1966). Solubility of gases in liquids. *Chemical Reviews*, 66 (4), 395-463.
- Brewer, P.G., Friederich, G., Peltzer, E.T., Franklin, M. Orr., (1999). Direct experiments on the ocean disposal of fossil fuel CO₂. *Science*, 284, 943-945.
- Culberson, O.L., McKetta, J.J, Jr., (1951). Phase equilibria in hydrocarbon-water systems. III. The solubility of methane in water at pressures to 10,000 psia. *Transactions of the American Institute of Mining and Metallurgical Engineers*, 192, 223-226.
- Englezos, P., (1993). Clathrate hydrates. *Industrial and Engineering Chemistry Research*, 32, 1251-1274.

- Handa, Y.P., (1990). Effect of hydrostatic-pressure and salinity on the stability of gas hydrates. *Journal of Physical Chemistry*, 94 (6), 2652-2657.
- Holder, G.D., Corbin, G., Papadopoulos, K.D., (1980). Thermodynamic and molecular properties of gas hydrate from mixtures containing methane, argon and krypton. *Industrial and Engineering Chemistry Fundamentals*, 19, 282-286.
- Kim, Y.S., Ryu, S.K., Yang, S.O., Lee, C.S., (2003). Liquid water-hydrate equilibrium measurements and unified predictions of hydrate-containing phase equilibria for methane, ethane, propane and their mixtures. *Industrial and Engineering Chemistry Research*, 42, 2409-2414.
- Klauda, J.B., Sandler, S.I., (2000). A fugacity model for gas hydrate phase equilibria. *Industrial and Engineering Chemistry Research*, 39, 3377-3386.
- Klauda, J.B., Sandler, S.I., (2003). Phase behavior of clathrate hydrates: a model for single and multiple gas component hydrates. *Chemical Engineering Science*, 58, 27-41.
- Lekvam, K., Bishnoi, P.R., (1997). Dissolution of methane in water at low temperatures and intermediate pressures. *Fluid Phase Equilibria*, 131, 297-309.
- Mork, M., Gudmundsson, J.S., (2002). Hydrate formation rate in a continuous stirred tank reactor: Experimental results and bubble-to-crystal model. In: *Proceeding of the 4th International Conference on Gas Hydrates*, Yokohama.
- Parrish, W.R., Prausnitz, J.M., (1972). Dissociation pressures of gas hydrates formed by gas mixtures. *Industrial and Engineering Chemistry Process Design and Development*, 11 (1), 26-35.
- Peng, D-Y., Robinson, D.B., (1976). A new two-constant equation of state. *Industrial and Engineering Chemistry Fundamentals*, 15 (1), 59-64.

- Saberian-Broudjenni, M., Wild, G., Kim, S.D., (1989). Liquid axial dispersion in gas-liquid-solid fluidized beds. *The Chemical Engineering Journal*, 40, 83-92.
- Servio, P., Englezos, P., (2001). Effect of temperature and pressure on the solubility of carbon dioxide in water in the presence of gas hydrate. *Fluid Phase Equilibria*, 190, 127-134.
- Servio, P., Englezos, P., (2002). Measurement of dissolved methane in water in equilibrium with its hydrate. *Journal of Chemical and Engineering Data*, 47, 87-90.
- Sloan, Jr. E.D., (1998). *Clathrate Hydrates of natural gases*. 2nd ed., New York: Marcel Dekker.
- Soave, G., (1972). Equilibrium constants from a modified Redlich-Kwong equation of state. *Chemical Engineering Science*, 27 (6), 1197-1203.
- Stewart, P.B., Munjal, P.K., (1970). Solubility of carbon dioxide in pure water, synthetic sea water, and synthetic sea water concentrates at -5° to 25 °C and 10- to 45- atm. pressure. *Journal of Chemical and Engineering Data*, 15, 67-71.
- Tabe, Y., Hirari, S., Okazaki, K., Kawamura, K., Hijikata, K., (1998). Thermodynamical explanation of dissolution mechanism of liquid CO₂ with clathrate-hydrate film. In: *Heat Transfer, Proceeding of 11th IHTC, Korea*, 5, 75-80.
- Thomas, S., Dawe, R.A., (2003). Review of ways to transport natural gas energy from countries which do not need the gas for domestic use. *Energy*, 28, 1461-1477.
- Treble, M.A., Bishnoi, P.R., (1987). Development of a new four-parameter cubic equation of state. *Fluid Phase Equilibria*, 35, 1-18.
- Treble, M.A., Bishnoi, P.R., (1988). Extension of the Treble-Bishnoi equation of state to fluid mixtures. *Fluid Phase Equilibria*, 40 (1-2), 1-21.

- Valtz, A., Chapoy, A., Coquelet, C., Paricaud, P., Richon, D., (2004). Vapor-liquid equilibria in the carbon dioxide-water system, measurement and modeling from 278.2 to 318.2 K. *Fluid Phase Equilibria*, 226, 333-344.
- van der Waals, J.H., Platteeuw, J.C., (1959). Clathrate solutions. *Advances in Chemical Physics*, 2, 1-57.
- Wang, L-K., Chen, G-J., Han, G-H., Guo, X-Q., Guo, T-M., (2003). Experimental study on the solubility of natural gas components in water with or without hydrate inhibitor. *Fluid Phase Equilibria*, 207, 143-154.
- Wendland, M., Hasse, H., Maurer, G., (1999). Experimental pressure-temperature data on three- and four-phase equilibria of fluid, hydrate, and ice phases in the system carbon dioxide-water. *Journal of Chemical and Engineering Data*, 44, 901-906.
- Yang, S.O., Yang, I.M., Kim, Y.S., Lee, C.S., (2000). Measurement and prediction of phase equilibria for water + CO₂ in hydrate forming conditions. *Fluid Phase Equilibria*, 175, 75-89.
- Yang, S.O., Cho, S.H., Lee, H., Lee, C.S., (2001). Measurement and prediction of phase equilibria for water + methane in hydrate forming conditions. *Fluid Phase Equilibria*, 185, 53-63.
- Zatsepina, O.Y., Buffet, B.A., (1997). Phase equilibrium of gas hydrate: Implications for the formation of hydrate in the deep sea floor. *Geophysical Research Letters*, 24 (13), 1567-1570.

Chapter 3

Gas Hydrate Growth Model in a Semi-Batch Stirred Tank Reactor

S. Hashemi¹, A. Macchi^{1*}, P. Servio²

Industrial and Engineering Chemistry Research, (2007), 46, 5907–5912

¹ Department of Chemical and Biological Engineering
University of Ottawa
161 Louis Pasteur Street
Ottawa, Ontario, K1N 6N5, Canada

² Department of Chemical Engineering
McGill University
3610 University Street
Montreal, Quebec, H3A 2B2, Canada

* Corresponding author: Arturo Macchi, Tel: +1 613 562 5800 ext: 6939, Fax: +1 613 562 5172, E-mail address: arturo.macchi@uottawa.ca

Abstract

The gas hydrate growth model of Englezos et al. (1987a) was modified based on a concentration driving force where the equilibrium concentration at the hydrate surface is determined at the surface pressure and temperature, with the latter varying between the bulk and three-phase equilibrium temperature depending on the rate of heat removal. In order to study hydrate growth kinetics, literature mole consumption rates and hydrate surface area obtained in a semi-batch stirred tank reactor were used. The extraction of the intrinsic kinetic rate constant is intimately linked to the estimated hydrate surface area, which is difficult to accurately measure. Theoretical estimation of the surface area using a population balance is also problematic since it does not account for the inherent presence of foreign particles, of unknown quantity and size distribution, serving as nucleation sites. Finally, mole consumption rates in such experimental systems may be controlled by gas-liquid interphase mass transfer suggesting that accurate interphase mass transfer coefficients are required for proper estimation of the intrinsic kinetic rate constant.

Keywords: carbon dioxide, growth kinetics, hydrate, solubility

3.1 Introduction

Gas hydrates are non-stoichiometric crystalline compounds that form when a single gas or a volatile liquid molecule occupies the cages of structured water (Sloan, 1998). Synthesis of gas hydrates is being regarded as a means to capture carbon dioxide from flue gases as well as an alternate method of transportation and storage of natural gas (Thomas and Dawe, 2003). In order to design multiphase reactors that will produce hydrate at a large scale, both transport phenomena and hydrate formation kinetics need to be studied.

Kinetic studies of hydrate growth are often carried out in a controlled environment using a semi-batch stirred tank reactor where liquid water and hydrate former gas are in contact at suitable temperature and pressure to form gas hydrate. The driving forces presented so far in the literature to quantitatively model the hydrate growth phenomenon can be divided into three categories: temperature, fugacity or chemical potential, and concentration (mole fraction). A temperature driving force was first applied by Vysniauskas and Bishnoi (1983, 1985) and was defined as the difference between the hydrate three-phase equilibrium temperature at the experimental pressure and the experimental, i.e., bulk, temperature. Bollavaram et al. (2000) also defined the driving force based on the difference between the hydrate surface temperature and that of the bulk. The hydrate surface temperature was assumed to be equal to the three-phase equilibrium temperature, although the existence of only two phases, solid hydrate and liquid, was reported. Alternatively, Varaminian (2002) presented the hydrate formation driving force as the difference between the hydrate-liquid interface and bulk temperatures.

The Englezos et al. (1987a) model, which includes both hydrate formation kinetics and interphase mass transfer, is based on the difference between the fugacity in the bulk and the fugacity at the bulk temperature and the corresponding three-phase equilibrium pressure. This driving force was combined with the two-film theory to describe the gas-liquid mass transfer and a population balance to account for the second moment of particle size distribution. The empirical correlation proposed by Gaillard et al. (1996) for the growth rate is based on the Englezos et al. (1987a) driving force. Monfort et al. (2000) also proposed a semi-empirical model with fugacity and temperature driving forces taken from Englezos et al. (1987a) and Vysniauskas and Bishnoi (1983, 1985), respectively. The approach of Englezos et al. (1987a) to extract the intrinsic kinetic rate constant was also followed by Clarke and Bishnoi (2005), who measured the hydrate size distribution using a particle size analyzer. Finally, Gnanendran and Amin (2004) also assumed that hydrate particles are formed at the bulk temperature and three-phase equilibrium pressure.

Skovborg and Rasmussen (1994) in contrast to Englezos et al. (1987a) suggested that, from the onset of hydrate nucleation, the gas consumption rate is controlled by the transport of gas molecules from the gas to the liquid phase and hence does not depend on the total surface area of the hydrate particles. Their proposed driving force is a difference between the gas hydrate former component mole fraction at the gas-liquid interface and that of the bulk. Herri et al. (1999) and Pic et al. (2000) adopted the idea that the gas dissolution rate was controlled by mass transfer at the gas-liquid interface, but also accounted for the particle size distribution in order to characterize hydrate crystallization.

Mork and Gudmundsson (2002) modeled the formation of gas hydrates in a continuous stirred tank slurry reactor with a driving force based on the difference in concentration at the gas-liquid interface and that at the hydrate surface at the experimental pressure and corresponding three-phase equilibrium temperature. According to their model, hydrate formation kinetics are fast and hydrate formation is controlled by both gas-liquid and liquid-solid interphase mass transfer. Herri et al. (1999) also assumed that hydrate growth kinetics were much greater than the interphase mass transfer rates.

This work examines the approach to extract the hydrate growth intrinsic kinetic rate constant from a semi-batch stirred tank reactor and proposes a driving force that accounts for heat transfer, thus not necessarily resulting in three-phase equilibrium conditions.

3.2 Hydrate Formation Model

Gas hydrate crystals grow by diffusion of gas hydrate former molecules through the gas and liquid phases and incorporation onto the surface of the crystal. In this work, a concentration gradient will represent the driving force for crystal growth. Mass transfer phenomena are usually modeled with a concentration gradient rather than temperature or pressure. Moreover, pressure should not be used as a driving force since a difference in pressure would cause a force imbalance between the phases, which is not possible (Sloan, 1998). Gas hydrate formation is exothermic, and the heat released must be consistently removed, otherwise the rate of hydrate formation will be significantly reduced or stopped. Thus, the effect of heat transfer will be addressed in the hydrate growth model.

Following the hydrate growth modeling approach proposed by Englezos et al. (1987a, 1987b), the global rate of reaction for an N -component gas mixture assuming that there is no accumulation in the liquid film around the spherical hydrate particles can be written in the form:

$$R(t) = \pi \mu_2 \sum_{i=1}^N K_i^* (C - C_{eq})_i \quad (3.1)$$

where

$$\frac{1}{K^*} = \frac{1}{k_r} + \frac{1}{k_s} \quad (3.2)$$

k_s and k_r are, respectively, the mass transfer coefficient for the diffusion of the dissolved gas from the bulk of the solution to the hydrate-liquid interface and the intrinsic kinetic rate constant of the incorporation of the gas molecules onto the surface of the hydrate particles.

μ_2 is the second moment of the particle size distribution (PSD), which is given by:

$$\mu_2 = \int_0^{\infty} s^2 \phi(s, t) ds \quad (3.3)$$

where the solid surface area a_s is $\pi\mu_2$.

C_{eq} in Eq. (3.1) is the gas hydrate former equilibrium concentration at the crystal surface estimated at the temperature and pressure of the hydrate surface. As mentioned, pressure is uniform among all phases and is equal to the experimental pressure (Sloan, 1998). However, temperature at the hydrate surface depends on the rate of heat removal and can vary between the experimental (bulk) and three-phase equilibrium temperature at the experimental pressure. This will be discussed in the next section.

Based on the two-film theory, gas hydrate former molecules diffuse through the film layers adjacent to the interface of gas and liquid phases. For sparingly soluble gases, the resistance for mass transfer in the gas phase is assumed negligible (Chisti, 1989; Levenspiel, 1999). By assuming that the rate of mass transfer in the film layer is low and there is no accumulation of gas at the gas-liquid interface, i.e. quasi-steady-state condition (Englezos et al., 1987a), the mass balance for gas molecules in the liquid film layer yields:

$$D_{g,i} \frac{d^2 C_i}{dy^2} = \pi K_i^* \mu_2 (C - C_{eq})_i \quad i = 1-N \quad (3.4)$$

Considering $Y_i = (C - C_{eq})_i$, the following boundary conditions satisfy Eq. (3.4):

$$Y_i = (C_{g-l} - C_{eq})_i \quad \text{at} \quad y = 0 \quad (3.5)$$

$$Y_i = (C_b - C_{eq})_i \quad \text{at} \quad y = y_L \quad (3.6)$$

where C_{g-l} is the gas hydrate former equilibrium concentration at the gas-liquid interface and is computed at the experimental temperature and pressure (Skovborg and Rasmussen, 1994; Herri et al., 1999; Mork and Gudmundsson, 2002) and C_b is the concentration in the bulk of the liquid phase.

Analytical solution of Eq. (3.4) can be found in the work of Englezos et al. (1987a). The rate of gas mole consumption and bulk concentration as a function of time can be written as follows:

$$\frac{dn_i}{dt} = \left(\frac{D_{g,i} \gamma_i A_{(g-l)}}{y_L} \right) \frac{((C_{g-l} - C_{eq})_i \cosh \gamma_i - (C_b - C_{eq})_i)}{\sinh \gamma_i} \quad i = 1-N \quad (3.7)$$

$$\frac{dC_{bi}}{dt} = \frac{D_{g,i} a \gamma_i}{y_L \sinh \gamma_i} ((C_{g-l} - C_{eq})_i - (C_b - C_{eq})_i \cosh \gamma_i) - \pi K_i^* \mu_2 (C_b - C_{eq})_i \quad i = 1-N \quad (3.8)$$

where γ is the Hatta number and y_L is the liquid film layer thickness given by:

$$\gamma_i = y_L \sqrt{\pi K_i^* \mu_2 / D_{g,i}} \quad (3.9)$$

The expressions presented above describe the hydrate growth phenomenon. Hence, the starting point for the model, nucleation point, must be defined. For Eq. (3.7), the initial condition is the number of moles dissolved into the liquid water phase at the turbidity point n_{tb} assuming instantaneous nucleation. The number of moles at the turbidity point is

determined from measurements and indicates the level of system supersaturation just before nuclei form. At the onset of turbidity, gas in excess of equilibrium is assumed to be consumed for hydrate formation. The concentration in the bulk thus drops to an equilibrium value, which is the initial condition for Eq. (3.8). This concentration is determined under liquid-hydrate or vapor-liquid-hydrate equilibrium depending on the rate of heat removal and is estimated with the model proposed by Hashemi et al. (2006). It is assumed that negligible amounts of water moles are consumed during an experiment.

In order to determine μ_2 as a function of time, a population balance is needed and can be written as follows (Randolph and Larson, 1971):

$$\frac{\partial \phi}{\partial t} + G \frac{\partial \phi}{\partial s} = B - D \quad (3.10)$$

In this expression, it is assumed that the growth rate $G = ds/dt$ is linear and independent of the particle size. The birth B and death D rates include primary nucleation, secondary nucleation, breakage and agglomeration.

3.2.1 Two-Phase Versus Three-Phase Equilibrium

Gas hydrate formation is exothermic leading to an increase in temperature across the liquid film at the liquid-hydrate interface. Similarly, a temperature difference occurs across the liquid film at the vapor-liquid interface due to heat released from the gas dissolution in water. Temperature is assumed uniform along the bulk of the liquid phase due to turbulent

mixing. The temperature difference across the liquid film at the liquid-hydrate interface can be determined as follows:

$$\Delta T_{film} = (T_b - T_s) = \frac{(dn/dt)(\Delta H_f)}{h_s \pi \mu_2 V_l} \quad (3.11)$$

The subsequent calculations are based on the experimental data of Clarke and Bishnoi (2005). The convective heat transfer coefficient h_s is at a minimum value when the Nusselt number is equal to 2, i.e. in a stagnant liquid. The heat of CO₂ hydrate formation and the thermal conductivity of water at 277.15 K are approximately 80 kJ/mol (Sloan, 1998) and 0.574 W/(m K), respectively. The ΔT_{film} is estimated at values of 6.21×10^{-5} and 1.4×10^{-10} °C for the measured second moment μ_2 and the calculated one using Eq. (3.14), respectively.

Experiments in the semi-batch stirred tank reactor are conducted at a constant temperature and pressure associated to the liquid-hydrate two-phase zone in a pressure-temperature diagram. Since the temperature at the surface of the hydrate crystal is nearly equal to that in the liquid bulk, the driving force for hydrate growth should be based on two- rather than three-phase equilibrium conditions. Fig. (3.1) illustrates that interphase heat transfer effects via surface temperature is included in the concentration driving force. As the temperature decreases, the vertical line representing the overall steady-state concentration driving force moves towards the left, resulting in a greater driving force. Similarly, a higher pressure enhances the driving force due to an increase in C_{g-l} . The effect of pressure is more

pronounced on the equilibrium of vapor-liquid than of hydrate-liquid systems (Hashemi et al., 2006).

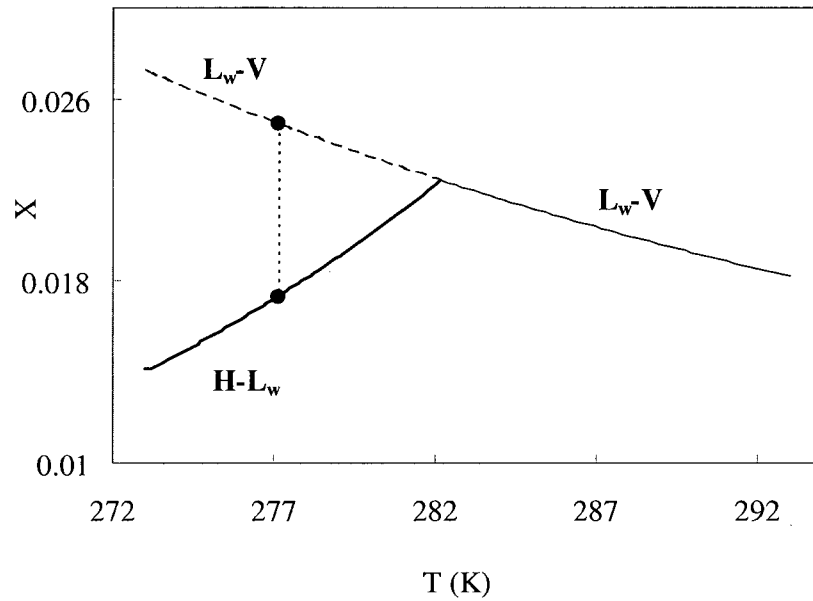


Figure (3.1). Carbon dioxide solubility in water under liquid water-vapor and liquid water-hydrate equilibrium at 35 bar (Hashemi et al., 2006).

The temperature, pressure and concentration driving forces within the liquid phase are summarized in Fig. (3.2).

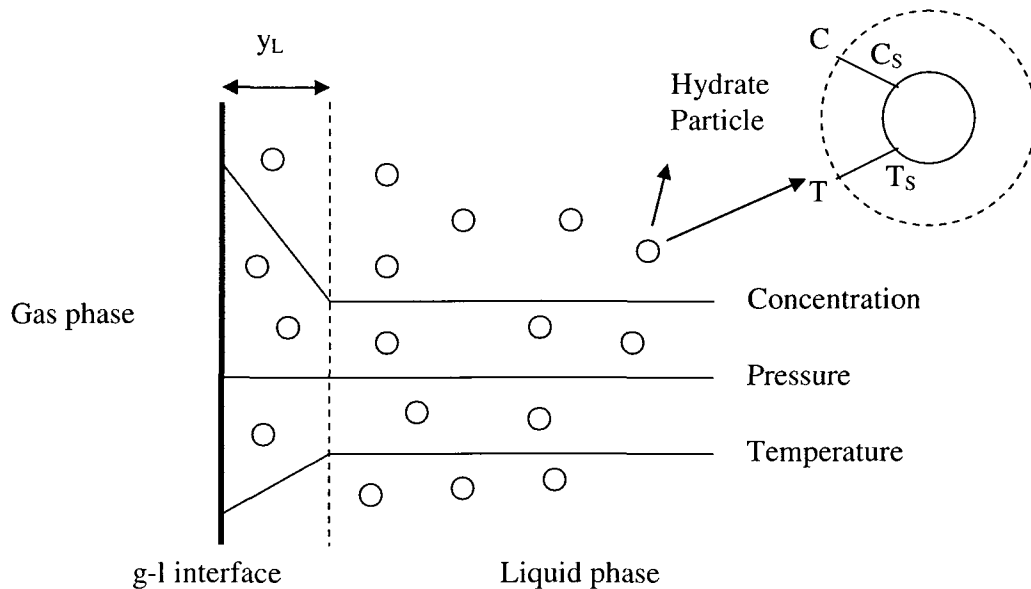


Figure (3.2). Temperature, pressure and concentration driving forces within the liquid phase. Dashed lines represent the liquid film boundary.

3.3 Results and Discussion

In this work, the experimental data of Clarke and Bishnoi (2005) obtained in a semi-batch stirred tank reactor were used for estimating the kinetics of CO₂ hydrate growth ($N = 1$). Since the pressure and temperature were kept constant during an experiment, the reactor does not reach the three-phase equilibrium condition. In addition to hydrate formation experiments, for each isotherm, solubility runs were conducted at a pressure slightly lower than the three-phase equilibrium pressure in order to determine the volumetric liquid-side mass transfer coefficient (apparent dissolution rate constant) $k_{l,a}$. Their experiments were designed to eliminate liquid-solid interphase heat and mass transfer resistances around the hydrate crystals by using a sufficiently high stirring rate, 450 rpm. Ultrapure water was employed in order to minimize the presence of foreign particles. The particle size distribution in the range of 0.5-1000 μm in diameter was measured in situ with a focused

beam reflectance method (FBRM) probe. For comparison purposes, the hydrate surface area and resulting intrinsic kinetic rate constant will also be estimated from a population balance.

3.3.1 Intrinsic Kinetic Rate Constant

For their experimental conditions, Clarke and Bishnoi (2005) show that the number of hydrate particles increases after the turbidity point but relatively quickly reaches a plateau suggesting that, after the nuclei have formed, the rate of gas consumption by crystal growth is much greater than by primary nucleation. From the constant number of particles, it was concluded that no particles in the range of 0.5-1000 μm in diameter were generated by agglomeration, breakage, or secondary nucleation.

The population balance presented in Eq. (3.10) can thus be simplified to the following equations (Kane et al., 1974; Malegaonkar, 1997) during the time period where the number of particles measured by Clarke and Bishnoi (2005) remains constant:

$$\frac{d\mu_0}{dt} = 0 \quad \mu_0(0) = \mu_0^0 \quad (3.12)$$

$$\frac{d\mu_1}{dt} = G\mu_0 \quad \mu_1(0) = \mu_1^0 \quad (3.13)$$

$$\frac{d\mu_2}{dt} = 2G\mu_1 \quad \mu_2(0) = \mu_2^0 \quad (3.14)$$

The linear growth rate can be defined as follows using the approach of Englezos et al. (1987a):

$$G_{avg} = \left(\frac{2M_H}{\rho_H L} \right) \left(y_L \sum_{i=1}^N K_i^* \frac{(C_{g-l} + C_b - 2C_{eq})_i (\cosh \gamma_i - 1)}{\gamma_i \sinh \gamma_i} + \sum_{i=1}^N K_i^* (L - y_L) (C_b - C_{eq})_i \right) \quad (3.15)$$

The excess amount of gas over the two-phase hydrate-liquid water equilibrium determines the initial conditions for Eq. (3.12) to (3.14). The number of particles per unit volume of liquid μ_0 at the turbidity point can be calculated by the excess gas converted to hydrate nuclei as follows:

$$\mu_0^0 = \frac{N_p}{V_l} = \frac{3M_H (n_{lb} - \sum_{i=1}^N n_{eq,i})}{4\pi V_l \rho_H r_{cr}^3} \quad (3.16)$$

The initial conditions for the first and second moments, respectively, are as follows (Englezos, 1987a):

$$\mu_1^0 = 2r_{cr} \mu_0^0 \quad (3.17)$$

$$\mu_2^0 = 4r_{cr}^2 \mu_0^0 \quad (3.18)$$

The initial size of particles can also be found from the following equation (Englezos et al., 1987a):

$$r_{cr} = \frac{-2\sigma}{\Delta g} \quad (3.19)$$

where

$$-\Delta g = \frac{RT_{\text{exp}}}{v_H} \left(\sum_{i=1}^N \theta_i \ln \frac{f_{ib}(T_{\text{exp}}, P_{\text{exp}}, X_{ib})}{f_{eq,i}(T_{\text{exp}}, P_{\text{exp}}, X_{eq,i})} + n_w \ln \frac{f_{w,ib}(T_{\text{exp}}, P_{\text{exp}}, (1 - X_{ib}))}{f_{w,eq}(T_{\text{exp}}, P_{\text{exp}}, (1 - \sum_{i=1}^N X_{eq,i}))} \right) \quad (3.20)$$

where X_{ib} and X_{eq} are the gas hydrate former mole fraction at the turbidity point and hydrate-liquid water equilibrium, respectively.

Transport parameters and mole consumption data were taken from Clarke and Bishnoi (2005), while physical properties were obtained from the work of Malegaonkar et al. (1997). The intrinsic kinetic rate constant was evaluated by fitting Eq. (3.7) to the experimental gas mole consumption rate along with the measured and computed particle surface area.

The resulting intrinsic kinetic rate constant k_r at 277.15 K and 21.87 bar is 1.20×10^{-8} m/s with the particle surface area obtained by the simplified population balance, while it is 4.25×10^{-5} m/s with the measured particle surface area. The large discrepancy is attributed to the difference in the theoretical and experimental particle surface areas, with the former being roughly 1000 times larger than the latter. The theoretical diameter of hydrate nuclei predicted by Eq. (3.19) is 48 nm, which is ~10 times smaller than the smallest size the probe

is capable of measuring. Experimentally, Nerheim (1993) found that the nuclei critical diameter for a (94%CH₄ + 6%C₃H₈) mixture varies between 6 and 160 nm. Although the size of particles predicted by the population balance is smaller than those measured by the probe, their number is $\sim 1 \times 10^7$ times greater.

The presence of impurities seen by the probe at the beginning of the Clarke and Bishnoi (2005) experiment suggests heterogeneous nucleation, while the population balance is based on homogeneous nucleation and does not account for foreign particles serving as nucleation sites. Homogeneous nucleation is difficult to achieve since even efficiently filtered solutions prepared in a controlled laboratory environment may still contain up to 1×10^3 particles/(mL of liquid), with those of 0.1-1 μm in diameter being the most active sites for nucleation (Mullin, 1992). The number of measured particles after nucleation ceases is ~ 2.8 times greater than the number of particles detected before nucleation. This suggests that not all foreign particles serving as nucleation sites were initially seen by the probe and/or that nucleation may not be solely heterogeneous. In both cases, there may still be particles that have not grown or coalesced with other particles to reach the probe detectable size range. Their relative contribution to the total solid surface will naturally depend on their number. More work is still required to obtain an accurate particle surface area resulting from experimentally measured particle size distributions.

3.3.2 Supersaturation

Fig. (3.3) shows the bulk supersaturation ratio C_b/C_{eq} as a function of time at 277.15 K and 21.87 bar using the second moment estimated from the population balance as well as that

from the experiment of Clarke and Bishnoi (2005). At the onset of nucleation, bulk concentration drops to the two-phase liquid-hydrate equilibrium value leading to a high gas dissolution driving force and a subsequent accumulation of gas in the liquid bulk. The increase in bulk concentration continues up to a point where the rate of gas dissolution is equal to the rate of gas hydrate formation. Afterward, the bulk concentration slowly decreases with a slope of $-8 \times 10^{-4} \text{ mol}/(\text{m}^3 \cdot \text{s})$ for both the calculated and experimental solid surface area. Gas consumption rates are observed to be apparently constant with time (Englezos et al., 1987a; Clarke and Bishnoi, 2005; Herri et al., 1999; Mork and Gudmundsson, 2002; Malegaonkar et al., 1997).

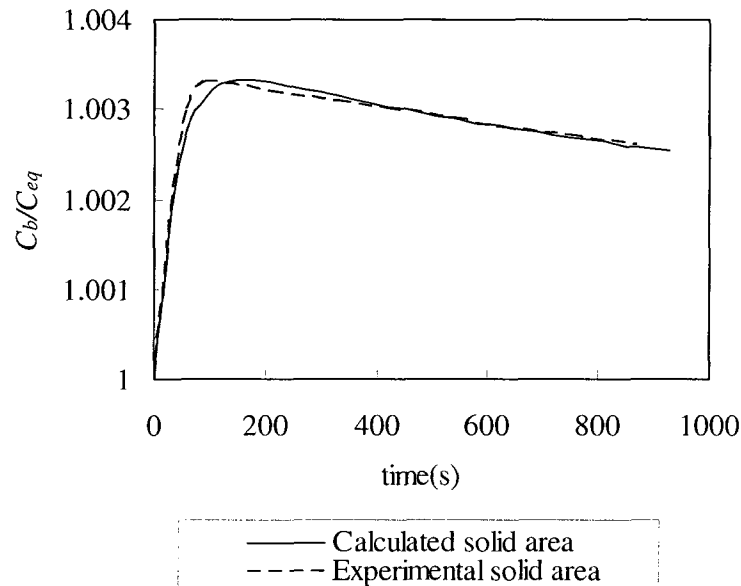


Figure (3.3). Supersaturation as a function of time at 277.15 K and 21.87 bar.

The increase in solid area has, thus, a subtle influence on the gas consumption rate as the bulk concentration reaches roughly a constant value, implying that the hydrate growth rate is

controlled by transport of molecules from the gas to the liquid phase rather than by surface reaction. Moreover, the supersaturation ratio is quite small, indicating that only a small growth driving force around the hydrate particles is required to match the rate of gas dissolution. The value of $k_{l,a} = 1.22 \times 10^{-3} \text{ s}^{-1}$ is an order of magnitude smaller than $k_{r,a,s}$, which is $2.43 \times 10^{-2} \text{ s}^{-1}$ at the onset of nucleation and $3.41 \times 10^{-2} \text{ s}^{-1}$ after 928 s.

In order to extract a proper intrinsic kinetic rate constant in such a semi-batch stirred tank reactor, it thus becomes important to use accurate values of $k_{l,a}$ and μ_2 as well as to attempt to increase $k_{l,a}$ through the stirring rate. Herri et al. (1999) observed that the value of $k_{l,a}$ increases from 1×10^{-3} to $1 \times 10^{-2} \text{ s}^{-1}$ when the stirring rate increases from 400 to 700 rpm. Although hydrate growth models solely based on gas-liquid interphase mass transfer may also fit the experimental moles consumption rates of the experimental setup (Skovborg and Rasmussen, 1994), most industrial agitated slurry reactors operate with orders of magnitude greater gas-liquid interphase mass transfer rates (Bouaifi et al., 2001; Lau et al., 2004), where now hydrate growth kinetics as well as heat removal rates become more influential.

3.4 Conclusions

The gas hydrate growth model of Englezos et al. (1987a) was reformulated based on a concentration driving force that incorporates an energy balance. For kinetic experiments performed in a semi-batch stirred tank reactor, the driving force depended on two- rather than three-phase equilibrium conditions due to efficient interphase heat transfer. A true intrinsic kinetic rate constant could not be identified as there are limitations in the estimation of the hydrate surface area. Moreover, in order to measure the intrinsic kinetic rate constant

in such experimental systems, the volumetric gas-liquid mass transfer coefficient should be maximized as the rate of gas consumption may be significantly controlled by the rate of gas dissolution into the liquid.

Nomenclature

a	gas-liquid interfacial area per unit volume of liquid, $m_{g-l}^2 m_{liq}^{-3}$
a_s	liquid-solid interfacial area per unit volume of liquid, $m_{hyd}^2 m_{liq}^{-3}$
A_{g-l}	gas-liquid interfacial area, m^2
B	birth of particles term in Eq. (3.10)
C	concentration, $mol\ m^{-3}$
D_g	diffusivity of gas component in liquid, $m^2\ s^{-1}$
D	death of particles term in Eq. (3.10)
f	fugacity, Pa
G	linear growth rate, $m\ s^{-1}$
h_s	liquid-solid convective heat transfer coefficient, $W\ m^{-2}\ K^{-1}$
H	hydrate phase
k_r	intrinsic kinetic rate constant, $m_{liq}^3 m_{hyd}^{-2}\ s^{-1}$
k_{μ}	volumetric gas-liquid mass transfer coefficient, s^{-1}
k_s	liquid-solid convective mass transfer coefficient, $m_{liq}^3 m_{hyd}^{-2}\ s^{-1}$
K^*	combined rate parameter, $m_{liq}^3 m_{hyd}^{-2}\ s^{-1}$
L	distance between (g-l) interface and the bottom of the reactor, m
L_w	water phase
M	molecular weight of the hydrate of the form $CO_2 \cdot n_w H_2O$

n	moles of gas consumed, mol
n_{tb}	number of gas molecules dissolved in the liquid water at the turbidity point, mol
n_w	hydration number
N	number of components in the gas mixture
N_p	number of particles in the liquid phase
P	pressure, Pa
r_{cr}	critical radius, m
R	gas constant, J mol ⁻¹ K ⁻¹
$R(t)$	global reaction rate, mol m _{liq.} ⁻³ s ⁻¹
s	diameter, m
t	time, s
T	temperature, K
V	vapor phase
V_l	liquid volume, m ³
X	molar fraction
y	distance from the (g-l) interface, m
y_L	liquid film thickness at (g-l) interface, m

Greek letters

ΔH_f	Enthalpy change of hydrate formation, J mol ⁻¹
Δg	free energy change per unit volume of product, J m ⁻³
γ	Hatta number defined in Eq. (3.9)
$\phi(s,t)$	particle size distribution

μ_n	n -th moment of particle distribution, $\text{m}^n \text{m}_{\text{liq.}}^{-3}$
μ_n^0	initial n -th moment of particle distribution
v	molar volume, $\text{m}^3 \text{mol}^{-1}$
θ	mole fraction of the gas in the hydrate phase on a water free basis
ρ	density, kg m^{-3}
σ	surface energy for a hydrate-water system, J m^{-2}

Subscripts

b	liquid bulk
d	dynamic
eq	hydrate-liquid water or hydrate-liquid water-vapor equilibrium
exp	experimental condition
$g-l$	gas-liquid interface
H	hydrate phase
i	gaseous component
p	particle
s	surface of solid

Acknowledgements

The authors are grateful to the Natural Sciences and Engineering Research Council of Canada for financial assistance.

References

- Bollavaram, P., Devarakonda, S., Selim, M.S., Sloan, Jr. E.D., (2000). Growth kinetics of single crystal sII hydrates: elimination of mass and heat transfer effects. *Annals of New York Academy of Sciences*, 912, 533-543.
- Bouaifi, M., Hebrard, G., Bastoul, D., Roustan, M., (2001). A comparative study of gas hold-up, bubble size, interfacial area and mass transfer coefficients in stirred gas-liquid reactors and bubble columns. *Chemical Engineering and Processing*, 40, 97-111.
- Chisti, M.Y., (1989). *Airlift bioreactors*. New York: Elsevier Science Publishers.
- Clarke, M.A., Bishnoi, P.R., (2005). Determination of the intrinsic kinetics of CO₂ gas hydrate formation using in situ particle size analysis. *Chemical Engineering Science*, 60, 695-709.
- Englezos, P., Kalogerakis, N., Dholabhai, P.D., Bishnoi, P.R., (1987a). Kinetics of formation of methane and ethane gas hydrates. *Chemical Engineering Science*, 42, 2647-2658.
- Englezos, P., Kalogerakis, N., Dholabhai, P.D., Bishnoi, P.R., (1987b). Kinetics of gas hydrate formation from mixtures of methane and ethane. *Chemical Engineering Science*, 42, 2659-2666.
- Gaillard, C., Monfort, J.P., Peytavy, J.L., (1996). Formation and growth kinetics of natural gas hydrate. In: *Proceeding of the 2nd International Conference on Gas Hydrates*, Toulouse.
- Gnanendran, N., Amin, R., (2004). Modeling hydrate formation kinetics of a hydrate promoter-water-natural gas system in a semi-batch spray reactor. *Chemical Engineering Science*, 59, 3849-3863.

- Hashemi, S., Macchi, A., Bergeron S., Servio, P. (2006). Prediction of methane and carbon dioxide solubility in water in the presence of hydrate. *Fluid Phase Equilibria*, 246 (1-2), 131-136.
- Herri, J.M., Pic, J.S., Gruy, F., Cournil, M., (1999). Methane hydrate crystallization mechanism from in-situ particle sizing. *AIChE Journal*, 45, 590-602.
- Kane, S.G., Evans, T.W., Brain P.L.T., Sarofim, A.F. (1974). Determination of the kinetics of secondary nucleation in batch crystallizers. *AIChE Journal*, 20, 855-862.
- Lau, R., Peng, W., Velazquez-Vargas, L.G., Yang, G.Q., Fan, L.S., (2004). Gas-liquid mass transfer in high pressure bubble columns. *Industrial Engineering Chemistry Research*, 43, 1302-1311.
- Levespiel, O., (2001). *Chemical reaction engineering*, 3rd ed. John Wiley & Sons.
- Malegaonkar, M.B., Dholabhai, P.D., Bishnoi, P.R., (1997). Kinetics of carbon dioxide and methane hydrate formation. *Canadian Journal of Chemical Engineering*, 75, 1090-1099.
- Monfort, J.P., Jussaume, L., El Hafaia, T., Canselier, J.P., (2000). Kinetics of gas hydrate formation and tests of efficiency of kinetic inhibitors, experimental and theoretical approaches. *Annals of the New York Academy of Sciences*, 912, 753-765.
- Mork, M., Gudmundsson, J.S., (2002). Hydrate formation rate in a continuous stirred tank reactor: Experimental results and bubble-to-crystal model. In: *Proceeding of the 4th International Conference on Gas Hydrates*, Yokohama.
- Mullin, J.W., (1992). *Crystallization*. 3rd ed. Butterworth Heinemann.
- Nerheim, A.R., (1993). Investigation of gas hydrate formation kinetics by laser light scattering. D. Ing. Thesis, Norwegian Institute of Technology, Trondheim.

- Pic, J.S., Herri, J.M., Cournil, M., (2000). Mechanisms of methane hydrate crystallization in a semi-batch reactor: Influence of a kinetic inhibitor: Polyvinylpyrrolidone. *Annals New York Academy of Sciences*, 912, 564-575.
- Randolph, A.D., Larson, M.A., (1971). *Theory of particulate processes: Analysis of techniques of continuous crystallization*. New York: Academic.
- Skovborg, P., Rasmussen, P., (1994). A mass transport limited model for the growth of methane and ethane gas hydrates. *Chemical Engineering Science*, 49, 1131-1143.
- Sloan, Jr. E.D., (1998). *Clathrate Hydrates of natural gases*. 2nd ed., New York: Marcel Dekker.
- Thomas, S., Dawe, R.A., (2003). Review of ways to transport natural gas energy from countries which do not need the gas for domestic use. *Energy*, 28, 1461-1477.
- Varaminian, F., (2002). The role of heat transfer in kinetics of hydrate formation. In: *Proceeding of the 4th International Conference on Gas Hydrates*, Yokohama.
- Vysniauskas, A., Bishnoi, P.R., (1983). A kinetic study of methane hydrate formation. *Chemical Engineering Science*, 38, 1061-1072.
- Vysniauskas, A., Bishnoi, P.R., (1985). Kinetics of ethane hydrate formation. *Chemical Engineering Science*, 40, 299-303.

Chapter 4

Gas-Liquid Mass Transfer in a Slurry Bubble Column Operated at Hydrate Forming Conditions

S. Hashemi¹, A. Macchi^{1*}, P. Servio²

Accepted to Chemical Engineering Science

¹ Department of Chemical and Biological Engineering
University of Ottawa
161 Louis Pasteur Street
Ottawa, Ontario, K1N 6N5, Canada

² Department of Chemical Engineering
McGill University
3610 University Street
Montreal, Quebec, H3A 2B2, Canada

* Corresponding author: Arturo Macchi, Tel: +1 613 562 5800 ext: 6939, Fax: +1 613 562 5172, E-mail address: arturo.macchi@uottawa.ca

Abstract

Gas-liquid interphase mass transfer coefficients were investigated in a three-phase slurry bubble column under CO₂ hydrate forming operating conditions. Modeling of gas hydrate formation requires knowledge of mass transfer behavior as well as the hydrodynamics of the system. The pressure was varied from 0.1 MPa to 4 MPa while gas velocity was increased up to 0.20 m/s. The effect of temperature was investigated at ambient as well as 277 K. Wettable ion-exchange resin particles were used to simulate the CO₂ hydrate physical properties affecting the system hydrodynamics. The slurry concentration was varied up to 10 vol.%. The volumetric mass transfer coefficient ($k_{l}a_{l}$) follows the trend in gas holdup which increases with superficial gas velocity as well as pressure. However, $k_{l}a_{l}$ and gas holdup both decrease with a decrease in temperature with the former being more sensitive. The effect of solid concentration on $k_{l}a_{l}$ and gas holdup was found to be insignificant in the range studied for high pressures. Both hydrodynamic and transport data were compared to best available correlations.

Keywords: bubble, bubble column, gas hydrates, hydrodynamics, mass transfer, phase holdup

4.1 Introduction

Synthesis of gas hydrates has recently been regarded as an alternate method of transportation and storage of natural gas as they eliminate the necessity of very low temperatures ($-160\text{ }^{\circ}\text{C}$ for Liquefied Natural Gas, LNG) and very high pressures (200 atm for Compressed Natural Gas, CNG). The hydrate contains about 160 Sm^3 of gas per m^3 of hydrate, which is comparable to LNG and CNG, at near ambient temperatures (0 to $-10\text{ }^{\circ}\text{C}$) and pressures (10 to 1 atm) (Thomas and Dawe, 2003). Gas hydrate has also been considered to recover CO_2 from flue gas by hydrate formation. This can be achieved by forming the mixed hydrate that preferentially removes CO_2 from the gaseous mixture (Seo et al., 2005).

The various multiphase systems that have been suggested to produce gas hydrate can be categorized into two groups such that liquid (Iwasaki et al., 2002) or gas (Mork and Gudmundsson, 2002) is the dispersed phase. The latter is preferred over the former as gas-liquid mass transfer can be improved by bubbling the gas into the liquid phase. In addition, systems with liquid as the continuous phase benefit from the greater heat capacity of water in order to remove the heat of hydrate formation. Hence, the multiphase reactor of choice in this work is a continuous sparged slurry bubble column. The interphase mass transfer coefficient needs to be determined in this type of system at operating conditions corresponding to gas hydrate formation and coupled with the gas-liquid and liquid-solid concentration driving forces as well as the intrinsic kinetic rate constant to formulate the hydrate formation rate (Hashemi et al., 2007).

The hydrodynamics of bubble columns at high pressure (Lau et al., 2004; Letzel et al., 1999; Jordan et al., 2003) as well as at atmospheric pressure have been extensively investigated (Kantarci et al., 2005), while research in slurry bubble columns at atmospheric pressure (Li and Prakash, 2000; Vandu et al., 2004; Vandu and Krishna, 2004; Ruthiya et al., 2006; Chilekar et al., 2007) and elevated pressure (Behkish et al., 2002; Luo et al. 1999; Inga and Morsi, 1999; Deckwer et al., 1980; Iliuta et al., 2008) were mostly conducted in the presence of dense particles. The density of suspended particles is usually above 2 g/ml which is high relative to those of hydrates, e.g. 1.1 g/ml for CO₂ hydrate. The liquid used is mostly organic particularly in high pressure studies. van der Schaaf et al. (2007) used liquid water, but the operating pressure was limited to 1.3 MPa. The objective of this work is thus to study the effect of pressure, temperature and superficial gas velocity as well as particle concentration on the gas-liquid mass transfer coefficient at CO₂ hydrate forming conditions, e.g. above 2 MPa at 277 K. In this work, CO₂ hydrate particles were simulated by wettable ion exchange resins.

4.2 Experimental

4.2.1 Apparatus

Experiments were performed in a SS316 column with an inner diameter of 0.1 m and a maximum possible bed height of 1.22 m. The gas velocity was varied up to 0.2 m/s for pressures up to 4 MPa. The experimental set-up is shown in Fig. (4.1). Two glass windows of 118.75 mm by 15.625 mm are located on the front and rear sides of the column to allow visual observation. Ports are installed along the column side in order to connect the differential pressure transducer (Rosemount, Model: 1151DP4S22C6Q4) and the dissolved

oxygen optical probe (Ocean Optics Inc., Foxy T-1000). The column wall is jacketed and the coolant temperature could be reduced to -10°C . National Instrument hardware and software was used for data acquisition.

Gas is circulated within the system via a single-stage reciprocating compressor (Hydro-Pac, Model: C01.5-10-30LX). Gas dampeners are located before and after the compressor to reduce the flow fluctuations. A pipe-in-pipe heat exchanger is used to remove the heat of compression and cool down the gas to a desired temperature. Gas is then sent to either the main column or the second column with the same geometry where it distributes through a perforated plate with 34 holes of 0.003175 m diameter on a square pattern with a pitch of 0.0159 m. Gas flow rates are measured using orifice plates (Rosemount, Model: 1195S010P1S0345CS4J3J1) and a pressure transmitter (Rosemount, Model: 8732CT12N0) and then controlled via the compressor stroke rate as well as in-line and by-pass manual valves. Gas is transferred to a demister pad to reduce any trace amounts of liquid entrained by the gas flow and recycled to the inlet gas dampeners.

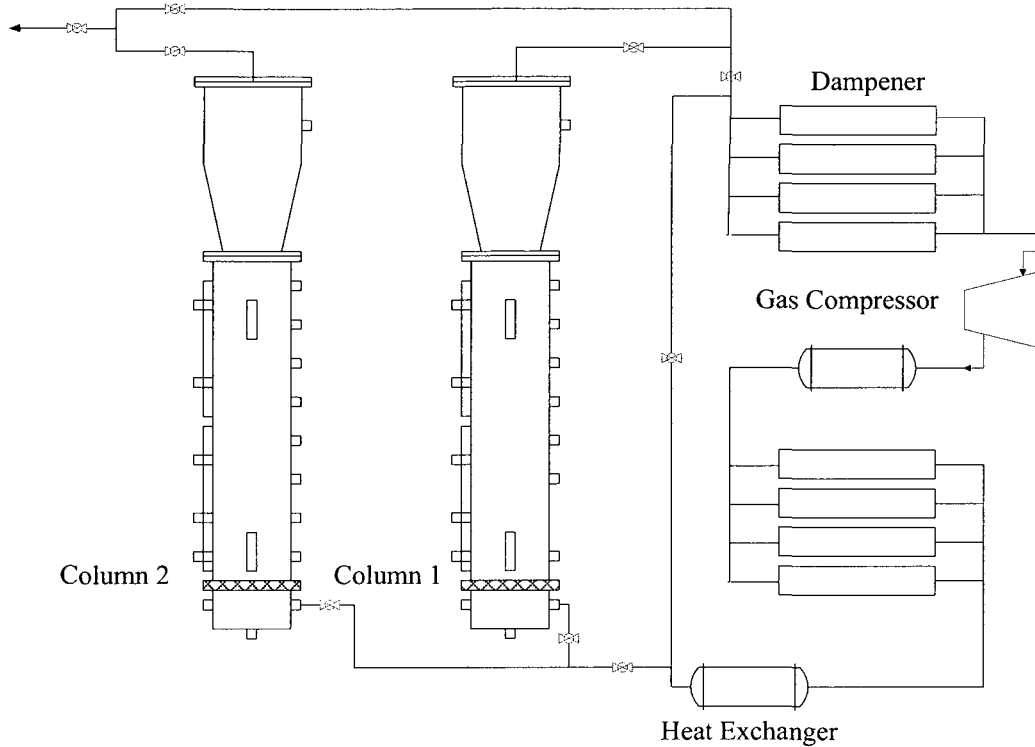


Figure (4.1). Slurry bubble column setup.

4.2.2 Procedure

An optical probe is used to measure the oxygen concentration in water. A 475 nm beam light excites the ruthenium at the tip of the probe where it fluoresces and emits energy at a wavelength of 600 nm. The energy is transferred once the fluoresced beam encounters an oxygen molecule and as a result the fluorescence intensity reduces. The rate of fluorescence quenching is proportional to oxygen concentration in the liquid phase or gas partial pressure.

The gas-liquid mass transfer coefficient at high pressure is measured by the pressure-step method (Letzel et al., 1999). The calibration of the probe is performed at each operating pressure and temperature. The signal is first set 0 % at the initial pressure which is 20-30%

lower than the desired pressure. Pressure is then increased to the desired value where the signal is set at 100%, which corresponds to the solubility at that pressure. The gas flow rate is adjusted in the second column and switched to the first column where the oxygen concentration as well as dynamic pressure gradient is monitored simultaneously. Experiments were repeated three times at the lowest and highest pressure at minimum and maximum superficial gas velocity for both no solids and 10 vol%. The relative difference is always less than 4%.

The liquid is tap water and the gas consists of a mixture of oxygen and nitrogen with concentrations detectable by the optical probe, i.e., 0 to 42 ppm at 295 K and atmospheric pressure. The solid particle is Dowex ® 50WX8, 200-400 mesh, ion-exchange resin. The volumetric solid concentration is given on gas-free basis and varies between 0% and 10%. Superficial gas velocity is varied between 0.025 to 0.2 m/s, while the pressure is increased from atmospheric to 4MPa. Ambient temperature is 295 K in this work. The mass balance on dissolved oxygen in the liquid phase can be written as:

$$\frac{dC}{dt} = k_l a_l (C^* - C) \quad (4.1)$$

where $k_l a_l$ is the volumetric liquid mass transfer coefficient, C is the dissolved oxygen concentration in water and C^* is the saturation concentration at the liquid interface. The concentration detected by the sensor can be obtained from the following equation:

$$\frac{dC_{sensor}}{dt} = k_{sensor} (C - C_{sensor}) \quad (4.2)$$

Eq. (4.1) and (4.2) were solved simultaneously for an initial concentration value of C_0 considering the probe response time of 0.4 s:

$$C_{sensor} = C^* - \frac{C^* - C_0}{k_{sensor} - k_l a_l} [k_{sensor} \exp(-k_l a_l t) - k_l a_l \exp(-k_{sensor} t)] \quad (4.3)$$

C_0 is zero as explained before. The optical probe results as well as the fit obtained with Eq. (4.3) are shown in Fig. 2(a) and 2(b). The graphs represent the data of bubble column system. The bubble rise velocity at atmospheric pressure is estimated as ~ 1 m/s, which is the same order as the liquid circulation velocity ($U_{circ.} \sim 3/4 U_b$) (Ellenberger (1995) cited by Letzel et al., 1999). The expanded bed height is calculated via $H_{initial}/(1-\varepsilon_g)$ which is 0.6-0.7 m at atmospheric conditions. As a result, τ_{mixing} is approximately 0.8-0.9 s, whereas $1/k_l a_l$ is of the order of 10 s. The assumption of perfectly mixed liquid is thus justified at low pressure as the condition of ($\tau_{mixing} \ll 1/k_l a_l$) is satisfied (Letzel et al., 1999). At higher pressures, the bubble rise velocity is lower and the mixing time is greater, e.g. roughly 2-3 s at 4MPa. Moreover, $k_l a_l$ is greater at higher pressures and hence the condition of ($\tau_{mixing} \ll 1/k_l a_l$) no longer holds true particularly at higher gas superficial velocity where $k_l a_l$ has the greatest value. However, studies show that there is either subtle difference in $k_l a_l$ determined by assuming the perfectly mixed model relative to the axial dispersion one (Lau et al., 2004), or $k_l a_l$ is independent of the axial dispersion coefficient (Deckwer et al. 1983; Tang et al. 1990). $k_l a_l$ could be determined by fitting Eq. (4.3) to the measured values of concentration.

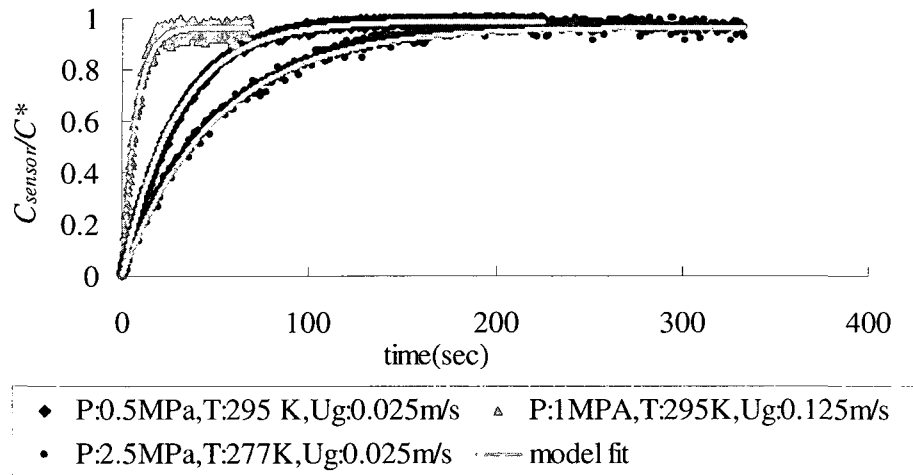


Figure (4.2)a. Oxygen absorption dynamics for water at 0.5, 1 and 2.5 MPa in the bubble column.

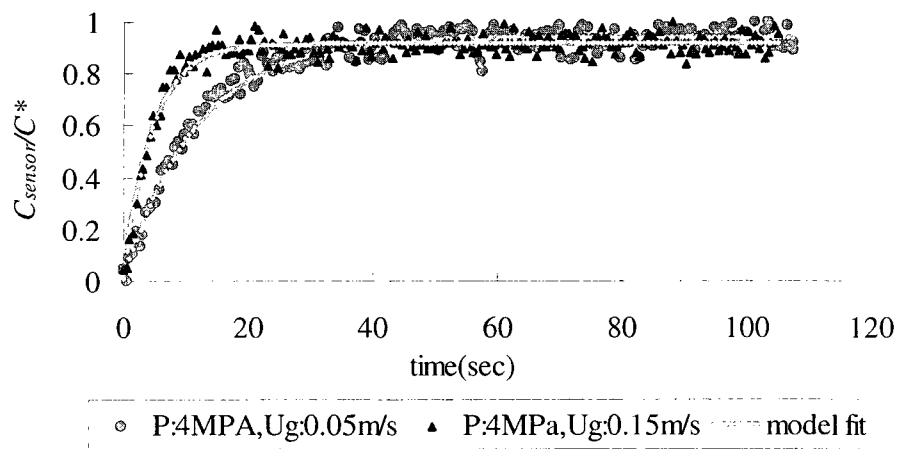


Figure (4.2)b. Oxygen absorption dynamics for water at 4MPa in the bubble column.

Experimental gas holdup was estimated based on the measured dynamic pressure drop which could be written as (Luo et al., 1999):

$$\left(\frac{\Delta P}{\Delta z}\right)_d = (\rho_g \varepsilon_g + \rho_l \varepsilon_l + \rho_s \varepsilon_s - \rho_l)g = \left\{ \frac{K(\rho_s - \rho_l)}{1+K} + \left[\frac{(1+K)\rho_g - (\rho_l + K\rho_s)}{1+K} \right] \varepsilon_g \right\} g \quad (4.4)$$

where K is defined as the solid-to-liquid volume ratio:

$$K = \frac{V_s}{V_l} \quad (4.5)$$

4.2.3 Particles

In this work, the effect of CO₂ hydrate particles on the system transport and hydrodynamic features was simulated with wettable ion-exchange resins with a density of 1.22-1.28 g/ml and a diameter ranging from 34.7 to 158.5 μm with a mean size of 84.8 μm measured by a Malvern 2000 particle size analyzer.

The slurry rheology was measured using an AR-G2 rotational rheometer. The results are shown in Fig. (4.3) which indicates that the slurry behavior shifts from Newtonian to shear-thinning at a volumetric concentration of 6-7%. The effective viscosity in a slurry bubble column can be based on the following equation ($2800 \text{ m}^{-1} U_g$), which is used to estimate the effective shear rate (cited by Nigam and Schumpe, 1996).

Fig. (4.3) shows that slurry viscosity, regardless of the solids concentration, tends to a viscosity value close to that of water at a shear rate around 100s^{-1} . Although no data were taken above 100s^{-1} due to rheometer geometry limitations, the slurry viscosity will likely plateau above the shear rate of 100s^{-1} . The shear-thinning behavior would not continue (i.e. slurry viscosity below that of water alone) based on the following theoretical equation (cited by Nigam and Schumpe, 1996):

$$\frac{\mu_{ls}}{\mu_l} = 1 + f(\alpha_s) \quad (4.6)$$

where α_s is the solid volume concentration, μ_{ls} and μ_l are the slurry and liquid viscosity, respectively. The resin slurry viscosity in the slurry bubble column will thus likely remain close to that of water for the operating condition chosen in this work with the maximum gas superficial velocity of 0.2 m/s , i.e. shear rate of 560s^{-1} , and maximum solid concentration of 10%.

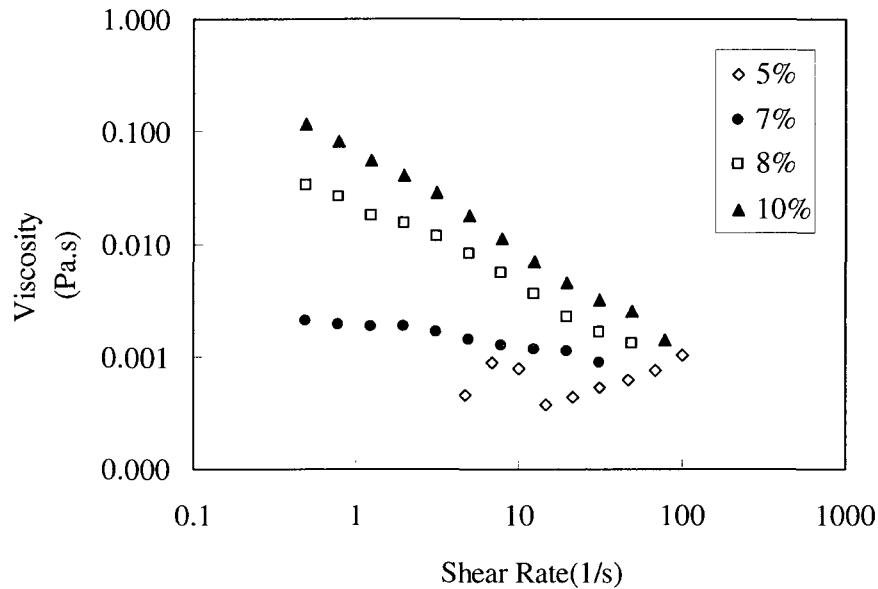


Figure (4.3). Rheology for ion-exchange resin slurry in water.

Andersson and Gudmundsson (2000) results with methane hydrate indicate that the slurry starts to deviate from Newtonian to Bingham at a concentration around 5-8% while the viscosity increases from 1.5×10^{-3} to 3.5×10^{-3} Pa·s by increasing the volumetric hydrate concentration from 1% to 13-14%. The viscosity of methane hydrate slurry above the mentioned concentration was reported to be shear-thinning. However, the authors stated that it was difficult to accurately measure the slurry viscosity at concentrations above 15 vol %. Based on the correlation of Lau et al. (2004), increasing the viscosity by a factor of almost 3.5 (3.5×10^{-3} to 1×10^{-3} for water), k_{1a1} only changes by 12% suggesting that the particles chosen in this work would have a fairly close rheology behavior to those of methane hydrates at the chosen operating condition. More work is needed to study the rheology of carbon dioxide hydrates slurries.

4.3 Results and Discussion

Fig. (4.4) and (4.5) represent the effect of pressure and gas superficial velocity on gas holdup and $k_i a_i$ for the bubble column at ambient temperature. Gas velocity determines the bubble column flow regime. By increasing gas velocity, the regime switches from the dispersed bubble flow where the bubble size is uniform to coalesced bubble flow where the bubble size distribution becomes broader. Gas holdup as well as $k_i a_i$ increase with gas superficial velocity with the rate being more pronounced in the dispersed bubble flow regime. An increase in superficial gas velocity enhances mixing in the liquid resulting in higher k_i . The rate of bubble coalescence is higher at high gas velocities. Nevertheless, there is a net increase in gas holdup as well as interfacial area available for transfer, a_i .

Gas holdup and gas-liquid mass transfer coefficient both increase with the operating pressure with the effect more noticeable in the coalesced bubble flow regime. An increase in pressure enhances bubble break-up due to a decrease in surface tension and an increase in gas density (Luo et al., 1999) and results in an increase in gas holdup and interfacial mass transfer area. By comparing Fig. (4.4) and (4.5) it could be concluded that the volumetric mass transfer coefficient increases with pressure and gas superficial velocity primarily due to an increase in interfacial area, a_i rather than mass transfer coefficient, k_i . The transition gas velocity from the dispersed bubble flow to the coalesced bubble flow was estimated based on the drift-flux model (cited by Luo et al., 1997). Increasing pressure delays the onset of bubble coalescence and hence, the dispersed flow regime occurs at higher gas holdup. By increasing the pressure from 0.1 to 4 MPa, the transition velocity increases from 0.078 to 0.125 m/s and resulting gas holdup increases from 0.15 to 0.36.

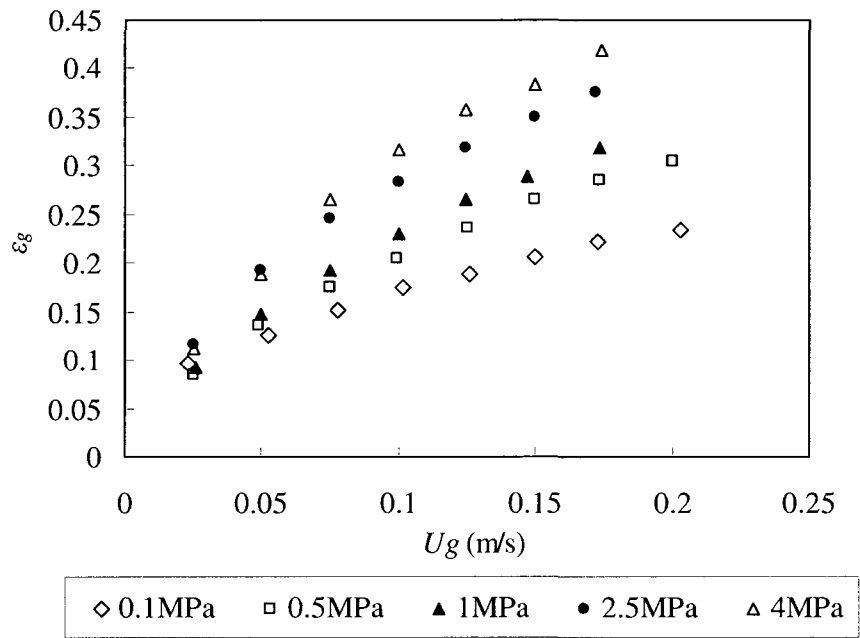


Figure (4.4). Effect of pressure on gas holdup in the bubble column at ambient temperature.

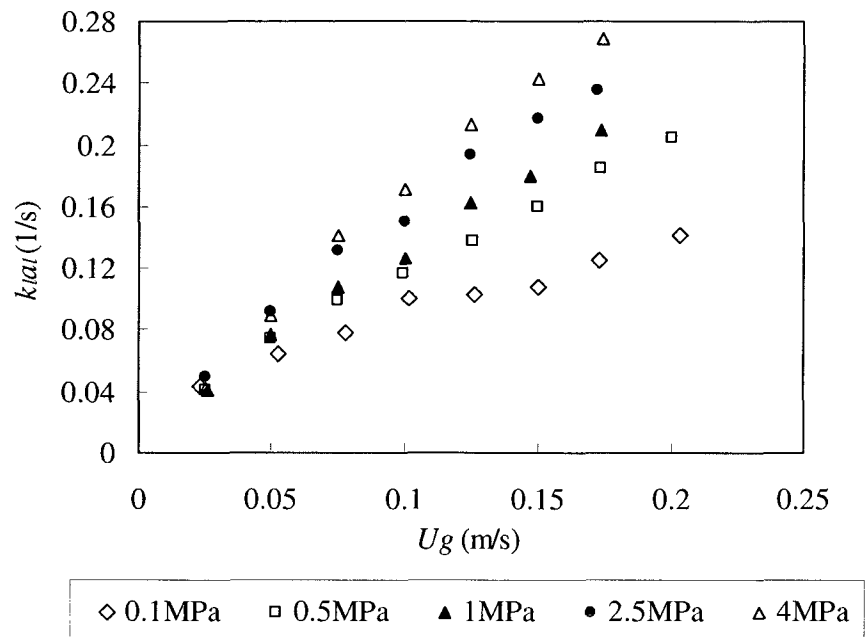


Figure (4.5). Effect of pressure on volumetric mass transfer coefficient in the bubble column at ambient temperature.

Fig. (4.6) and (4.7) shows the effect of solid volume concentration on gas holdup and volumetric mass transfer coefficient at 2.5 MPa and ambient temperature where the results of two concentrations of 5% and 10% were compared with those of bubble column. As could be seen, the effect of solid concentration on the hydrodynamics and mass transfer is negligible. Solid concentration did not influence the hydrodynamics even at higher concentration up to 20%. Effect of solid at other pressures also appears to be insignificant as displayed in Fig. (4.8) and (4.9). The insignificant influence of solids on the physical properties of the liquid explains the similarity between the hydrodynamic behavior of the slurry bubble column and that of the bubble column. For lower size of particles, the penetration of particles into the gas-liquid film layer and an increase in mass transfer coefficient, k_L , is not expected due to the low density of solids (Öztürk and Schumpe, 1987).

Dense solid appears to decrease the gas holdup and k_{La} at atmospheric pressure (Vandu and Krishna, 2004) as well as at elevated pressures (Luo et al., 1999; Behkish et al., 2002; Inga and Morsi, 1999). Solid particles increase the suspension viscosity in these systems and enhance bubble coalescence. The liquid phase used in these studies is organic mixtures.

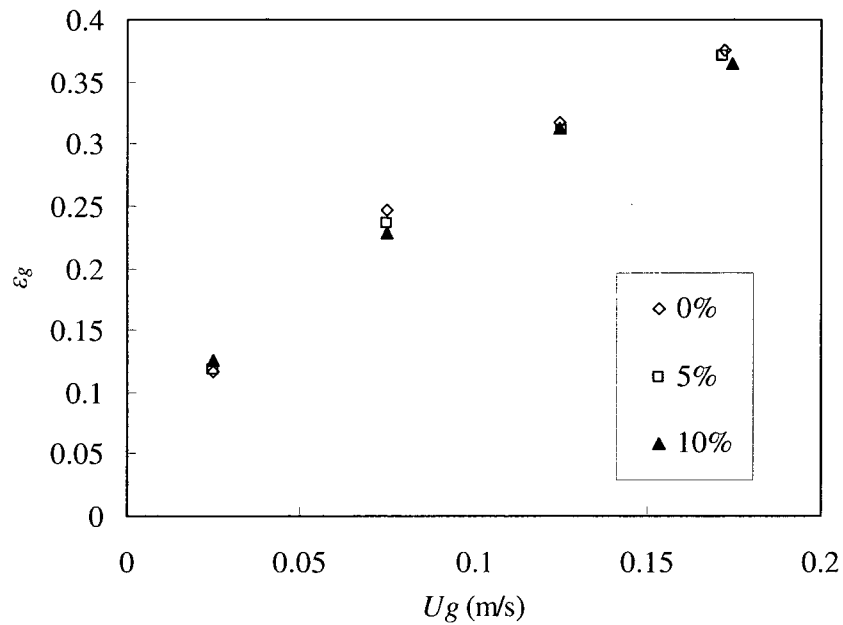


Figure (4.6). Effect of solid volume concentration on gas holdup at 2.5 MPa and ambient temperature.

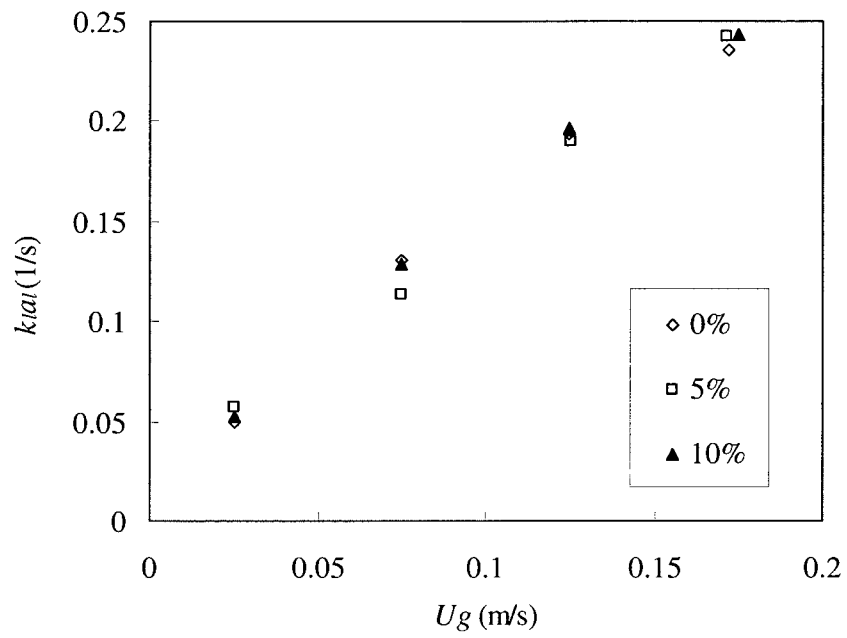


Figure (4.7). Effect of solid volume concentration on volumetric mass transfer coefficient at 2.5 MPa and ambient temperature.

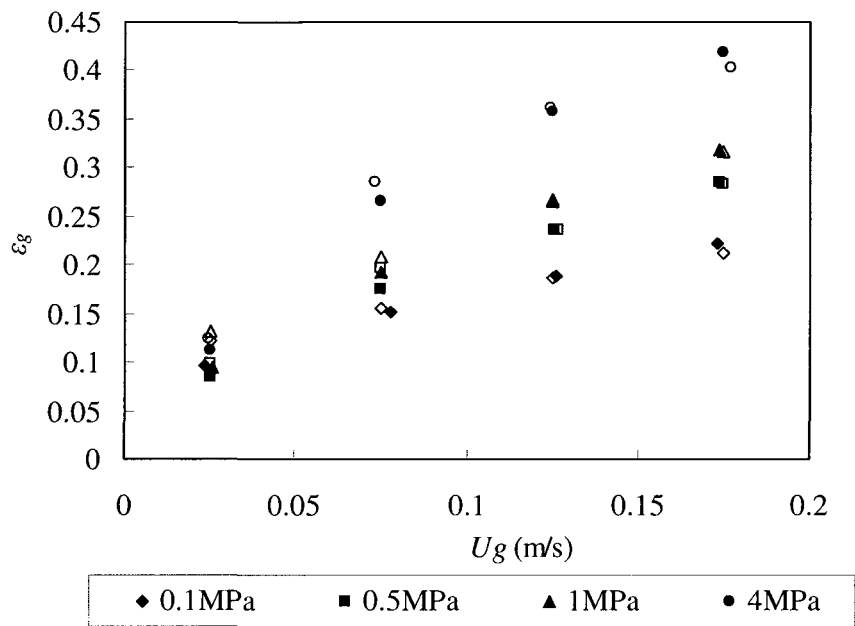


Figure (4.8). Effect of solid volume concentration and pressure on gas holdup at ambient temperature. closed symbols: 0%; open symbols: 10%.

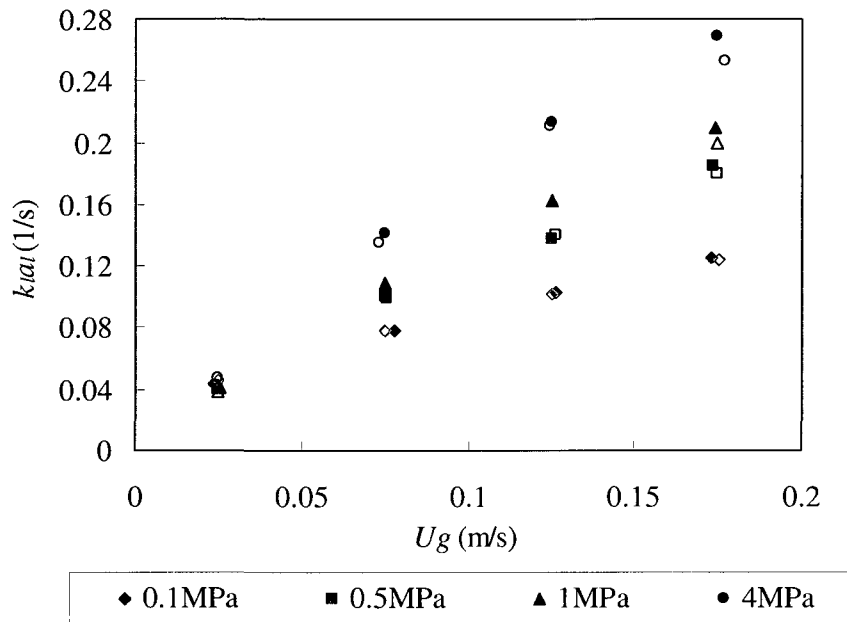


Figure (4.9). Effect of solid volume concentration and pressure on volumetric mass transfer coefficient at ambient temperature. closed symbols: 0%; open symbols: 10%.

Effect of temperature in the bubble column is displayed in Fig. (4.10) and (4.11) for gas holdup and the volumetric mass transfer coefficient, respectively at 2.5 MPa, at two different solid concentrations of 0 and 10%. At lower temperatures, surface tension and liquid viscosity are higher. As a result, bubble sizes are larger and gas holdup is lower. Fig. (4.10) and (4.11) show that reduction in $k_l a_l$ with a decrease in temperature is mainly attributed to a decrease in k_l which suggests that the effect of temperature on k_l is more influential than that on interfacial area, a_l . k_l is directly proportional to diffusivity and inversely proportional to the liquid viscosity which explain the reduction of k_l at low temperatures. On the other hand, as liquid surface tension increases, bubble size and in turn bubble rise velocity increases. As a result, k_l increases due to the reduced contact time between gas and liquid phases (Chang and Morsi, 1992). Surface tension effect does not dominate over that of viscosity as k_l

eventually decreases with a decrease in temperature. The effect of surface tension on increasing k_t is less pronounced at high gas velocity where the average bubble rise velocity is initially higher. Effect of solid concentration as could be seen is again negligible at low temperature.

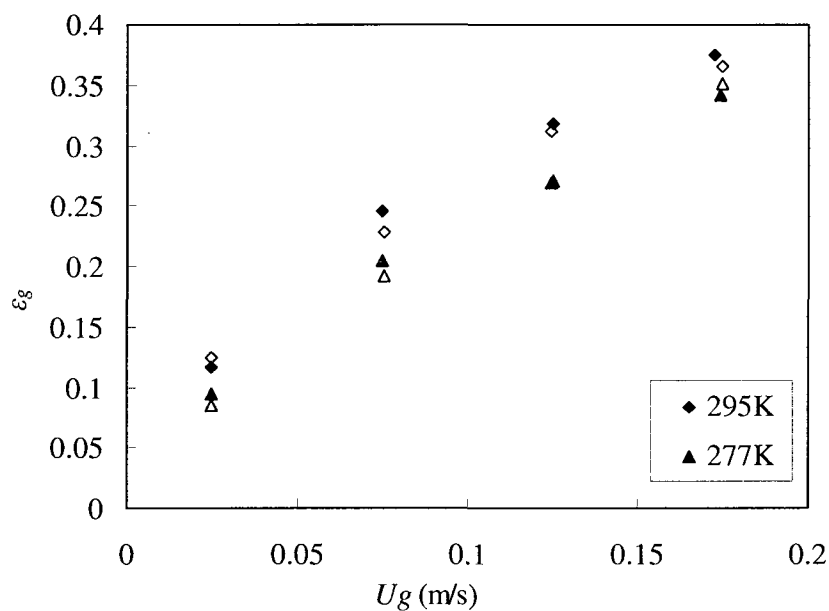


Figure (4.10). Effect of temperature on gas holdup at 2.5MPa. closed symbols: 0%; open symbols: 10%.

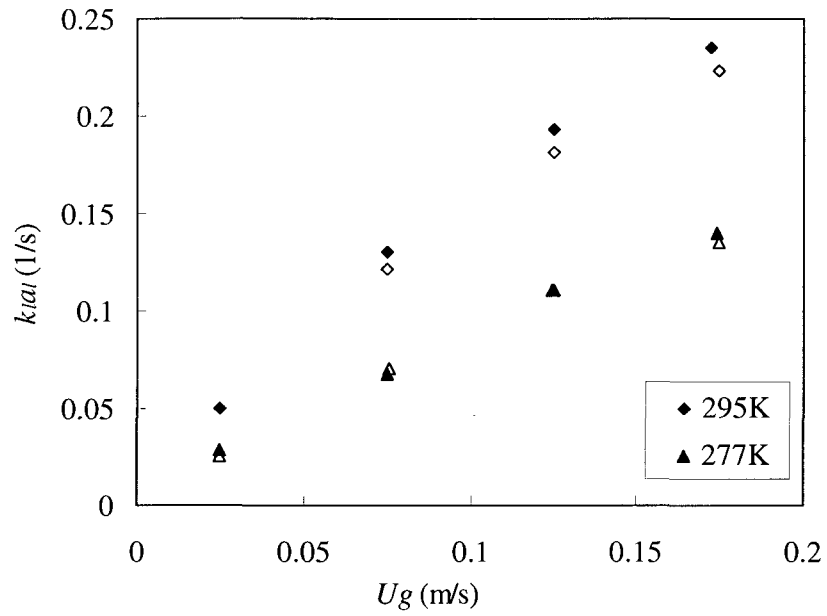


Figure (4.11). Effect of temperature on volumetric mass transfer coefficient at 2.5MPa.

closed symbols: 0%; open symbols: 10%.

The relation between $k_l a_l$ and gas holdup could be expressed in the following analytical term (Schügerl 1981; Shah et al. 1982).

$$k_l a_l = \frac{6k_l \varepsilon_g}{d_b (1 - \varepsilon_g)} \quad (4.7)$$

where d_b is the mean bubble size. By taking natural log from Eq. (4.7):

$$\ln k_l a_l = \ln \left(\frac{6k_l}{d_b} \right) + \ln \frac{\varepsilon_g}{(1 - \varepsilon_g)} \quad (4.8)$$

Eq. (4.8) could be used to verify the validity of the experimental data. $\ln k_1 a_1$ versus $\ln(\epsilon_g/(1-\epsilon_g))$ was plotted in Fig. (4.12) for the bubble column data at various pressures and ambient temperature. As could be seen, the slope is fairly close to one for all pressures studied in this work. The same trend was observed at lower temperature, e.g. the slope is 1.03 at 2.5 MPa and 277 K.

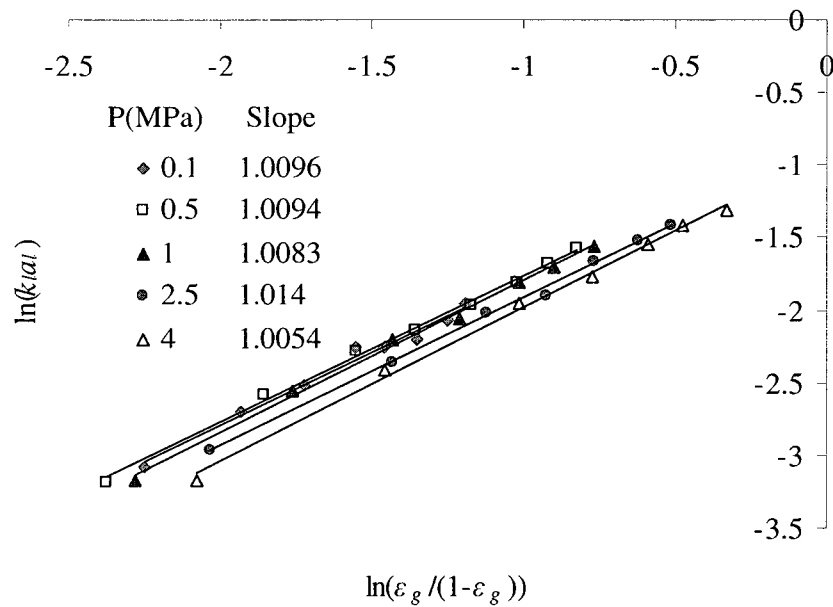


Figure (4.12). Mass transfer versus gas holdup in the bubble column at ambient temperature.

Rearranging Eq. (4.7) results in:

$$\frac{k_l}{d_b} = \frac{k_1 a_1 (1 - \epsilon_g)}{6 \epsilon_g} \quad (4.9)$$

k_l/d_b was plotted as a function of superficial gas velocity using the experimental data of bubble column at ambient temperature in Fig. (4.13). The ratio of k_l/d_b is relatively constant over the range of superficial gas velocity investigated, which is in agreement with the result obtained by Chisti (1989) in bubble column with air-water system. The value of k_l/d_b ratio at atmospheric pressure and ambient temperature is 0.073 s^{-1} using the correlation proposed by Chisti at zero solid concentration:

$$\frac{k_l}{d_b} = 5.63 \times 10^{-5} \left(\frac{g \rho_l^2 D \sigma}{\mu_l^3} \right)^{1/2} e^{-0.131 C_s^2} \quad (4.10)$$

where D is the molecular diffusivity of the solute in the liquid phase, σ is the surface tension, ρ_l is the liquid density and C_s (dry wt./vol. %) is the solid concentration in the liquid phase. The experimental value of k_l/d_b ratio at atmospheric pressure is $0.075 \pm 0.004 \text{ s}^{-1}$ which is fairly close to the predicted one by the correlation. The predicted values deviate from experimental data at higher pressure and lower temperature due to the fact that the correlation was obtained at atmospheric pressure and ambient condition. However, the trend seems to remain valid. At 2.5 MPa, the average experimental result for k_l/d_b ratio is $0.067 \pm 0.003 \text{ s}^{-1}$ for ambient temperature and $0.046 \pm 0.004 \text{ s}^{-1}$ for 277 K while the predicted values are respectively 0.072 s^{-1} and 0.025 s^{-1} . The Chisti correlation is no longer valid for the slurry bubble column data obtained in this work as it shows the decreasing value of the k_l/d_b ratio with solid concentration.

The dependency of k_l correlations on d_b varies in literature. k_l is proportional to $d_b^{0.5}$ for Akita and Yoshida (1974) and $d_b^{-0.25}$ for Schügerl et al. (1978), whereas k_l was found to be independent of bubble size by Calderbank and Moo-Young (1961).

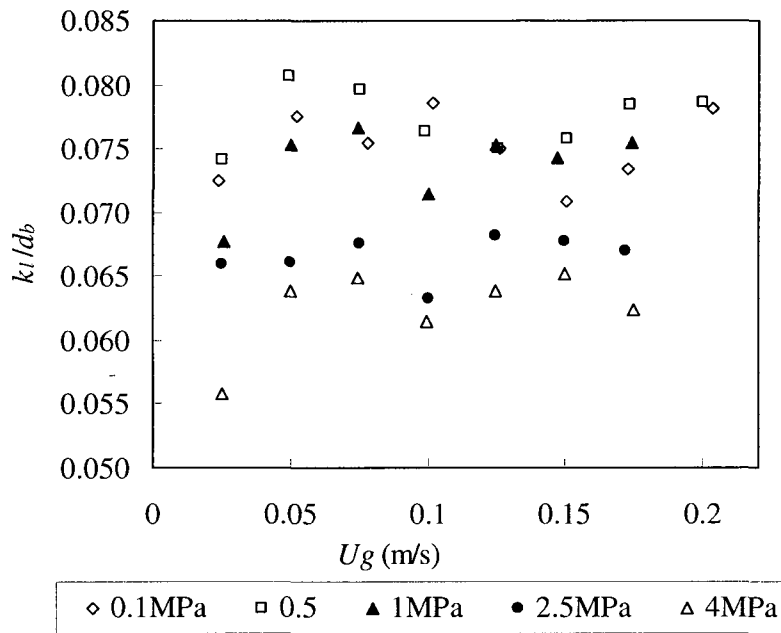


Figure (4.13). Mass transfer coefficient-to-bubble diameter ratio in the bubble column at ambient temperature.

It could be shown that $k_l a / \epsilon_g$ follows the same trend as k_l / d_b , where $k_l a$ is the volumetric mass transfer coefficient per total unit volume (gas + liquid + solid) and for the gas-liquid system could be defined by the following equation:

$$k_l a = k_l a_l (1 - \epsilon_g) \quad (4.11)$$

By, comparing Eq. (4.7) and Eq. (4.11), the values of $k_L a / \epsilon_g$ ratio are six times greater than those shown in Fig. (4.13) for k_L / d_b ratio. The average of $k_L a / \epsilon_g$ ratio is 0.45 at atmospheric pressure. The results of Vandu and Krishna (2004) for an air-water system at atmospheric condition, ambient temperature and a column diameter of 0.1 m show that at lower gas superficial velocities, the $k_L a / \epsilon_g$ ratio is initially at a maximum and then decreases to a constant value between 0.4-0.5 as the gas velocity increases and the coalesced bubble flow regime is reached. It should be noted that $k_L a / \epsilon_g$ ratio increases with gas superficial velocity as shown in Fig. (4.14).

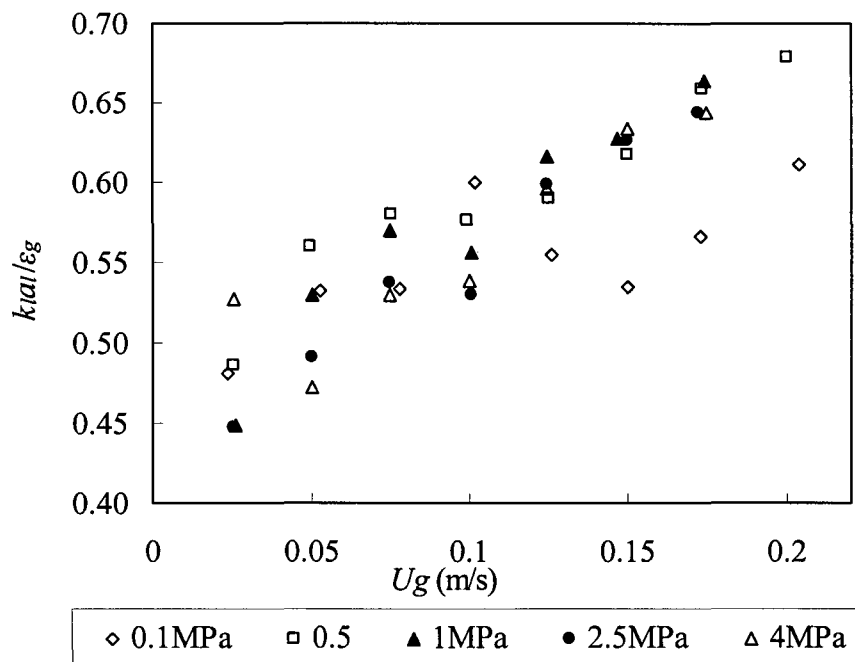


Figure (4.14). Mass transfer coefficient-to-gas holdup ratio in the bubble column at ambient temperature.

Experimental results were also compared to comprehensive correlations in the literature. The gas holdup results obtained in this work for the bubble column were compared to the

correlations proposed by Behkish et al. (2006) and Luo et al. (1999) as shown in Fig. (4.15)a for 2.5 MPa at ambient condition. The current data is consistently lower than both predicted results. Similar behavior was observed at high and low pressures. At atmospheric condition, as shown in Fig. (4.15)b the overall error was found to be lower relative to other pressures (AARE: 14%). This might be due to the fact that more literature data had been applied in order to obtain the correlations. Hence, the difference in the predicted results of two correlations also became smaller at atmospheric pressure. At lower temperature the average relative error is larger for both correlations as could be seen in Fig. (4.15)c. Overall, the Behkish et al. correlation seems to have a relatively better agreement to the experimental data than the Luo et al. correlation.

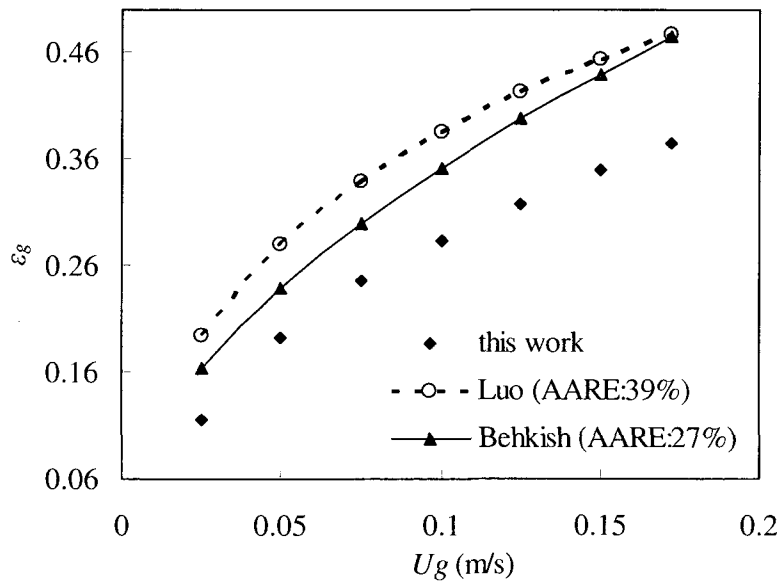


Figure (4.15)a. Gas holdup in the bubble column at 2.5 MPa and 295K comparing the current experimental data with Luo et al. as well as Behkish et al. correlations.

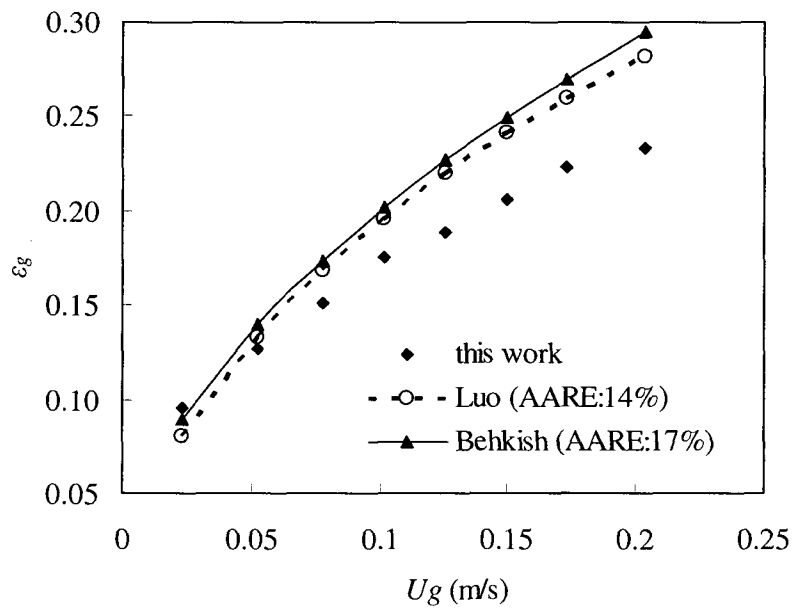


Figure (4.15)b. Gas holdup in the bubble column at 0.1 MPa and 295K comparing the current experimental data with Luo et al. as well as Behkish et al. correlations.

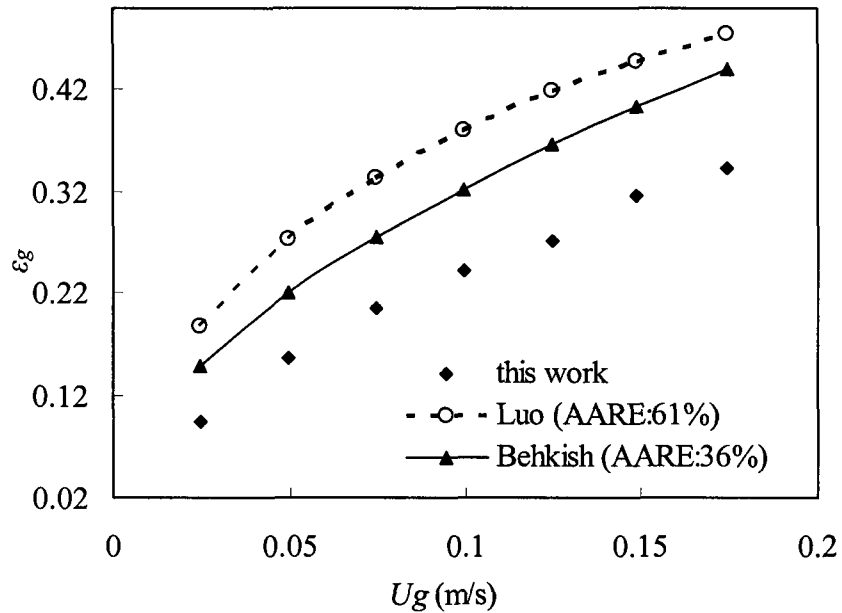


Figure (4.15)c. Gas holdup in the bubble column at 2.5 MPa and 277K comparing the current experimental data with Luo et al. as well as Behkish et al. correlations.

Fig. (4.16)a to (4.16)c present experimentally obtained volumetric mass transfer coefficients in the bubble column compared to Lau et al. (2004) as well as Lemoine et al. (2008) correlations. At ambient temperature, the experimental results are closer to the predicted values of Lau et al. correlation particularly at higher pressures (AARE: 11%). At lower temperatures, the Lau et al. correlation overestimated $k_L a_v$, while Lemoine et al. underestimated it. Gas holdup and volumetric mass transfer coefficients predicted using these correlations show a decreasing trend as a function of solid concentration.

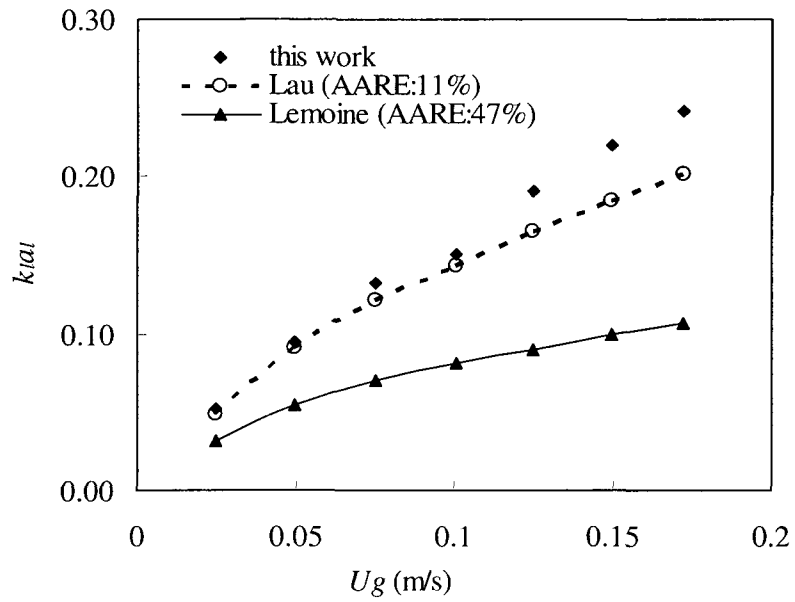


Figure (4.16)a. Volumetric mass transfer coefficient in the bubble column at 2.5 MPa and 295 K comparing the current experimental data with Lau et al. as well as Lemoine et al. correlations.

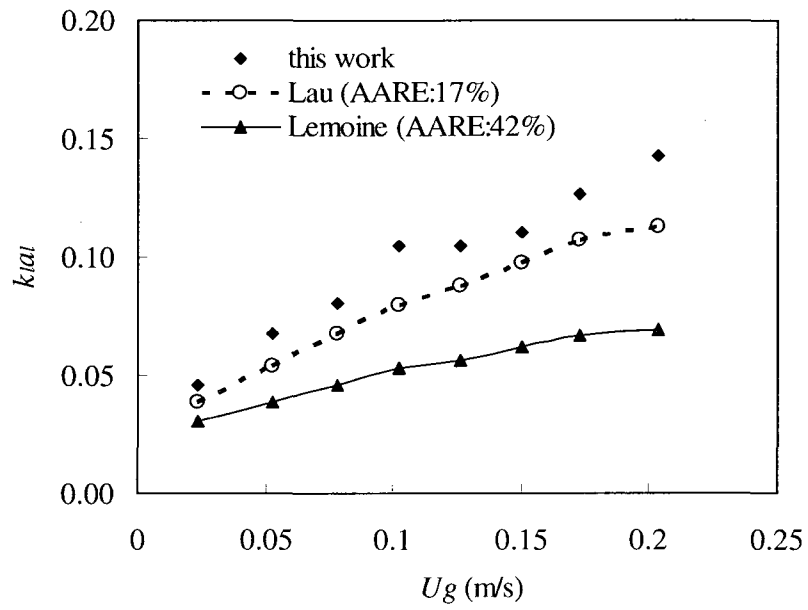


Figure (4.16)b. Volumetric mass transfer coefficient in the bubble column at 0.1 MPa and 295 K comparing the current experimental data with Lau et al. as well as Lemoine et al. correlations.

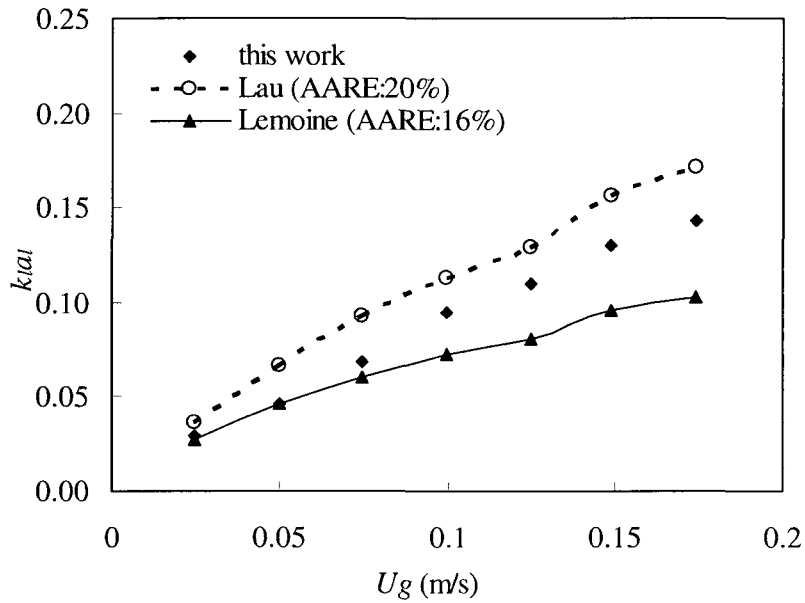


Figure (4.16)c. Volumetric mass transfer coefficient in the bubble column at 2.5 MPa and 277 K comparing the current experimental data with Lau et al. as well as Lemoine et al. correlations.

The ratio of carbon dioxide gas holdup and k_{L,a_1} to those obtained in this work was estimated based on Behkish et al. (2006) and Lemoine et al. (2008) correlations, respectively and presented in Fig. (4.17). It should be noted that the surface tension of water in presence of carbon dioxide is sensitive to pressure (Jho et al., 1977; Kvamme et al., 2007), and its values were estimated via the correlation proposed by Kvamme et al. (2007).

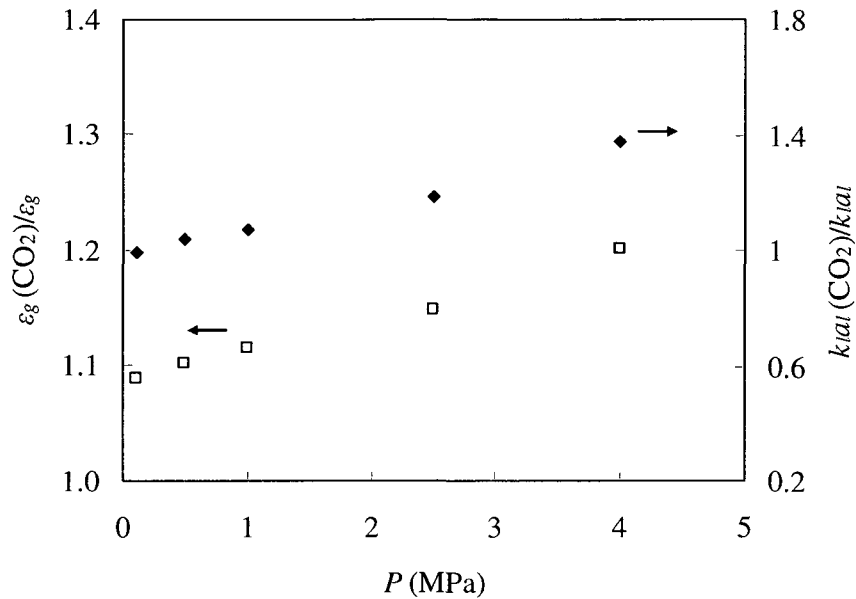


Figure (4.17). The ratio of CO₂ volumetric mass transfer coefficient and gas holdup to those reported in this work at 295 K.

4.4 Conclusions

Effect of gas superficial velocity, temperature, pressure and solid concentration on hydrodynamics and mass transfer behavior in a slurry bubble column was investigated under CO₂ hydrate forming condition. Gas holdup as well as k_{La} were found to increase with superficial gas velocity and pressure while decrease with temperature. The effect of pressure is dominant on the interfacial area due to the increase in the rate of bubble breakup. However, mass transfer coefficient was found to be more sensitive to lower temperatures than interfacial area due to a decrease in diffusivity. Effect of solid concentration was not noticeable in the range investigated for higher pressures.

Nomenclature

a_l	interfacial area per unit volume, $\text{m}^2_{\text{g}}\text{m}^{-3}_l$
C	dissolved gas concentration, molm^{-3}
C_0	dissolved gas concentration at t_0 , molm^{-3}
C^*	saturation concentration, molm^{-3}
C_s	solid concentration in the liquid phase, dry wt./vol. %
D	gas diffusivity in liquid, m^2s^{-1}
g	gravitational acceleration, ms^{-2}
$k_l a_l$	volumetric mass transfer coefficient based on liquid volume, s^{-1}
$k_l a$	volumetric mass transfer coefficient based on total volume, s^{-1}
k_l	liquid mass transfer coefficient, $\text{m}^3\text{m}^{-2}_{\text{g}}\text{s}^{-1}$
P	pressure, Pa
t	time, s
U_g	superficial gas velocity, ms^{-1}
V	volume, m^3
z	height, m

Greek letters

α_s	solid volume fraction
ε	holdup
μ_l	liquid viscosity, Pa.s
μ_s	slurry viscosity, Pa.s
ρ	density, kgm^{-3}

σ surface tension of liquid, Nm^{-1}

Subscripts

b bubble

g gas

l liquid

Acknowledgements

The authors are grateful to the Canadian Foundation for Innovation, the Ontario Innovation Trust and the Natural Sciences and Engineering Research Council of Canada for financial assistance.

References

- Akita, K., Yoshida, F., (1974). Bubble size, interfacial area, and liquid phase mass transfer coefficients in bubble columns. *Industrial and Engineering Chemistry Process Design and Development*, 13, 84-91.
- Andersson, V., Gudmundsson, J.S., (2000). Flow properties of hydrate-in-water slurries. *Annals of the New York Academy of Sciences*, 912, 322-329.
- Behkish, A., Lemoine, R., Oukaci, R., Morsi, B.I., (2006). Novel correlations for gas holdup in large-scale slurry bubble column reactors operating under elevated pressures and temperatures. *Chemical Engineering Journal*, 115, 157-171.

- Behkish, A., Men, Z., Inga, J.R, Morsi, B.I., (2002). Mass transfer characteristics in a large-scale slurry bubble column reactor with organic liquid mixtures. *Chemical Engineering Science*, 57, 3307-3324.
- Calderbank, P.H., Moo-Young, M.B., (1961). The continuous phase heat and mass-transfer properties of dispersions. *Chemical Engineering Science*, 16, 39-54.
- Chang, M-Y., Morsi, D.I., (1992). Mass transfer in a three-phase reactor operating at elevated pressures and temperatures. *Chemical Engineering Science*, 47, 1779-1790.
- Chilekar, V.P., Singh, C., van der Schaaf, J., Kuster, B.F.M, Schouten, J.C., (2007). A gas hold-up model for slurry bubble columns. *AIChE Journal.*, 53(7), 1687-1702.
- Chisti, M.Y., (1989). *Airlift bioreactors*. New York: Elsevier Science Publishers.
- Deckwer, W.-D., Lousi, Y., Zaldi, A., Ralek, M., (1980). Hydrodynamic properties of the Fischer-Tropsch Slurry Process. *Industrial and Engineering Chemistry Process Design and Development*, 19, 699-708.
- Deckwer, W.-D., Nguyen-Tien, K., Kelkar, B.G., Shah, Y.T., (1983). Applicability of axial dispersion model to analyze mass transfer measurements in bubble columns. *AIChE J.*, 29, 915-922.
- Hashemi, S., Macchi, A., Servio, P., (2007). Dynamic simulation of gas hydrate formation in an agitated three-phase slurry reactor. In: *Proceeding of the 12th International Conference on Fluidization*, Vancouver.
- Hikita, H., Asai, S., Tanigawa, K., Segawa, K., Kitao, M., (1980). Gas hold-up in bubble columns. *Chemical Engineering Journal*, 20, 59-67.
- Inga, J.R., Morsi, B.I., (1999). Effect of operating variables on the gas holdup in a large-scale slurry bubble column reactor operating with an organic liquid mixture. *Industrial and Engineering Chemistry Research*, 38, 928-937.

- Iliuta, I., Larachi, F., Desvigne, D., Anfray, J., Dromard, N., Schweich, D., (2008). Multicompartment hydrodynamic model for slurry bubble columns. *Chemical Engineering Science*, 63, 3379-3399.
- Iwasaki, S., Kimura, T., Yoshikawa, K., Nagayasu, H., (2002). The pre-investigation of natural gas transportation and storage system as gas hydrates for development of marginal natural gas fields. In: *Proceeding of the 4th International Conference on Gas Hydrates*, Yokohama.
- Jho, C., Nealon, D., Shogbola, S., King, JR., A.D., (1977). Effect of pressure on the surface tension of water: Adsorption of hydrocarbon gases and carbon dioxide on water at temperatures between 0 and 50 °C. *Journal of Colloid and Interface Science*, 65, 141-154.
- Jordan, U., Saxena, A.K., Schumpe, A., (2003). Dynamic gas disengagement in a high-pressure bubble column. *The Canadian Journal of Chemical Engineering*, 81, 491-498.
- Kantarci, N., Borak, F., Kutlu, O.U., (2005). Review bubble column reactors. *Process Biochemistry*, 40, 2263-2283.
- Kvamme, B., Kuznetsova, T., Hebach, A., Oberhof, A., Lunde, E., (2007). Measurements and modeling of interfacial tension for water + carbon dioxide systems at elevated pressures. *Computational Material Science*, 38, 506-513.
- Lau, R., Peng, W., Velazquez-Vargas, L.G., Yang, G.Q., Fan, L-S., (2004). Gas-liquid mass transfer in high pressure bubble columns. *Industrial and Engineering Chemistry Research*, 43, 1302-1311.
- Lemoine, R., Behkish, A., Sehabiague, L., Heintz, Y.J., Oukaci, R., Morsi, B.I., (2008). An algorithm for predicting the hydrodynamic and mass transfer parameters in bubble column and slurry bubble column reactors. *Fuel Processing Technology*, 89, 322-343.

- Letzel, H.M., Schouten, J.C., Krishna, R., van den Bleek, C.M., (1999). Gas holdup and mass transfer in bubble column reactors operated at elevated pressures. *Chemical Engineering Science*, 54, 2237-2246.
- Li, H., Prakash, A., (2000). Influence of slurry column concentrations on bubble population and their rise velocities in a three-phase slurry bubble column. *Powder Technology*, 113,158-167.
- Luo, X., Jiang, P., Fan, L-S., (1997). High-pressure three-phase fluidization: hydrodynamics and heat transfer. *AIChE Journal*, 43, 2432-2445.
- Luo, X., Lee, D.J., Lau, R., Yang, G., Fan, L-S., (1999). Maximum stable bubble size and gas holdup in high-pressure slurry bubble columns. *AIChE Journal*, 45, 665-680.
- Mork, M., Gudmundsson, J.S., (2002). Hydrate formation rate in a continuous stirred tank reactor: Experimental results and Bubble-to-Crystal model. In: *Proceeding of the 4th International Conference on Gas Hydrates*, Yokohama.
- Nigam, K.D.P., Schumpe, A., (1996). *Three-phase sparged reactors*. Amsterdam: Gordon and Breach Publishers.
- Öztürk S.S., Schumpe, A., (1987). The influence of suspended solids on oxygen transfer to organic liquids in a bubble column. *Chemical Engineering Science*, 42, 1781-1785.
- Ruthiya, K.C., van der Schaaf, J., Kuster, B.F.M., Schouten, J.C., (2006). Influence of particles and electrolyte on gas hold-up and mass transfer in a slurry bubble column. *International Journal of Chemical Reactor Engineering*, 4(A13), 1-37.
- Schügerl, K., Lücke, J., Lehmann, I., Wanger, F., (1978). Application of tower bioreactors in cell mass production. *Advances in Biochemical Engineering*, 8, 63-131.
- Schügerl, K., (1981). Oxygen transport into highly viscous media. *Advances in Biochemical Engineering*, 19, 71-1741.

- Seo, Y-T., Moudrakovski, I., Ripmeester J.A., Lee, J-W., Lee, H., 2005. Efficient recovery of CO₂ from flue gas by clathrate hydrate formation in porous silica gels. *Environmental Science and Technology*, 39, 2315-2319.
- Shah, Y.T., Kelkar, B.G., Godbole, S.P., Deckwer, W.-D., (1982). Design parameter estimations for bubble column reactors. *AIChE Journal*, 28, 353-379.
- Tang, W.-T, Fan, L.-S., (1990). Gas –liquid mass transfer in a three phase fluidized bed containing low density particles. *Industrial and Engineering Chemistry Research*, 29, 128-133.
- Thomas, S., Dawe, R.A., (2003). Review of ways to transport natural gas energy from countries which do not need the gas for domestic use. *Energy*, 28, 1461-1477.
- Vandu, C.O., Krishna, R., (2004). Volumetric mass transfer coefficients in slurry bubble columns operating in the churn-turbulent flow regime. *Chemical Engineering and Processing*, 43, 987-995.
- Vandu, C.O., Koop, K., Krishna, R., (2004). Volumetric mass transfer coefficients in slurry bubble columns operating in the heterogeneous flow regime. *Chemical Engineering Science*, 59, 5417-5423.

Appendix:

The effect of pressure on the surface tension of water/CO₂ is shown in Fig. (A.1) based on the correlation proposed by Kvamme et al. (2007).

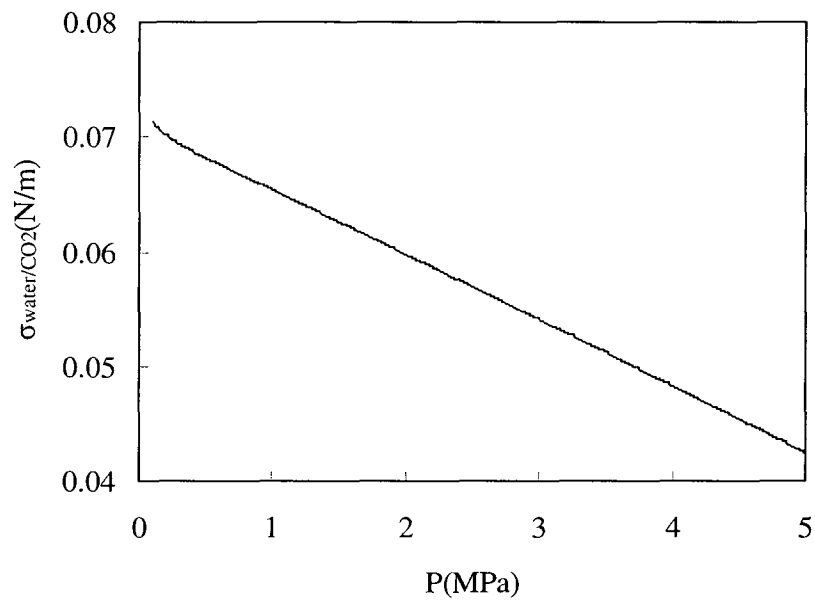


Figure (A.1). Surface tension of water in presence of CO₂ as a function of pressure at 295 K.

Chapter 5

Dynamic Simulation of Gas Hydrate Formation in a Three-Phase Slurry Reactor

S. Hashemi¹, A. Macchi^{1*}, P. Servio²

Submitted to **Industrial and Engineering Chemistry Research**

¹ Department of Chemical and Biological Engineering
University of Ottawa
161 Louis Pasteur Street
Ottawa, Ontario, K1N 6N5, Canada

² Department of Chemical Engineering
McGill University
3610 University Street
Montreal, Quebec, H3A 2B2, Canada

* Corresponding author: Arturo Macchi, Tel: +1 613 562 5800 ext: 6939, Fax: +1 613 562 5172, E-mail address: arturo.macchi@uottawa.ca

Abstract

A dynamic hydrate formation model that incorporates growth kinetics as well as system hydrodynamics and interphase heat and mass transfer rates is presented. Supersaturation ratios and gas consumption rates were evaluated as a function of time for different gas and liquid superficial velocities. The effect of temperature and pressure was also investigated based on available kinetic information in the literature. Finally, the influence of mass transfer resistance over kinetic resistance was also discussed.

Keywords: Dynamic model; Gas Hydrates; Kinetics; Slurry Reactor; Transport Phenomena

5.1 Introduction

Gas hydrates are non-stoichiometric crystalline compounds made of ice-like lattice linked together through hydrogen bonding. Gas hydrates form when the cages of structured water are stabilized by gas molecules via weak van der Waals forces (Sloan, 1998). Gas hydrate metastability can be achieved at higher temperature and lower pressure levels than those required for liquefaction and compression, respectively (Chatti et al., 2005). This characteristic of gas hydrate as well as high storage capacity, 160 Sm³ per m³ of hydrate, makes it a viable alternative for transportation and storage of natural gas. Natural gas hydrate becomes more prominent for medium- or small-scale natural gas fields where using liquefied natural gas or pipeline transportation is not as economical (Hao et al., 2008; Watanabe et al., 2008).

The various multiphase systems that have been suggested to produce gas hydrate can be categorized into two groups such that liquid (Iwasaki et al., 2002) or gas (Mork and Gudmundsson, 2002) is the dispersed phase. The latter is preferred over the former as gas-liquid mass transfer can be improved by bubbling the gas into the liquid phase (Levenspiel, 2001). In addition, systems with liquid as the continuous phase benefit from the greater heat capacity of water in order to remove the heat produced from hydrate formation. In this work, a dynamic model that depicts CO₂ hydrate formation in a slurry reactor is presented. The effect of gas and liquid superficial velocity, temperature and pressure is discussed. A parametric analysis to study the influence of interphase mass transfer and kinetics is also performed.

5.2 Model Development

The hydrate growth system is represented by gas bubbles and growing hydrate particles dispersed in liquid water. Initially gas is dissolved into the liquid in order to create a supersaturated solution. Then, at a specific time called the turbidity point, nucleation occurs generating the seed hydrate particles. Afterwards, by ensuring low supersaturation conditions, gas consumed is assumed to be utilized for growth of already formed hydrates rather than for nucleation (Clarke and Bishnoi, 2005). Thus, gas molecules transfer from the bubbles to the gas-liquid interface, then diffuse through the liquid film to the bulk and finally incorporate onto the surface of hydrate particles. Gas and liquid phases are assumed to be at equilibrium at the interface where the concentration is evaluated at the temperature and pressure of the system (Herri et al., 1999). For sparingly soluble gases, the gas-liquid mass transfer resistance is restricted within the liquid film (Levespiel, 2001).

Based on the theory of gas hydrate crystallization (Englezos et al., 1987), gas is adsorbed onto the surface of hydrate crystals in two consecutive steps. Gas molecules first diffuse through the liquid film surrounding the crystal towards the surface where they are then adsorbed onto the surface of the crystal due to the lower energy provided at the surface. The enclathration of gas onto the surface is controlled by the equilibrium concentration, which is the solubility of the gas hydrate former in water at the crystal surface temperature (Hashemi et al., 2007) and system pressure as it is uniform among all phases (Sloan, 1998). Equilibrium concentrations at the gas-liquid and hydrate-liquid interfaces were estimated using the model proposed by Hashemi et al. (2006). There is no concentration or temperature gradient across the crystal. Moreover, temperature differences across the liquid films at the gas-liquid and hydrate-liquid interfaces due to respectively the heat of dissolution and

hydrate formation were found to be negligible. This will be discussed later. Fig. (5.1) summarizes the pressure, temperature and concentration gradients across the different phases.

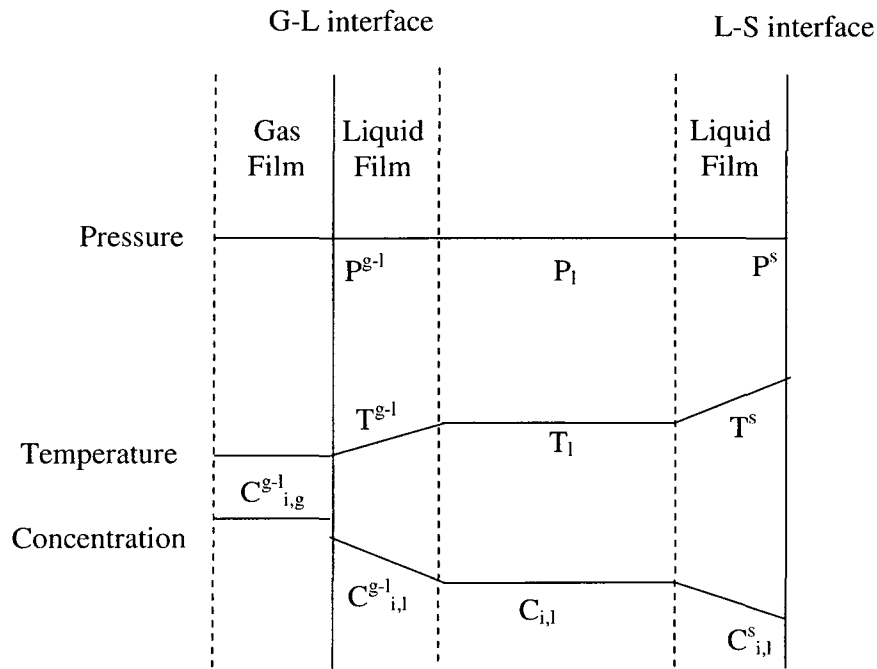


Figure (5.1). Temperature, pressure and concentration driving forces within the gas, liquid and solid phases.

5.2.1 Mass Balance

The slurry bubble flow structure can be divided into three compartments (Fig. (5.2)b). Each compartment represents one of the three phases. The mass balance of component i in the gas, liquid and solid phases for the slurry bubble column reactor presented in Fig. (5.2)a is given by Eq. (5.1) to (5.3), respectively. It is assumed that the rate of mass transfer in the liquid

film layers is low and there is no accumulation of gas at the gas-liquid and hydrate-liquid interfaces. Water is in excess and is assumed not to limit the rate of hydrate formation.

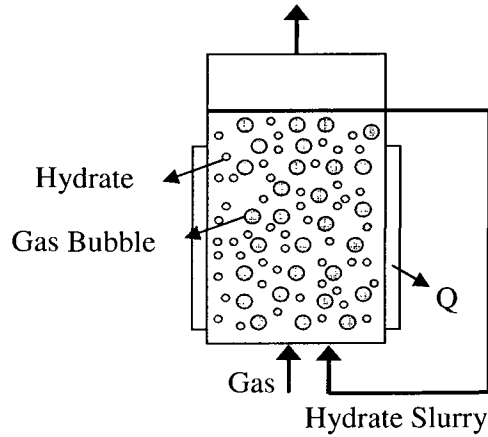


Figure (5.2)a. Schematic of the experimental apparatus .

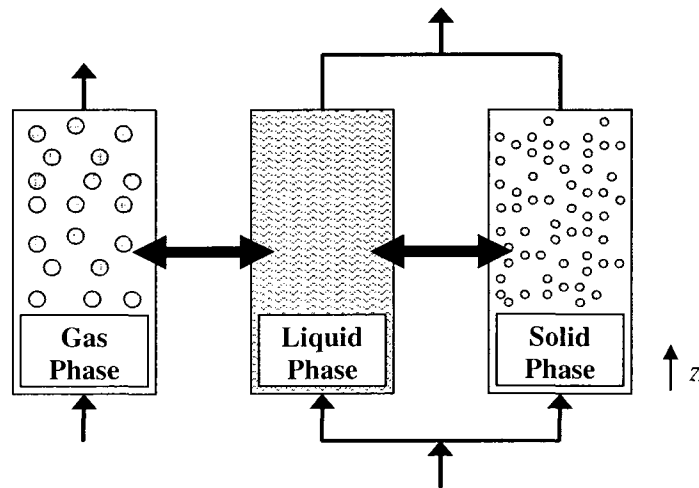


Figure (5.2)b. Schematic representation of slurry bubble column reactor.

$$\frac{\partial}{\partial z} \left(E_{i,g} \epsilon_g \frac{\partial C_{i,g}}{\partial z} \right) - \frac{\partial}{\partial z} (U_g C_{i,g}) - k_l a_l \epsilon_l (C_{i,l}^{g-l} - C_{i,l}) = \frac{\partial}{\partial t} (C_{i,g} \epsilon_g) \quad (5.1)$$

$$\frac{\partial}{\partial z} \left(E_{i,l} \varepsilon_l \frac{\partial C_{i,l}}{\partial z} \right) - \frac{\partial}{\partial z} (U_l C_{i,l}) + k_l a_l \varepsilon_l (C_{i,l}^{g-l} - C_{i,l}) - k_s a_s (C_{i,l} - C_{i,l}^s) = \frac{\partial}{\partial t} (C_{i,l} \varepsilon_l) \quad (5.2)$$

$$k_s a_s (C_{i,l} - C_{i,l}^s) = k_r a_s (C_{i,l}^s - C_{i,l}^{eq}) \quad (5.3)$$

The concentration of gas molecules at the solid surface $C_{i,l}^s$ can be eliminated by combining the two terms in Eq. (5.3) and introducing a combined mass transfer and kinetic resistance around the solid hydrate particles ($1/K^*$):

$$\frac{1}{K^*} = \frac{1}{k_r} + \frac{1}{k_s} \quad (5.4)$$

Assuming pure carbon dioxide as the inlet gas, Eq. (5.1) can be rewritten as:

$$-\frac{\partial}{\partial z} (U_g C_g) - k_l a_l \varepsilon_l (C_{i,l}^{g-l} - C_{i,l}) = \frac{\partial}{\partial t} (C_g \varepsilon_g) \quad (5.5)$$

An overall momentum balance ignoring acceleration effects and friction at the wall results in:

$$C_g = \frac{P + (\rho_l \varepsilon_l + \rho_s \varepsilon_s + \rho_g \varepsilon_g)(H_D - z)g}{ZRT} \quad (5.6)$$

Considering the fact that liquid phase velocity is relatively constant throughout the column (liquid in excess), Eq. (5.2) can also be expressed as:

$$\frac{\partial}{\partial z} \left(E_l \varepsilon_l \frac{\partial C_l}{\partial z} \right) - U_l \frac{\partial C_l}{\partial z} + k_l a_l \varepsilon_l (C_l^{s-l} - C_l) - K^* a_s (C_l - C_l^{eq}) = \frac{\partial}{\partial t} (C_l \varepsilon_l) \quad (5.7)$$

It has been assumed that at the turbidity point, the bulk concentration drops to the equilibrium value and gas in excess of equilibrium is consumed for hydrate formation (Englezos et al., 1987). As a result, the initial condition for Eq. (5.7) for $0 \leq z \leq H_p$ is as follows:

$$C_l = C_l^{eq} \quad (5.8)$$

It has also been assumed that nuclei are uniformly generated throughout the column at the turbidity point and growing particles are continuously recycled. The recycle line volume is assumed sufficiently small so that the liquid concentration at the inlet of the reactor is equal to that at the outlet, i.e. no reaction in the recycle line. The boundary conditions are as follows:

The open-open vessel boundary condition can be applied:

$$-E_l \varepsilon_l \frac{\partial C_l}{\partial z} \Big|_{z=H_p} + U_l C_l^{H_p} = -E_l \varepsilon_l \frac{\partial C_l}{\partial z} \Big|_{z=0} + U_l C_l^0 \quad (5.9)$$

$$C_l^0 = C_l^{H_D} \quad (5.10)$$

Boundary condition for gas velocity is consistent with the initial condition at $z = 0$:

$$U_G = U_G^0 \quad (5.11)$$

The particle surface area, a_s , and the solid holdup, ε_s , per unit volume of reactor can be obtained from the second and third moment of a population balance. Following Randolph and Larson (1971) and assuming that there is no particle breakage or agglomeration in the system:

$$\frac{\partial \phi}{\partial t} = E_s \nabla^2 \phi - \nabla \cdot (v\phi) \quad (5.12)$$

where

$$v = v_e + v_i \quad (5.13)$$

v_e is the external particle velocity which is the convective solid velocity on an external coordinate of the reactor, i.e. z . The convective solid velocity calculation will be discussed later. v_i is the internal particle velocity which is a function of the state of the particle. Given a particle size L , the linear growth rate is defined as $G = dL/dt$. Growth rate is essentially the

convective velocity of a particle along the internal L axis (Randolph and Larson, 1971).

Assuming the growth only occurs along the z axis of the slurry bubble column, Eq. (5.12)

can be rewritten as:

$$\frac{\partial \phi}{\partial t} = E_s \frac{\partial^2 \phi}{\partial z^2} - \frac{\partial}{\partial z} (U_s \phi) - \frac{\partial}{\partial L} (G \phi) \quad (5.14)$$

where G is expressed by the following equation:

$$G = \frac{2K^* M_H (C_l - C_l^{eq})}{\rho_H} \quad (5.15)$$

where M_H and ρ_H are the molecular weight and density of the hydrate particle, respectively.

By defining the j^{th} moment of the size distribution as:

$$\mu_j = \int_0^{\infty} \phi L^j dL \quad (5.16)$$

the population balance can be averaged in the L dimension by multiplying Eq. (5.14) by $L^j dL$ and integrating from zero to infinity:

$$\int_0^{\infty} \frac{\partial \phi}{\partial t} L^j dL = \int_0^{\infty} E_s \frac{\partial^2 \phi}{\partial z^2} L^j dL - \int_0^{\infty} \frac{\partial}{\partial z} (U_s \phi) L^j dL - \int_0^{\infty} \frac{\partial}{\partial L} (G \phi) L^j dL \quad (5.17)$$

The first and the second terms on the right hand side of the Eq. (5.17) as well as the left hand side of the equation can be rewritten in the form of Eq. (5.18) to Eq. (5.20) by reversing the order of integration and differentiation:

$$\int_0^{\infty} \frac{\partial \phi}{\partial t} L^j dL = \frac{\partial}{\partial t} \left(\int_0^{\infty} \phi L^j dL \right) = \frac{d\mu_j}{dt} \quad (5.18)$$

$$\int_0^{\infty} E_s \frac{\partial^2 \phi}{\partial t^2} L^j dL = E_s \frac{\partial^2}{\partial t^2} \left(\int_0^{\infty} \phi L^j dL \right) = E_s \frac{\partial^2 \mu_j}{\partial t^2} \quad (5.19)$$

$$\int_0^{\infty} \frac{\partial}{\partial z} (U_s \phi) L^j dL = \frac{\partial}{\partial z} \left(U_s \int_0^{\infty} \phi L^j dL \right) = \frac{\partial}{\partial z} (U_s \mu_j) \quad (5.20)$$

It was assumed in Eq. (5.20) that U_s is independent of L . The last term on the right hand side of Eq. (5.17) can be integrated by parts:

$$\int_0^{\infty} \frac{\partial}{\partial L} (G\phi) L^j dL = G \left(\phi L^j \Big|_0^{\infty} - j \int_0^{\infty} L^{j-1} \phi dL \right) = -jG\mu_{j-1} \quad (5.21)$$

The first part of the integration result in Eq. (5.21) is zero as the particle size distribution at size zero as well as infinity is nil. In order to integrate Eq. (5.21), it was assumed that the growth rate remains independent of particle size. This is known as McCabe's law, which

often holds true (Randolph and Larson, 1971). Combination of Eq. (5.17) to Eq. (5.21) gives:

$$\frac{\partial \mu_j}{\partial t} = E_s \frac{\partial^2 \mu_j}{\partial z^2} - \frac{\partial}{\partial z} (U_s \mu_j) + jG\mu_{j-1} \quad (5.22)$$

a_s and ε_s could be obtained from the second ($j = 2$) and third moment ($j = 3$) of particle size distribution, respectively.

The number of particles per unit volume of reactor, μ_0 , at the turbidity point can be calculated by the excess gas converted to hydrate nuclei as follows:

$$\mu_0^0 = \frac{N_p}{V_R} = \frac{3M_H(n_{tb} - n_{eq})}{4\pi V_R \rho_H r_{cr}^3} \quad (5.23)$$

where n_{tb} and n_{eq} are number of gas moles dissolved in water at turbidity point and H-L_w equilibrium, respectively. r_{cr} , defined as the critical radius, is the radius of nuclei at the turbidity point.

The initial conditions for the first, second and third moments are (Englezos et al., 1987):

$$\mu_j^0 = 2^j (r_{cr})^j \mu_0^0 \quad j = 1, 2, 3 \quad (5.24)$$

The initial size of particles can also be found from the following equation (Englezos et al., 1987):

$$r_{cr} = \frac{-2\sigma}{\Delta g} \quad (5.25)$$

where

$$-\Delta g = \frac{RT_{exp}}{v_H} \left(\ln \frac{f_{th}(T_{exp}, P_{exp}, X_{th})}{f_{eq}(T_{exp}, P_{exp}, X_{eq})} + n_w \ln \frac{f_{w,th}(T_{exp}, P_{exp}, (1 - X_{th}))}{f_{w,eq}(T_{exp}, P_{exp}, (1 - X_{eq}))} \right) \quad (5.26)$$

Here X_{th} and X_{eq} are the gas hydrate former mole fraction at the turbidity point and at equilibrium, respectively. The number of moles dissolved in the liquid at the turbidity point is assumed equal to that at L_w-V equilibrium. The difference between the measured n_{th} by Clarke and Bishnoi (2005) and calculated one based on L_w-V equilibrium is roughly 4% at 277.15 K and 2.187 MPa. X_{eq} is determined under L_w-H or L_w-H-V equilibrium depending on the rate of heat removal from the hydrate particle, see next section.

The boundary conditions are similar to those of Eq. (5.9):

$$-E_s \varepsilon_s \left. \frac{\partial \mu_j}{\partial z} \right|_{z=H_D} + U_s \mu_j^{H_D} = -E_s \varepsilon_s \left. \frac{\partial \mu_j}{\partial z} \right|_{z=0} + U_s \mu_j^0 \quad j = 1, 2, 3 \quad (5.27)$$

$$\mu_j^0 = \mu_j^{H_D} \quad j = 1, 2, 3 \quad (5.28)$$

The convective particles velocity, U_s , can be calculated from the solid momentum balance:

$$F_B - F_D - F_G = \rho_s V_s \left[\frac{\partial U}{\partial t} + U \frac{\partial U}{\partial z} \right] \quad (5.29)$$

where F_G is the gravity force, F_B is the buoyancy force and F_D is the drag force exerted by the liquid phase. U is the relative velocity between solid and liquid. Due to the small effect of gas velocity on the terminal velocity of particles smaller than 460 μm (Fan, 1989), the bubble-wake particle interaction force was neglected. Drag force was calculated based on the Stokes law ($Re_p < 0.1$). It was found that solids are moving along the column with the velocity almost equal to that of the liquid indicating that friction is negligible.

Gas holdup, ε_g , and volumetric liquid-side mass transfer coefficient, k_{La} , were taken from the experimental work of Hashemi et al. (2009) in a high-pressure slurry bubble column. The liquid-solid convective mass transfer coefficient k_s and the gas diffusivity were estimated using the equations proposed by Beenackers and Van Swaaij (1993) and Wilke and Chang (1955), respectively. Hydrate physical parameters were obtained from the work of Malegaonkar et al. (1997) while the intrinsic kinetic rate constant, k_r , was taken from the theoretical results of Hashemi et al. (2007).

5.2.2 Energy Balance

The temperature difference across the liquid film at the liquid-hydrate interface can be determined as follows:

$$(T_l - T^s) = \frac{(dn_H / dt)(\Delta H_f)}{h_{l-s} \pi \mu_2 V_R} \quad (5.30)$$

As a conservative estimate, the liquid-solid convective heat transfer coefficient h_{ls} is at a minimum value when the Nusselt number is equal to 2, i.e. in a stagnant liquid. The heat of CO₂ hydrate formation and the thermal conductivity of water at 277.15 K is approximately -80 kJ/mol (Sloan, 1998) and 0.574 W/(m K), respectively. From the simulation results presented in the following sections, the temperature gradient across the liquid film was found to be less than 7×10^{-9} °C, which is negligible.

Similarly, the temperature difference across the liquid film at the gas-liquid interface can be determined as follows:

$$(T^{g-l} - T_l) = \frac{d_b (dn_{tot} / dt)(\Delta H_{dis})}{6h_{g-l} \varepsilon_g V_R} \quad (5.31)$$

The enthalpy change of CO₂ dissolution in water ΔH_{dis} is -19.43 kJ/mol at 298 K (Sloan, 1998). The gas-liquid convective heat transfer coefficient, h_{gl} of a rigid bubble can be estimated by the following correlation (Bird et al., 2002):

$$Nu = 2 + 0.60 Re^{0.5} Pr^{0.33} \quad (5.32)$$

The maximum stable bubble size $(d_b)_{max}$ can be estimated by (Luo et al., 1999):

$$(d_b)_{max} = 3.27\sqrt{\gamma/g\rho_g} \quad (5.33)$$

where ρ_g and γ are respectively the gas density and gas-liquid surface tension. This approach can be considered conservative since the average bubble diameter is smaller. Again, it was found that temperature gradient across the liquid film was small at less than 0.16 °C.

Experiments in a slurry reactor are conducted at a constant temperature and pressure associated to the L_w-H two-phase zone in a pressure-temperature diagram, i.e. above the three-phase equilibrium line in Fig. (5.3). Since the temperature at the surface of the hydrate crystal is nearly equal to that in the liquid bulk, the driving force for hydrate growth should be based on L_w-H rather than L_w-H-V equilibrium conditions (Hashemi et al., 2007).

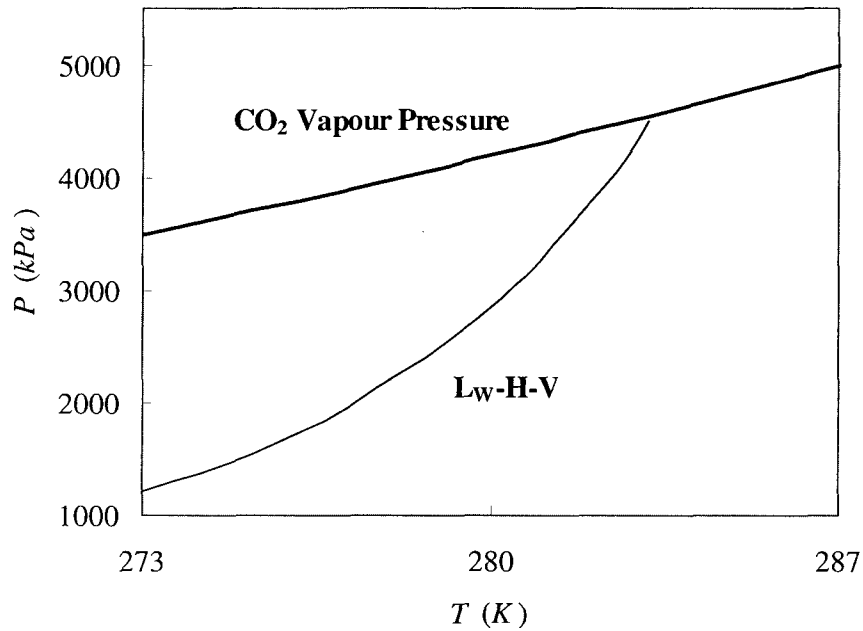


Figure (5.3). Phase diagram of carbon dioxide-water system.

Fig. (5.4) illustrates that interphase heat transfer effects via surface temperature is included in the concentration driving force. As the temperature decreases, the vertical line representing the overall steady-state concentration driving force moves towards the left, resulting in a greater driving force. Similarly, a higher pressure enhances the driving force due to an increase in C^{g-l} . The effect of pressure is more pronounced on the equilibrium of liquid-vapor than of hydrate-liquid systems (Hashemi et al., 2006).

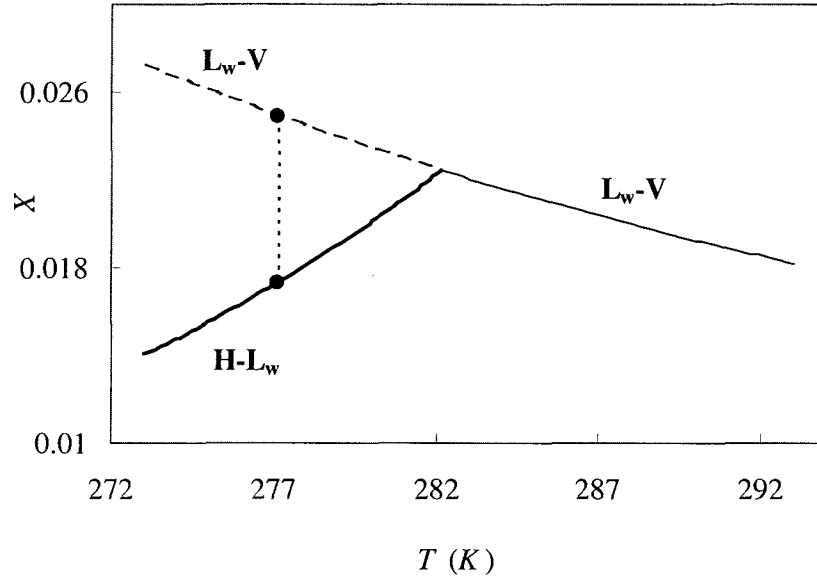


Figure (5.4). Carbon dioxide solubility in water under liquid water-vapor and liquid water-hydrate equilibrium at 3.5 MPa (Hashemi et al., 2006).

The amount of heat, Q ($J/s.m^3$), to be removed in order to keep the reactor temperature constant, can be determined from an overall energy balance:

$$\begin{aligned}
 & \frac{\partial}{\partial z} \left[(\kappa_l \varepsilon_l + \kappa_g \varepsilon_g + \kappa_s \varepsilon_s) \frac{\partial}{\partial z} (T - T^{ref}) \right] - \frac{\partial}{\partial t} \left[C_g \varepsilon_g C_{p,g} (T - T^{ref}) \right] - \frac{\partial}{\partial t} \left[C_l \varepsilon_l C_{p,l} (T - T^{ref}) \right] \\
 & - \frac{\partial}{\partial t} \left[\frac{\rho_s}{M_s} \varepsilon_s C_{p,s} (T - T^{ref}) \right] - \frac{\partial}{\partial z} \left[C_g U_g C_{p,g} (T - T^{ref}) \right] - \frac{\partial}{\partial z} \left[C_l U_l C_{p,l} (T - T^{ref}) \right] \\
 & - \frac{\partial}{\partial z} \left[\frac{\rho_s}{M_s} U_s C_{p,s} (T - T^{ref}) \right] + \Delta H_{dis}^{ref} k_l a_l \varepsilon_l (C_l^{g-l} - C_l) + \Delta H_f^{ref} K^* a_s (C_l - C_l^{eq}) = Q \quad (5.34)
 \end{aligned}$$

The required surface area of the heat exchanger can be obtained based on an estimated overall heat transfer coefficient and coolant driving force.

5.2.3 Pressure Balance

The system pressure is constant and uniform among all phases at a given axial position. The axial pressure drop, ignoring acceleration effects and friction at the walls, is given by:

$$\frac{-dp}{dz} = (\varepsilon_s \rho_s + \varepsilon_l \rho_l + \varepsilon_g \rho_g) g \quad (5.35)$$

This equation was included in Eq. (5.6) as presented before. The hydrostatic pressure and its effect on the axial gas concentration in water was found insignificant since the reactor is operated at high pressure of around 2 MPa and above.

5.3 Results and Discussion

The system was first solved for plug flow regime (PF) i.e., $E_l = E_s = 0$. Fig. (5.5) shows the bulk supersaturation ratio C_l/C_{eq} of carbon dioxide in water as a function of time at 277.15 K and 2.187 MPa, gas and liquid superficial velocity of 0.025 and 0.002 m/s, respectively. The intrinsic rate constant, k_r , is 1.20×10^{-8} m/s and is taken from the theoretical work of Hashemi et al. (2007). The hydrodynamic bed height and the reactor diameter are 1.35 m and 0.1 m, respectively. Fig. (5.5) compares the results of the plug flow regime at the outlet of the reactor with an alternative case where all phases are assumed to be completely stirred (CST). This could be obtained by integrating Eq. (5.5), (5.7) and (5.22) for dz from zero to H_D as follows:

$$C_{i,g} (U_{g,in} - U_{g,out}) - k_l a_l \epsilon_l (C_l^{g-l} - C_l) H_D = H_D \frac{d(C_g \epsilon_g)}{dt} \quad (5.36)$$

$$k_l a_l \epsilon_l (C_l^{g-l} - C_l) - K^* a_s (C_l - C_l^{eq}) = \frac{d(C_l \epsilon_l)}{dt} \quad (5.37)$$

$$jG\mu_{j-1} = \frac{d\mu_j}{dt} \quad \mu_j(0) = \mu_j^0, \quad j = 0, 1, 2, 3 \quad (5.38)$$

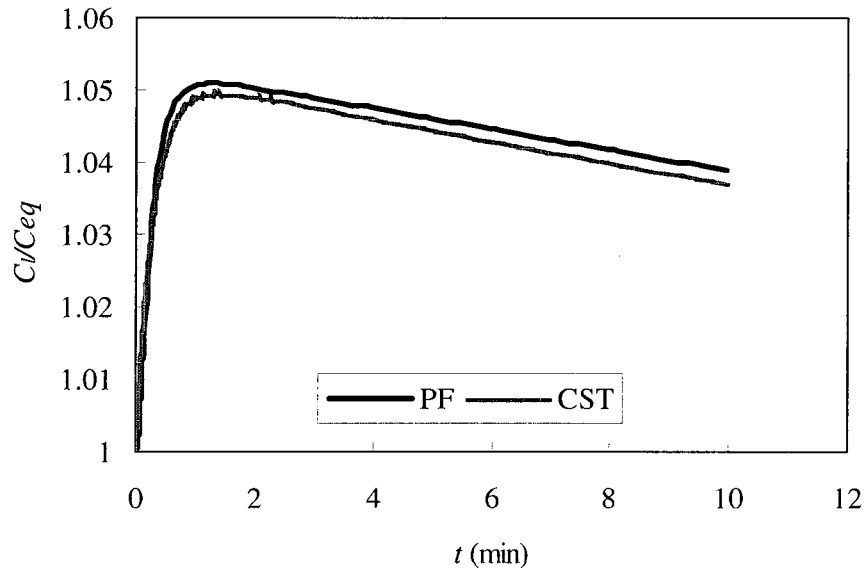


Figure (5.5). Supersaturation ratio of carbon dioxide in water as a function of time at 277.15 and 2.187 MPa; PF at $z = H_D$; gas and liquid superficial velocities are 0.025 and 0.002 m/s, respectively.

Eq. (5.36) to (5.38) were hence solved simultaneously for CST condition. The set of partial differential equations in case of fully PF reactor was solved in MATLAB[®] with the Explicit i.e. Forward method, and the set of ordinary differential equations in case of CST was solved using ODE15s(), which is an implicit solver in MATLAB[®] for stiff differential equations. The small difference in two curves as presented in Fig. (5.5) suggests that the effect of the phase flow pattern on system performance is insignificant. Bulk concentration profile indicates a negligible change along the column (less than 0.4%). An increase in the bed height results in an increase in the supersaturation ratio due to a greater residence time. However, the effect was found insignificant. By increasing the hydrodynamic bed height four times, the supersaturation ratio increases by less than 1% with negligible distribution along the bed. The rest of the study was conducted at CST.

It should be noted that the simulation was not continued for a time period beyond 10 minutes as the probability of particles forming agglomerates or large particles breaking due to particle-particle and particle-wall collisions would be even greater (Englezos et al., 1987). In order to take these phenomena into account the particle size distribution needs to be measured in-situ. Time equal to zero corresponds to the turbidity point where no more particles are generated by nucleation. The liquid-solid mass transfer resistance ($1/k_s$) was found insignificant relative to the kinetic resistance ($1/k_r$) with the former 10^7 times smaller than the latter. It was assumed that at the onset of turbidity, the gas hydrate former concentration drops to the two-phase L_w-H equilibrium value. This leads to a high gas dissolution driving force as $(C_l^{s-l}-C_l)$ is larger than $(C_l-C_l^{eq})$ resulting in the accumulation of gas in the liquid bulk, see Eq. (5.37). The increase in the bulk concentration proceeds to a point where the rate of gas dissolution is equal to the rate of gas hydrate formation.

Afterwards, the consistent increase in solid area results in a decrease in the bulk concentration, see Eq. (5.37), and hence a lower driving force, see Eq. (5.15), which in turn impedes the particles growth, see Eq. (5.38) for $j = 2$. The rate of gas dissolution remains almost equal to the rate of gas hydrate formation as the bulk concentration decreases with a slope around -0.002 s^{-1} . The slope becomes less steep as gas superficial velocity increases. The quasi-steady state can also be seen in Fig. (5.6). Here for the CST system, the total gas consumption rate is equal to the sum of the gas consumption rate in the liquid bulk and at the hydrate surface: i.e. $dn_{tot}/dt = dn_l/dt + dn_H/dt$. The operating conditions are the same as Fig. (5.5).

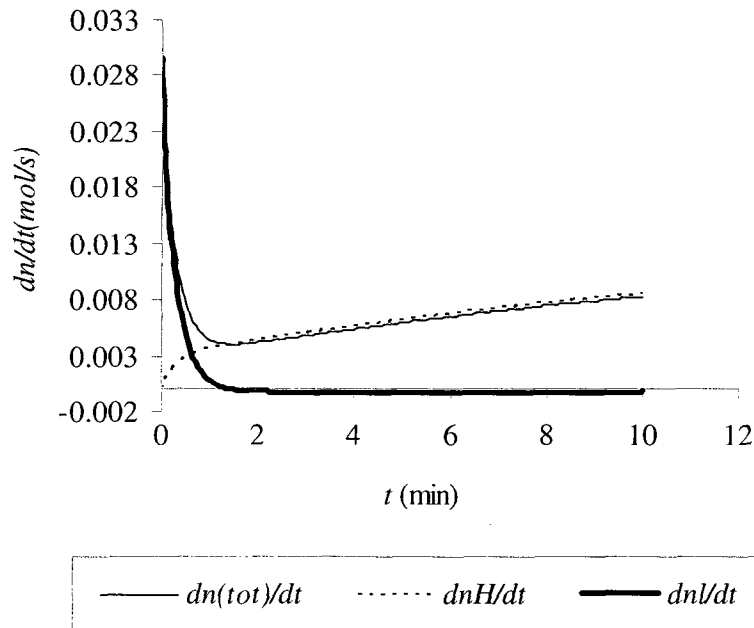


Figure (5.6). Gas consumption rate as a function time at 277.15 K and 2.187 MPa; gas and liquid superficial velocities are 0.025 and 0.002 m/s, respectively; CST for all phases.

The mole consumption rate slowly increases during this time with a maximum (at 10 minutes) of 0.0061, 0.0083 and 0.012 mol/s at gas velocities of 0.01, 0.025 and 0.15 m/s, respectively. The average rate of CO₂ mole consumption rate measured by Bergeron and Servio (2008b) is approximately 6×10^{-5} mol/s at 279 K and 3.05 MPa. Similarly, the methane/THF mole consumption rate reported by Luo et al. (2007) is 7×10^{-5} mol/s at maximum superficial gas velocity of 0.01 m/s at 277.65 K and 0.5 MPa. The former was obtained in a semi-batch stirred tank reactor where the system is essentially surface aerated while the latter was determined in a bubble column with inner diameter of 2.54 cm. A bubble column system provides more surface area for gas-liquid contact, i.e. higher dissolution rate. As reported by the authors, gas hydrates mostly formed on the surface of gas bubbles avoiding more gas dissolution in water.

Considering the system as quasi steady-state at 277.15 K and 2.187 MPa and the intrinsic rate constant of 1.20×10^{-8} m/s, the kinetic resistance ($1/k_r a_s$) was found to be more influential than the gas-liquid mass transfer resistance ($1/k_l a_l \epsilon_l$) with the effect naturally more pronounced at higher gas velocities resulting in greater supersaturation ratios, see Fig. (5.7). The kinetic resistance gradually decreases after turbidity point while the mass transfer resistance increases. However, with the operating condition mentioned above, the kinetic resistance remains more influential than the mass transfer resistance within 10 minutes. At gas superficial velocity of 0.025 m/s, the rate of increase in ($1/k_l a_l \epsilon_l$) is around 30% during 10 minutes of simulation and the rate of decrease in ($1/k_r a_s$) is around 70%, while at gas superficial velocity of 0.15 m/s, the increase in ($1/k_l a_l \epsilon_l$) and decrease in ($1/k_r a_s$) are 25% and 76%, respectively. From Bergeron and Servio (2008a), the experimental propane mole consumption rate results show that the system is kinetically controlled at the onset of growth

and gradually becomes more mass transfer limited within 42 minutes of experiment. It should be noted that even by assuming a constant dissolved gas mole concentration (quasi-steady state right after the turbidity point), the system is not necessarily controlled by the kinetic resistance at the onset of growth as reported by Bergeron and Servio (2008a). If the driving force is high enough, the initial particle surface area can be sufficiently large to result in the mass transfer resistance being dominant. This is shown later in Fig. (5.12)a and (5.13)a. The supersaturation ratio increases with an increase in liquid velocity although the effect is less noticeable than that of gas velocity since $k_l a_l$ is more sensitive to the gas than the liquid velocity. An increase in the column diameter also leads to lower gas holdup and gas-liquid surface area and hence lower supersaturation ratio. However, the effect is not significant as doubling the reactor diameter twice only decreases the supersaturation ratio by less than 1%.

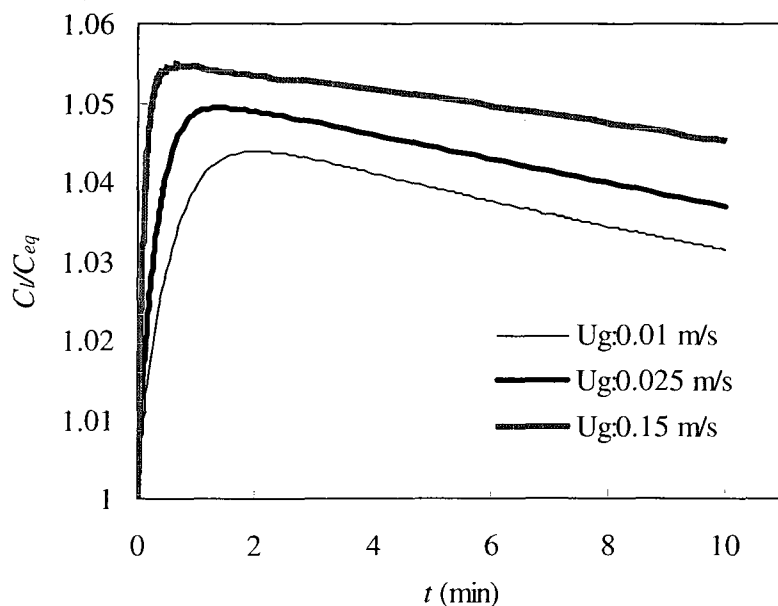


Figure (5.7). Supersaturation ratio of carbon dioxide in water as a function of time at 277.15 K and 2.187 MPa; liquid velocity is 0.002 m/s; CST for all phases.

Fig. (5.8) displays the heat produced in the system at 277.15 K, 2.187 MPa and a liquid superficial velocity of 0.002 m/s for the gas superficial velocities of 0.01, 0.025 and 0.15 m/s. In order to determine the heat to be removed from the system, Eq. (5.34) should be multiplied by dz and integrated from zero to H_D . The temperature is constant throughout the reactor as well as the recycle line and is equal to the operating temperature.

$$\begin{aligned}
& -C_{P,g}(T-T^{ref})H_D \frac{d}{dt}(C_g \varepsilon_g) - C_{P,l}(T-T^{ref})H_D \frac{d}{dt}(C_l \varepsilon_l) - \frac{\rho_s}{M_s} C_{P,s}(T-T^{ref})H_D \frac{d}{dt}(\varepsilon_s) \\
& + C_g C_{P,g}(T-T^{ref})(U_{g,in} - U_{g,out}) + \Delta H_{dis}^{ref} k_l a_l \varepsilon_l (C_l^{g-l} - C_l) H_D \\
& + \Delta H_f^{ref} K^* a_s (C_l - C_l^{eq}) H_D = Q
\end{aligned} \tag{5.39}$$

At the turbidity point, the heat released is mainly due to the gas dissolution, which decreases gradually while the heat due to the hydrate formation increases. Eventually, the gas dissolution rate is almost equal to gas hydrate formation rate, see Fig. (5.6), while the enthalpy of hydrate formation (80.3 kJ/mol) is higher than that of gas dissolution (19.43 kJ/mol) at 298K. At higher superficial gas velocity, the rate of gas-liquid interphase mass transfer and as a result the rate of heat released due to gas dissolution in water is higher.

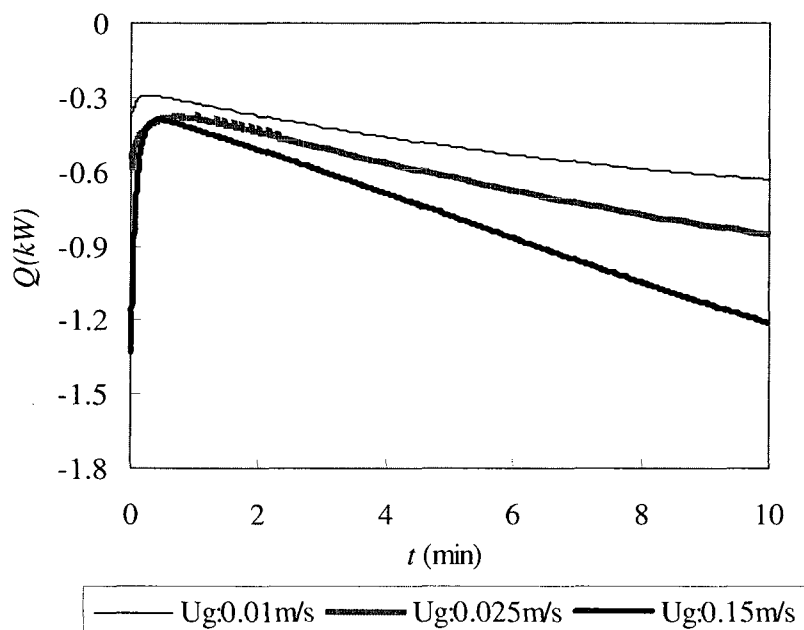


Figure (5.8). Heat produced as a function of time at 277.15 K and 2.187 MPa; liquid velocity is 0.002 m/s; CST for all phases.

Recently, Bergeron and Servio (2008b) obtained new intrinsic rate constants for carbon dioxide hydrate system in a semi-batch stirred tank reactor. The model is based on Hashemi et al. (2007) driving force while the bulk concentration was measured in-situ and found relatively constant at the onset of growth onwards (Bergeron and Servio, 2008c). Their results on measured carbon dioxide concentration suggests that the bulk concentration at the turbidity point and thereafter always remains close to the L_w -H two-phase equilibrium indicating low supersaturation ratio (1.006 at 277.5 K), which is similar to what was shown here in this work (maximum 1.05) as well as our previous work (maximum 1.003) (Hashemi et al., 2007). Moreover, the error associated with the assumption of L_w -H two-phase equilibrium value at the turbidity point should thus be insignificant. This could be further

investigated by measuring the dissolved gas concentration in a pilot-scale slurry bubble column. The mass transfer coefficient in a bubble column, 0.05 s^{-1} at 0.025 m/s , 277.15 K and 2.5 MPa (Hashemi et al., 2009), is an order of magnitude greater than that in the stirred tank reactor, 0.00122 s^{-1} at 277.15 K (Clarke and Bishnoi, 2005), which should result in higher dissolved gas concentration and in turn a greater supersaturation ratio.

Bergeron and Servio (2008b) kinetic study shows that the intrinsic rate constant obtained experimentally are in a good agreement with the theoretical model based on the population balance and experimental growth rate as well as purely theoretical population balance of Hashemi et al. (2007). The population balance is based on large number (1.69×10^{19}) of small nuclei (diameter of 97 nm) (at 277.15 K and 2.187 MPa) with the surface area in good agreement with those measured by Bergeron and Servio (2008b) with the particle size range of $0.6\text{-}6000 \text{ nm}$. In addition, n_{tb} and n_{eq} assumptions are valid as explained before. Thus, the population balance used in this work should fairly describe the hydrate growth rate provided that breakage and agglomeration is negligible within the 10 minutes simulation period.

The effect of pressure is shown in Fig. (5.9) at 277.5 K , at 2.187 MPa as well as 2.495 MPa at gas and liquid superficial velocity of 0.01 and 0.002 m/s , respectively. A higher pressure results in a greater driving force and as a result larger surface area at the onset of growth. Therefore, the mole consumption rate is greater at higher pressure. With the k_r of $4.5 \times 10^{-8} \text{ m/s}$, $k_{a,s}$ is 0.006 s^{-1} for 2.187 MPa , while 0.09 s^{-1} for 2.495 MPa at the turbidity point. Due to the higher $k_{a,s}$, the supersaturation curve reaches its maximum in a shorter amount of time and afterwards decreases with a larger slope. At 2.495 MPa , the supersaturation slope is -0.01 s^{-1} which is an order of magnitude greater than that at 2.187 MPa . If both conditions

were considered at quasi-steady state, mole consumption rate increases with time when the system is mostly controlled by kinetic resistance, i.e., 2.187 MPa while decreases when it is mass transfer limited i.e., 2.495 MPa. It has to be noted that at higher supersaturation ratio, i.e. driving force, the number of particles may no longer remain constant due to the formation of new nuclei (Clarke and Bishnoi, 2005). As a result, the population balance based on constant number of nuclei is more reliable at lower driving force.

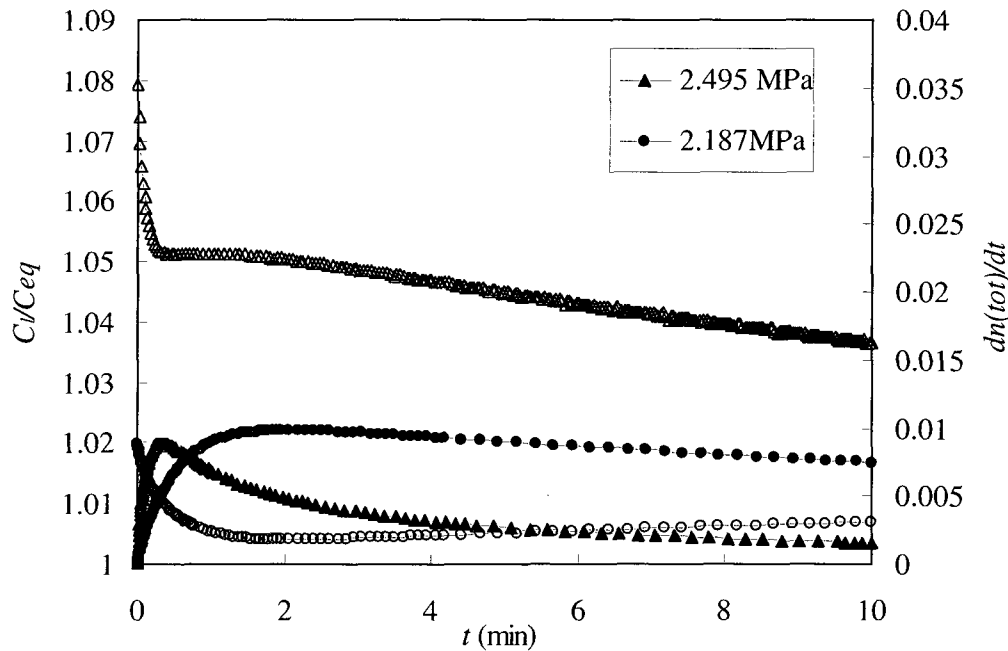


Figure (5.9). Effect of pressure at 277.5 K; gas and liquid superficial velocities are 0.01 and 0.002 m/s, respectively. Open and close symbols represent mole consumption rate and supersaturation ratio, respectively; CST for all phases.

The effect of temperature is displayed in Fig. (5.10) and (5.11). By decreasing the temperature, the supersaturation ratio increases resulting in a higher mole consumption rate.

The operating conditions chosen in Fig. (5.9) to (5.11) correspond to the dispersed bubble flow regime where the effect of temperature and pressure on the hydrodynamics (ϵ_g and $k_L a_L$) is not significant (Hashemi et al., 2009).

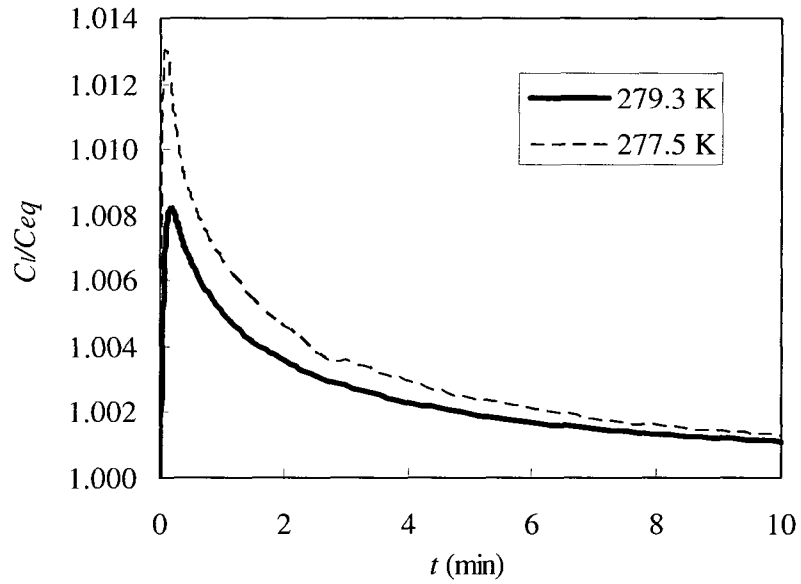


Figure (5.10). Effect of temperature on supersaturation at 3.04 MPa; gas and liquid superficial velocities are 0.01 and 0.002 m/s, respectively; CST for all phases.

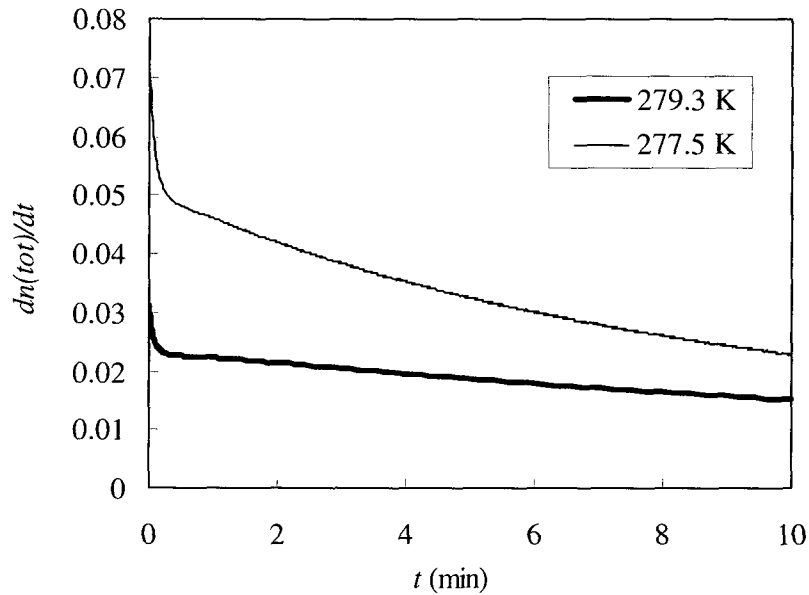


Figure (5.11). Effect of temperature on mole consumption rate at 3.04 MPa; gas and liquid superficial velocities are 0.01 and 0.002 m/s, respectively; CST for all phases.

Fig. (5.10) suggests that the system is mostly limited by mass transfer resistance at quasi steady-state condition. At 277.5 K the ratio of mass transfer resistance to the kinetic resistance is 191 while it is 66 at 279.3 K at time equal to 10 min. This ratio is 31 and 0.74 at 2.495 MPa and 2.187 MPa respectively at 277.5 K.

The ratio of mass transfer resistance to kinetic resistance, i.e. $k_{r,a_s} / k_{l,a_l} \epsilon_l$ as well as $k_{l,a_l} \epsilon_l$ and k_{r,a_s} are presented in Fig. (5.12) to (5.13). As the temperature decreases, pressure increases and/or reaction time increases, the ratio of mass transfer resistance to kinetic resistance will increase due to an increase in k_{r,a_s} and decrease in $k_{l,a_l} \epsilon_l$. At 2.187 MPa and 277.5 K, the effect of kinetic resistance is still more pronounced. For other conditions investigated, the

system is always controlled by the mass transfer resistance with the effect more pronounced at lower temperature and high pressure due to the higher driving force.

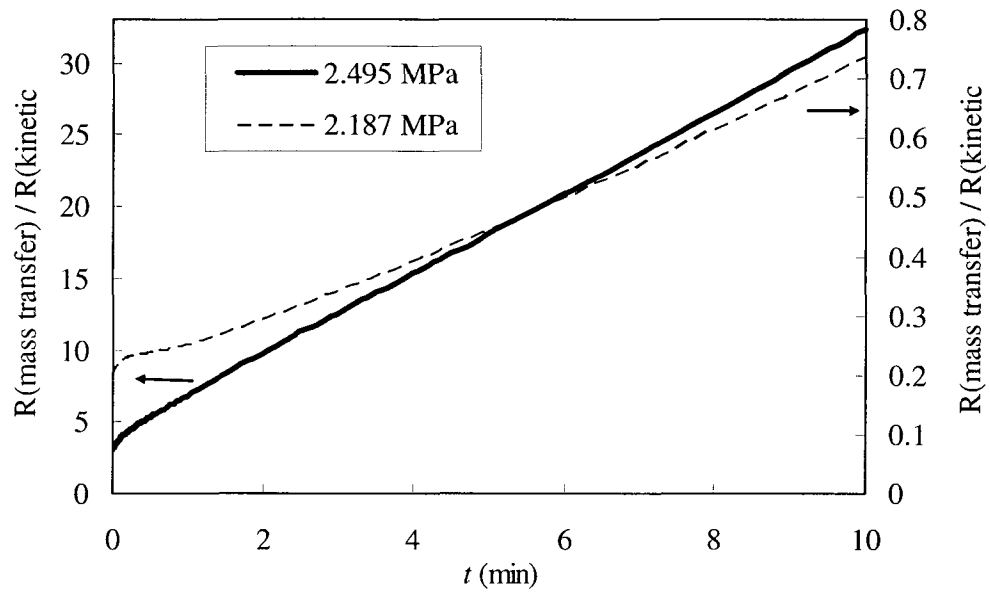


Figure (5.12)a. Effect of pressure on the ratio of resistances at 277.5 K; gas and liquid superficial velocities are 0.01 and 0.002 m/s, respectively; CST for all phases.

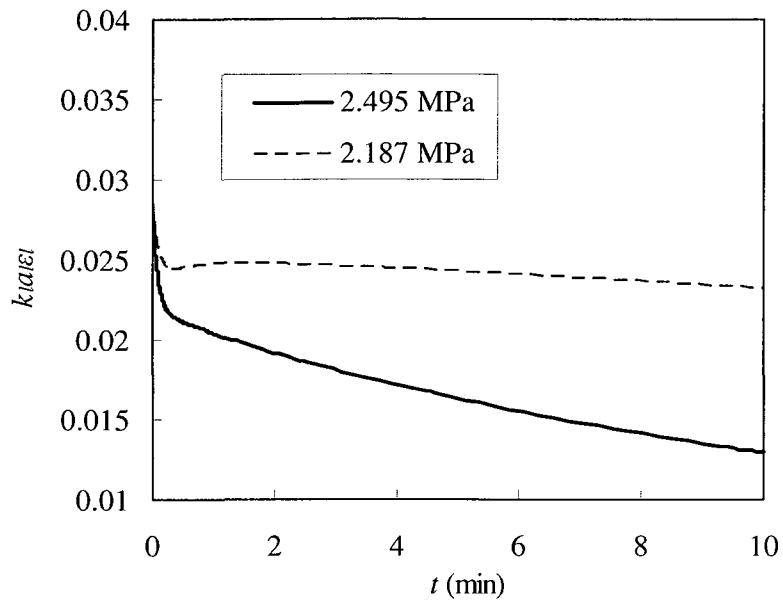


Figure (5.12)b. Effect of pressure on $k_{l|a|ε|_l}$ at 277.5 K; gas and liquid superficial velocities are 0.01 and 0.002 m/s, respectively; CST for all phases.

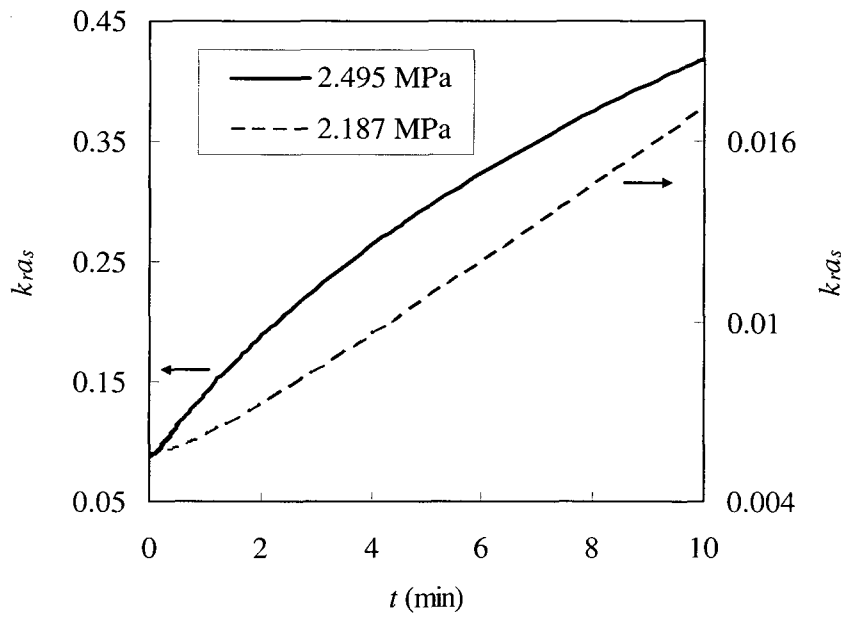


Figure (5.12)c. Effect of pressure on k_{r,a_s} at 277.5 K; gas and liquid superficial velocities are 0.01 and 0.002 m/s, respectively; CST for all phases.

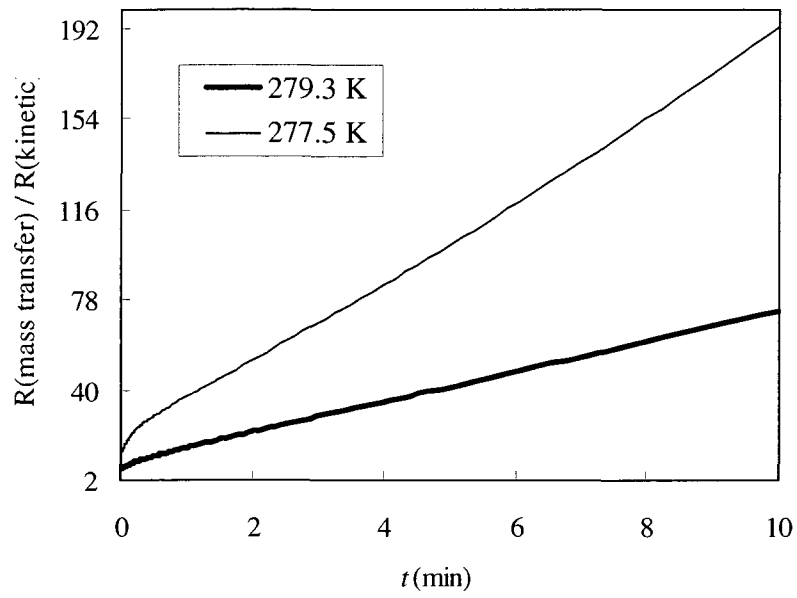


Figure (5.13)a. Effect of temperature on the ratio of resistances at 3.04 MPa; gas and liquid superficial velocities are 0.01 and 0.002 m/s, respectively; CST for all phases.

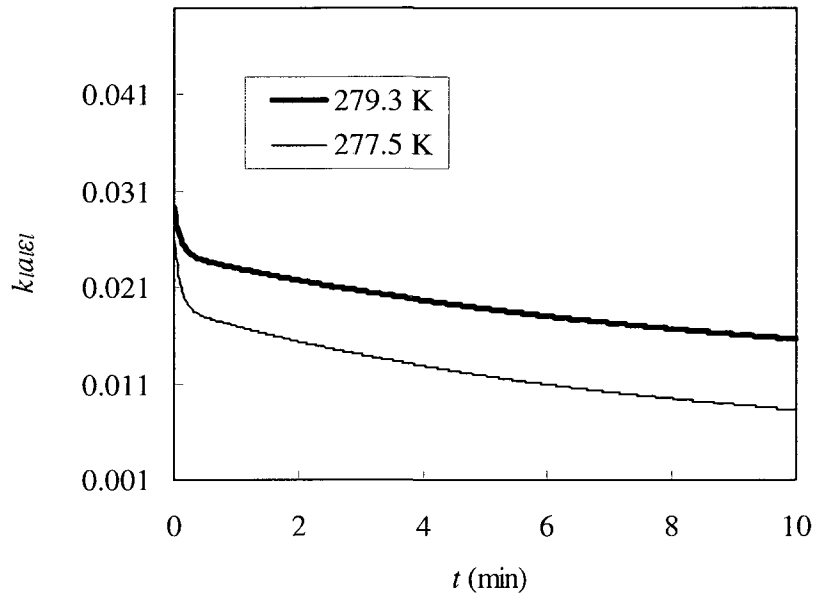


Figure (5.13)b. Effect of temperature on $k_l a_i \epsilon_i$ at 3.04 MPa; gas and liquid superficial velocities are 0.01 and 0.002 m/s, respectively; CST for all phases.

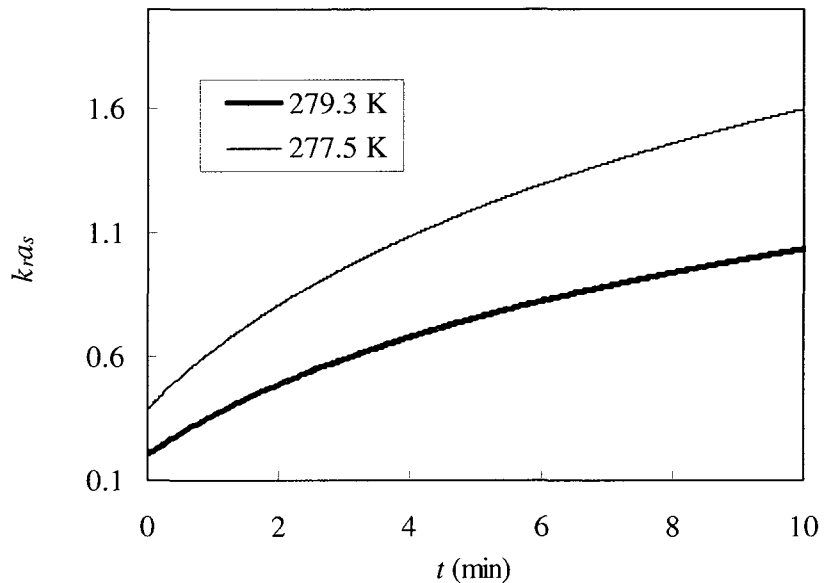


Figure (5.13)c. Effect of temperature on k_{g,a_s} at 3.04 MPa; gas and liquid superficial velocities are 0.01 and 0.002 m/s, respectively; CST for all phases.

As mentioned, the technology for large-scale synthesis of gas hydrates is still in the conceptual mode and there is almost no data available in the open literature. To our knowledge, the only published studies for similar systems to this work are from Mork and Gudmundsson (2002) and Luo et al. (2007) who produced methane and natural gas hydrates in a sparged stirred tank reactor and THF/methane hydrates in a slurry bubble column, respectively. Mork and Gudmusson (2002) reported an apparently constant mole consumption rate with time suggesting that the hydrate formation rate is controlled by interphase mass transfer rather than kinetics. Further evidence came from the much stronger influence of gas velocity than temperature on the gas consumption rate. In their case, they were limited to relatively low gas superficial velocities below 0.002 m/s. In order to link the

effects of temperature change on the hydrate growth kinetics through mole consumption rates, it is important to account for the change in driving force via solubility. Luo et al. (2007) found that a decrease in temperature, and increase in pressure and a rise in gas flow rate increased the gas consumption rate. They operated at low superficial gas velocities below 0.01 m/s and without mechanical agitation. In such conditions, hydrates quickly formed at the bubble surface and remained there during its rise through the column. They concluded that turbulence would help continuously replenish the surface of the bubble. Thus, at much greater shear stress due to liquid mixing by mechanical agitation, pneumatics (e.g. draft tube airlift) or greater gas velocities resulting in larger bubble size and rise velocities, one can speculate that hydrates particle may also grow in the bulk as the gas bubble surface would be free of hydrate. Moreover, if supersaturation exists at the turbidity point onwards as a result of dissolution process, the hydrate formation can occur everywhere in the liquid water and is not restricted to the gas-liquid film interface (Englezos et al., 1987).

5.4 Conclusion

A dynamic gas hydrate growth model was proposed for a slurry bubble column reactor based on a theoretical population balance as well as driving forces that require estimates of gas-liquid and liquid-hydrate equilibrium concentrations. The effect of gas and liquid superficial velocity based on transport properties at hydrate forming conditions was discussed. Mole consumption rate increases with superficial gas velocity while it is less sensitive to the liquid superficial velocity. The relative importance of mass transfer and kinetic resistances at different temperatures and pressures was also investigated. The intrinsic rate constant was found to be in good agreement with those available in literature. A higher pressure and lower

temperature increases the driving force, the mole consumption rate and the ratio of mass transfer to kinetic resistance.

Nomenclature

a_s	liquid-solid interfacial area per unit volume of reactor, $\text{m}_{\text{hyd.}}^2 \text{m}_{\text{R}}^{-3}$
C	concentration, mol m^{-3}
C_p	heat capacity, $\text{J mol}^{-1} \text{K}^{-1}$
D	diffusivity in liquid, $\text{m}^2 \text{s}^{-1}$
dp	pressure drop, Pa
d_p	particle diameter, μ_1 / μ_0 , m
d_b	bubble diameter, m
E	axial dispersion coefficient, $\text{m}^2 \text{s}^{-1}$
F	force, kg m s^{-2}
f	fugacity, Pa
G	linear growth rate, m s^{-1}
g	gravitational acceleration, m s^{-2}
h	convective heat transfer coefficient, $\text{W m}^{-2} \text{K}^{-1}$
H_D	hydrodynamic bed height, m
k_r	intrinsic kinetic rate constant, $\text{m}_{\text{liq.}}^3 \text{m}_{\text{hyd.}}^{-2} \text{s}^{-1}$
k_{a_l}	volumetric liquid-side mass transfer coefficient, s^{-1}
k_s	liquid-solid convective mass transfer coefficient, $\text{m}_{\text{liq.}}^3 \text{m}_{\text{hyd.}}^{-2} \text{s}^{-1}$
K^*	combined rate parameter, $\text{m}_{\text{liq.}}^3 \text{m}_{\text{hyd.}}^{-2} \text{s}^{-1}$
L	internal particle axis

M	molecular weight of the hydrate of the form $CO_2 \cdot n_w H_2O$
n	moles of gas consumed, mol
N_p	number of particles in the liquid phase
Nu	Nusselt number, hd / κ
Q	rate of heat removal, kJ s^{-1}
R	gas constant, $\text{J mol}^{-1} \text{K}^{-1}$
Re	Reynolds number, $\rho U_b d_b / \mu$
P	pressure, Pa
r_c	critical radius, m
Pr	Prandtl number, $C_p \mu / \kappa$
T	temperature, K
t	time, s
U	superficial velocity, m s^{-1}
V	volume, m^3
X	mole fraction
z	external coordinate on the reactor, m
Z	compressibility factor

Greek letters

ΔH_{dis}	Heat of gas dissolution, kJ mol^{-1}
ΔH_f	Heat of hydrate formation, kJ mol^{-1}
Δg	free energy change per unit volume of product, J m^{-3}
κ	thermal conductivity, $\text{W m}^{-1} \text{K}^{-1}$

γ	surface tension for a gas-liquid system, J m^{-2}
ε	phase holdup
μ	viscosity, Pa s
μ_j	n-th moment of particle distribution, $\text{m}^j \text{m}_R^{-3}$
μ_j^0	initial n-th moment of particle distribution
v	molar volume, $\text{m}^3 \text{mol}^{-1}$
v	particle velocity, m s^{-1}
ρ	density, kg m^{-3}
σ	surface tension for a hydrate-water system, J m^{-2}
ϕ	particle size distribution

Subscripts and Superscripts

b	bubble
B	buoyancy
D	drag
e	external
eq	equilibrium
exp	experimental condition
G	gravity
g	gas phase
$g-l$	gas-liquid interface
H	hydrate phase
i	gas component, internal

<i>l</i>	liquid bulk
<i>l-s</i>	liquid-solid interface
<i>R</i>	reactor
<i>Ref</i>	reference
<i>s</i>	surface of solid, solid(hydrate) phase
<i>tb</i>	turbidity point
<i>tot</i>	total
<i>w</i>	water

Acknowledgements

The authors are grateful to the Canadian Foundation for Innovation, the Ontario Innovation Trust and Natural Sciences and Engineering Research Council of Canada for financial assistance.

References

- Beenackers, A.A.C.M., Van Swaaij, W.P.M., (1993). Mass transfer in gas-liquid slurry reactors. *Chemical Engineering Science*, 48, 3109-3139.
- Behkish, A., Lemoine, R., Oukaci, R., Morsi, B.I., (2006). Novel correlations for gas holdup in large-scale slurry bubble column reactors operating under elevated pressures and temperatures. *Chemical Engineering Journal*, 115, 157-171.
- Bergeron, S., Servio, P., (2008a). Reaction rate constant of propane hydrate formation. *Fluid Phase Equilibria*, 265, 30-36.

- Bergeron, S., Servio, P., (2008b). Reaction rate constant of CO₂ hydrate formation and verification of old premises pertaining to hydrate growth kinetics. *AIChE Journal*, 54 (11), 2964-2970.
- Bergeron, S., Servio, P., (2008c). CO₂ and CH₄ mole fraction measurements during hydrate growth in a semi-batch stirred tank reactor. Accepted to *Fluid Phase Equilibria*.
- Chatti, I., Delahaye, A., Fournaison, L., Petitet, J-P., (2005). Benefits and drawbacks of clathrate hydrates: a review of their areas of interest. *Energy Conversion and Management*, 46, 1333-1343.
- Clarke, M.A., Bishnoi, P.R., (2005). Determination of the intrinsic kinetics of CO₂ gas hydrate formation using in situ particle size analysis. *Chemical Engineering Science*, 60, 695-709.
- Bird, R.B., Stewart, W.E., Lightfoot, E.N., (2002). *Transport Phenomena*, 2th ed., John Wiley & Sons.
- Englezos, P., Kalogerakis, N., Dholabhai, P.D., Bishnoi, P.R., (1987). Kinetics of formation of methane and ethane gas hydrates. *Chemical Engineering Science*, 42, 2647-2658.
- Fan, L-S, (1989). *Gas-liquid-solid fluidization engineering*, Boston: Butterworths.
- Hao, W., Wang, J., Fan, S., Hao, W., (2008). Evaluation and analysis method for natural gas hydrate storage and transportation processes. *Energy Conversion and Management*, 49, 2546-2553.
- Hashemi, S., Macchi, A., Bergeron S., Servio, P., (2006). Prediction of methane and carbon dioxide solubility in water in the presence of hydrate. *Fluid Phase Equilibria*, 246, 131-136.
- Hashemi, S., Macchi, A., Servio, P., (2007). Hydrate growth model in a semi-batch stirred tank reactor. *Industrial Engineering Chemistry Research*, 46, 5907-5912.

- Hashemi, S., Macchi, A., Servio, P., (2009). Gas-liquid mass transfer in a slurry bubble column operated at hydrate forming conditions. Accepted to Chemical Engineering Science.
- Herri, J.M., Pic, J.S., Gruy, F., Cournil, M., (1999). Methane hydrate crystallization mechanism from in-situ particle sizing. *AIChE Journal*, 45, 590-602.
- Iwasaki, S., Kimura, T., Yoshikawa, K., Nagayasu, H., (2002). The pre-investigation of natural gas transportation and storage system as gas hydrates for development of marginal natural gas fields. In: *Proceeding of the 4th International Conference on Gas Hydrates*, Yokohama.
- Lau, R., Peng, W., Velazquez-Vargas, L.G., Yang, G.Q., Fan, L-S., (2004). Gas-liquid mass transfer in high pressure bubble columns. *Industrial and Engineering Chemistry Research*, 43, 1302-1311.
- Levespiel, O., (2001). *Chemical reaction engineering*, 3rd ed. John Wiley & Sons.
- Luo, X., Lee, J.D., Lau, R., Guoqiang Y., Fan, L-S., (1999). Maximum stable bubble size and gas holdup in high-pressure slurry bubble columns. *AIChE Journal*, 45, 665-680.
- Luo, Y.-T., Zhu, J.H., Fan, S.-S., Chen, G.-J., (2007). Study on the kinetics of hydrate formation in a bubble column. *Chemical Engineering Science*, 62, 1000-1009.
- Malegaonkar, M.B., Dholabhai, P.D., Bishnoi, P.R., (1997). Kinetics of carbon dioxide and methane hydrate formation. *Canadian Journal of Chemical Engineering*, 75, 1090-1099.
- Mork, M., Gudmundsson, J.S., (2002). Hydrate formation rate in a continuous stirred tank reactor: Experimental results and bubble-to-crystal model. In: *Proceeding of the 4th International Conference on Gas Hydrates*, Yokohama.

- Randolph, A.D., Larson, M.A., (1971). Theory of particulate processes: Analysis of techniques of continuous crystallization. New York: Academic.
- Sloan, Jr. E.D., (1998). Clathrate Hydrates of natural gases. 2nd ed., New York: Marcel Dekker.
- Watanabe, S., Takahashi, S., Mizubayashi, H., Muratal, S., Murakami, H., (2008). A demonstration project of NGH land transportation system. In: Proceeding of the 6th International Conference on Gas Hydrates, Vancouver.
- Wilke, C.R., Chang, P., (1955). Correlation of diffusion coefficients in dilute solutions. AIChE Journal, 1, 264-270.

Chapter 6

Conclusions and Future Research

6.1 Conclusions

The technology of gas hydrate synthesis for the purpose of transportation and storage of natural gas is being developed. However, there are still many unknowns on reactor design as well as kinetics and transport phenomena of hydrate systems and there is little data in open literature for production of gas hydrate. In order to address the existing issues, the thermodynamics, kinetics and hydrodynamics of a leading technology, the slurry bubble column, were studied in this work. First, a general model was developed to predict the solubility of carbon dioxide and methane in water in the presence of gas hydrate. Then issues in the estimation of the intrinsic kinetic rate constant were extensively discussed using a model based on a driving force which takes interphase heat transfer into account. Hydrodynamics of a three-phase slurry bubble column was also studied at carbon dioxide hydrate forming conditions. Finally, a reactor model was developed that accounts for kinetics, hydrodynamics as well as interphase heat and mass transfer rates. The important conclusions from the above works are presented in this chapter:

Vapor-liquid water (L_w -V), vapor-liquid water-hydrate (H- L_w -V) and hydrate-liquid water (H- L_w) equilibrium need to be determined as they define the driving forces within gas-liquid and liquid-solid film layers in the three-phase slurry system. Henry's law has been the common approach to predict the gas hydrate former/water equilibrium in the presence of gas

hydrate. However, Henry's law estimates the solubility at the three-phase equilibrium (H-L_w-V) rather than two-phase hydrate liquid water equilibrium (H-L_w). The influence of pressure on the gas solubility in the (H-L_w) zone was found insignificant over the range investigated. Therefore, a slight change in pressure from two-phase (H-L_w) to three-phase (H-L_w-V) equilibrium does not significantly affect the solubility which explains the good agreement between the Henry's law and experimental results. In this work, the Trebble-Bishnoi equation of state was applied along with the van der Waals and Platteeuw, and Holder models to predict the gas solubility in water at (H-L_w) and (H-L_w-V) equilibrium for methane-water and carbon dioxide-water systems. The Trebble-Bishnoi equation of state was chosen due to its simplicity relative to other equations of state used in literature and relative success in predicting (L_w-V) equilibrium of a methane-water system and (H-L_w) equilibrium of a carbon dioxide-water system over other cubic equations of state such as Peng-Robinson and Soave-Redlich-Kwong. The model with the original parameters appears to always underestimate the solubility at two as well as three phase zone of methane/water and carbon dioxide/water system. In order to improve the accuracy of the present model, binary interaction parameters of Trebble-Bishnoi equation of state as well as reference parameters of the Holder model were readjusted to (L_w-V) and (H-L_w-V) equilibrium data, respectively. The model covered a larger temperature range and the Average Absolute Relative Error (AARE) for both gases was below 10%.

The intrinsic rate constant for CO₂ hydrate formation was determined in a semi-batch stirred tank reactor. The model is based on a concentration driving force rather temperature or pressure, while it accounts for heat transfer as hydrate formation is exothermic. The driving force does not necessarily result in three-phase equilibrium (H-L_w-V) condition at hydrate

surface. Temperature at the surface of hydrate depends on the rate of heat removal and can vary between the experimental (bulk) and three-phase equilibrium temperature at the experimental pressure. It was found that with minimum heat removal, the temperature gradient within the liquid-solid film layer is almost nil. Hence, the temperature at the surface of hydrate is nearly equal to the bulk temperature. It was also shown that the pressure and interphase heat transfer effects via surface temperature is included in the concentration driving force. A decrease in temperature or increase in pressure increases the driving force. The rate of hydrate growth was taken into account using a population balance as well as available experimental data in literature. The discrepancy within the intrinsic rate constant results were significant. The measured size of particles was limited to 0.5-1000 micron and the measured surface area does not appear to account for all the particles present in the system at the turbidity point. The experimental results also suggest the existence of foreign particles although it is not clear if the nucleation is absolutely heterogeneous. Therefore, the presence of particles with a size lower than detectable size range of the probe might significantly influence the hydrate surface area depending on their size and number. In addition, it was found that the data previously used in literature to extract the intrinsic rate constant is limited by gas dissolution rate, which requires a more accurate mass transfer coefficient. Recent studies in literature with the particle size from 0.6-6000 nm indicates a good agreement between the experimental and theoretical intrinsic rate constant suggesting that that a theoretical population balance is able to predict the surface area fairly well provided that effect of breakage, agglomeration and secondary nucleation is insignificant.

The interphase mass transfer coefficient needs to be determined at operating conditions corresponding to gas hydrate formation. Hydrodynamics of a three-phase slurry system at

CO₂ hydrate was studied in a high pressure pilot-scale slurry bubble column. Effect of superficial gas velocity, temperature, pressure and volumetric solid concentration on gas holdup and gas-liquid interphase mass transfer coefficient were investigated. The pressure was varied from 0.1 MPa to 4 MPa while gas velocity was increased up to 0.20 m/s. The effect of temperature was investigated at ambient as well as 277 K. The effect of carbon dioxide hydrate was simulated by wettable ion-exchange resins with the density close to that of CO₂ hydrate i.e. 1.22-1.28 g/ml with the average particle size of 85 microns. Gas holdup as well as $k_l a_l$ were found to increase with superficial gas velocity and pressure while decrease with temperature. The effect of pressure is dominant on the interfacial area due to the increase in the rate of bubble breakup. However, k_l was found to be more sensitive to lower temperatures than interfacial area, a_l due to the decrease in diffusivity. Effect of pressure is more pronounced at coalesced bubble flow regime and lower pressures. Increasing pressure delays the onset of bubble coalescence and hence, the dispersed flow regime occurs at higher gas holdup. Particle concentration was increased up to 10% vol. on gas free basis. Effect of solid concentration was not noticeable in the range investigated. Rheology of the particle slurry was also studied and it was found that at shear rate encountered in the bubble column, the rheology of the system resembles that of water alone. The similarity between the rheology and density of the slurry and water explains the negligible influence of solid on the hydrodynamic and transport properties of the system. The mass transfer coefficient was found independent of bubble size over the range of superficial gas velocity investigated. As a result, the ratio of volumetric mass transfer coefficient per total unit volume over gas holdup is constant.

A dynamic gas hydrate growth model was proposed for a slurry bubble column reactor which incorporates kinetics and hydrodynamics as well as interphase heat and mass transfer rates. The model is based on mass, energy and momentum balances coupled with a theoretical population balance to account for the hydrate growth surface area. The driving forces require estimates of gas-liquid (L_w-V) and hydrate-liquid ($H-L_w$) equilibrium concentrations taken from the results obtained in Chapter 2. The intrinsic rate constant was taken from Chapter 3 as well as recent literature data. Gas holdup as well as volumetric mass transfer coefficient was calculated using the literature correlations modified for hydrate forming conditions based on the experimental data obtained in Chapter 4 using a high-pressure slurry bubble column. The effect of gas and liquid superficial velocity based on transport properties at hydrate forming conditions was discussed. Mole consumption rate increases with superficial gas velocity while it is less sensitive to the liquid superficial velocity. The effect of flow regime was found insignificant on the performance of the system. The enclathration of the gas to the surface of the crystals was found to be mainly controlled by kinetic resistance. In fact, using the theoretical intrinsic rate constant from Chapter 3, kinetic resistance was found to be more influential than the gas-liquid mass transfer resistance with the operating conditions investigated. The supersaturation trend was discussed after the turbidity point showing the system eventually reaches to a quasi-steady state where the rate of hydrate formation remains close to the rate of gas consumption. The amount of heat to be removed in order to have isothermal operation was also calculated based on an energy balance. Higher pressure and lower temperature was found to increase the driving force, the ratio of mass transfer resistance to that of kinetic and mole consumption rate.

6.2 Future Research

The following recommendations are proposed for further research and studies in the field of thermodynamics, kinetics and hydrodynamics of hydrate formation:

- Extend the thermodynamic model to electrolytes i.e. inhibitors/promoters and multi component gas mixtures.
- Measure the particle size distribution in-situ in a pilot-scale slurry bubble column to verify the validity of population balance.
- Measure CO₂ mole consumption rate in a pilot-scale slurry bubble column in order to verify the simulation results.
- Study the effect of surface- active agents on system hydrodynamics as well as gas hydrate mole consumption rate.
- Study the effect of particle size on the hydrodynamics of the system.
- Investigate further the effect of solids on the hydrodynamics of the system at high concentrations.
- Evaluate the effect of reactor geometry (gas distributor, draft-tube) and operating conditions (gas superficial velocity, temperature, pressure, presence of inert particles) on the process stability and mole consumption rate.
- Study the rheology of CO₂ hydrate slurry.
- Extend the system to multi-component mixtures (natural gas).